Investigation on Design and Control of Energy Storage Systems for DC Microgrid

Submitted in partial fulfilment of the requirements
for the award of the degree of

Doctor of Philosophy
in
Electrical Engineering

By

Arunkumar C. R.
(Roll no: 718018)

Supervisor
Dr. Udaya Bhasker Manthati

Department of Electrical Engineering
National Institute of Technology Warangal
June 2022

APPROVAL SHEET

This Thesis entitled **"Investigation on Design and Control of Energy Storage Systems for DC Microgrid "** by **Mr. Arunkumar C. R.** is approved for the degree of Doctor of Philosophy

Examiners

_____

_____

_____

Supervisor

Dr. Udaya Bhasker Manthati

Assistant Professor

EED, NIT Warangal

Chairman

Prof. D. M. Vinod Kumar

Professor,

EED, NIT Warangal

Date:_____

Department of Electrical Engineering

National Institute of Technology,

Warangal- 506004, Telangana, India

Department of Electrical Engineering

National Institute of Technology Warangal - 506004

CERTIFICATE

This is to certify that the thesis entitled "**Investigation on Design and Control of Energy Storage Systems for DC Microgrid**" being submitted by **Arunkumar C. R. (718018)** is a bonafide research work carried out under my supervision and guidance in fulfillment of the requirement for the award of the degree of **Doctor of Philosophy** in the Department of Electrical Engineering, National Institute of Technology Warangal-506004, Telangana, India. The matter embodied in this thesis is original and has not been submitted to any other University or Institute for the award of any other degree.

Place: Warangal
Date: 13/06/2022

Dr. Udaya Bhasker Manthati
Assistant Professor
Department of Electrical Engineering
NIT Warangal

DECLARATION

This is to certify that the work presented in the thesis entitled "**Investigation on Design and Control of Energy Storage Systems for DC Microgrid**" is a bonafide work done by me under the supervision of **Dr. M. Udaya Bhasker**, Assistant Professor, Department of Electrical Engineering, National Institute of Technology Warangal and was not submitted elsewhere for the award of any degree.

I declare that this written submission represents my ideas in my own words and where others ideas or words have been included, I have adequately cited and referenced the original sources. I also declare that I have adhered to all principles of academic honesty and integrity and have not misrepresented or fabricated or falsified any idea / data / fact / source in my submission. I understand that any violation of the above will be a cause for disciplinary action by the Institute and can also evoke penal action from the sources which have thus not been properly cited or from whom proper permission has not been taken when needed.

Arunkumar C. R.

(**718018**)

Date: 13/06/2022

ACKNOWLEDGEMENTS

It would not have been possible to write this thesis without the help and support of the kind people around me, to only some of whom it is possible to give a particular mention here.

Foremost, I would like to express my deepest gratitude to my respected research supervisor, **Dr. Udaya Bhasker Manthati**, Assistant Professor, Department of Electrical Engineering, National Institute of Technology Warangal, for his guidance, scholarly input and consistent encouragement. This work is possible only because of the unconditional moral support provided by him. I had great freedom to plan and execute my ideas in research without any pressure. This made me identify my strengths and drawbacks and boosted my self-confidence.

I am very much thankful to **Prof. D. M. Vinod Kumar**, Chairman of DSC, Department of Electrical Engineering for his constant technical suggestions, encouragement, support and cooperation.

I wish to express my sincere thanks to **Prof. N.V. Ramana Rao**, Director, NIT Warangal for his official support and encouragement.

I take this privilege to thank all my DSC Committee members, **Prof. N. Viswanathan**, Department of Electrical Engineering, **Dr. A. Kirubakaran**, Assistant Professor, Department of Electrical Engineering and **Dr. J. Ravi Kumar**, Associate Professor, Department of Electronics and Communication Engineering, for their detailed technical review, constructive suggestions and excellent advice during the progress of this research work.

I am very much thankful to **Prof. M. Sailaja Kumari**, Head, Department of Electrical Engineering for her constant encouragement, support and cooperation.

I also appreciate the encouragement from teaching, non-teaching members, and the Department of Electrical Engineering fraternity of NIT Warangal. They have always been encouraging and supportive.

I would also like to thank the technical and support staff of the department for their support and help whenever I needed it. I cannot forget to thank my senior Ph.D. colleagues **Dr. Punna Srinivas**, **Dr. Laxman**, **Dr. Anil Kumar**, **Mr. Sumon Dhara**, **Mr.**

Hema Sundara Rao, **Mr. Madhu Babu** and **Mr. Chinna K.** for their cooperation and memorable association. It was an immense pleasure to work alongside with them.

I am grateful to my contemporary research scholars **Mr. Ajit Kumar Mohanty**, **Mr. Vijay Vutla**, **Mr. Chinmay Kumar Das**, **Mr. Ramesh Guguloth**, **Mr. Manoj P.**, **Mr. Dinesh Ambati**, **Mr. Sunil Ankeshwarapu**, **Mr. V. Lokesh**, **Mr. Puli Rajanikanth**, **Mr. M. F. Baba** and **Mrs. Parvathy M. L.**. The discussion I used to have with you on various topics provided a relaxing time from research. Apart from this, your advice during my struggling period with research was of great significance.

My heartfelt thanks to teachers and mentors in my life **Prof. Dinesh Gopinath**, **Mrs. Anu A. G.**, **Dr. Sujil A.**, **Dr. Sreenu Sreekumar** and **Dr. Dileep G.** for their constant support during my journey.

Special thanks to my present and ex colleagues with whom I have enjoyed my past four years, starting from **Mr. Mahadhevan**, **Mr. Jerry Joseph**, **Mr. Chakrapani**, **Mr. Akhil K.**, **Mr. Abhijeet**, **Ms. Monika**, **Mr. Mahesh**, **Mr. Ajay** , **Mrs. Chinju R.**, **Mr. Prashanth**, **Mr. Vishnu P.**, **Dr. Nikhil T.**, **Mr. Sudharshan**, **Mr. Nandan** and **Mr. Milattu**.

I acknowledge my gratitude to all my teachers and colleagues at various places for supporting and encouraging me to complete the work.

Finally, I would like to express profound gratitude to my family members for all they have undergone to bring me up to this stage. I wish to express gratitude to my parents, **Sh. Raveendran** and **Smt. Santhamma**, for their kind support, the confidence and the love they have shown to me. You are my greatest strength, and I am blessed to be your son. I want to thank my wife, **Mrs. Vinny George** for her continuous support and belief in me. You always supported and motivated me and believed in me for who I am. I also would like to thank my sister, **Mrs. Sandhya** for being a good friend and understanding me well during this challenging situation.

At the end of my thesis, it is a pleasant task to express my thanks to all those who contributed directly or indirectly in many ways to the success of this study and made an unforgettable experience for me.

Arunkumar C. R.

ABSTRACT

DC microgrids have shown significant growth in the power sector due to the tremendous usage of renewable energy sources (RES), energy storage, and DC inherent loads. The fewer power conversion stages and the non-requirement of synchronization and reactive power compensation make the DC microgrid more efficient than AC microgrids. Nevertheless, more research is still needed to find an effective solution to mitigate the power quality issues arising from the intermittent nature of RES, effective system topology, and standards for a reliable and stable power supply. The energy storage devices (ESD) are integrated with the DC microgrid to reduce the RES intermittence and achieve power balance in the DC microgrid system. Moreover, ESD can convert the non-dispatchable RES generation into dispatchable power, increasing the utility of DC microgrids.

The selection of ESD plays a crucial role in peak load shaving and transient mitigation of DC microgrid by providing a fast response as well as a prolonged operation. Unfortunately, single energy storage cannot meet these goals; consequently, hybridization of energy storage with high specific energy and specific power is the solution for proper compensation for power fluctuations in autonomous microgrids. The comprehensive review realized that combining a lead-acid battery and a supercapacitor (SC) compensated the gap between high energy density and high power density, proving to be the optimum solution for hybrid energy storage applications and therefore employed as a hybrid energy storage system (HESS) in this study.

Integrating multiple ESDs with different frequency characteristics to the DC microgrid requires utmost care. Hence a detailed study of design, modelling and controller parameter estimation of actively configured HESS in DC microgrid is presented. The battery and SC are actively interfaced into the DC bus via independent bidirectional DC-DC converters. The battery supplies the average power demand, and SC compensates for the transient power based on the control strategy. In conventional controller design, the outer voltage control parameters are selected based on SC characteristics, and the battery characteristics are neglected for easiness. Hence, the proposed controller design aims to incorporate the characteristics of the battery, SC and low pass filter effect on the controller. As a result, the designed unified controller can regulate the operation of HESS in charging and discharging mode. Moreover, the proposed method provides enough phase margin and bandwidth for the controller, ensuring stability in the DC microgrid.

Unlike the battery, the SC voltage can vary during operation and may give rise to oscillations in DC bus voltage, battery current and SC current, causing instability in the DC microgrid. Further, low order LPF in the controller causes delayed dynamic performance and slow battery and SC current settling. Hence to address these issues, a variable bandwidth low pass filter (VBLPF) based modified power-sharing scheme and energy management strategy (EMS) is proposed for HESS integrated isolated PV- DC microgrid. The modified power-sharing scheme generates the battery reference current without the direct aid of LPF. The VBLPF generates the SC reference current by incorporating the SC voltage variation. The proposed EMS selects the bandwidth of VBLPF based on the RES generation, battery state of charge and SC voltage. Further, the energy supply capability of SC can be controlled based on SC voltage utilizing VBLPF, i.e. it supplies more energy at high SC voltage and less energy at low SC voltage.

The conventional control of HESS in an isolated DC microgrid follows a two-loop control strategy with three PI controllers. In addition to the delay introduced by LPF, PI also adds delay to the control system. Simultaneously tuning three PI controller parameters for optimum DC microgrid performance is tedious. Further, PI controllers cannot provide the optimum transient and steady-state performance together, and there is a trade-off between peak overshoot and settling time during controller design. Hence, a hybrid controller is proposed to eliminate the delay introduced by PI controllers and LPF. In the proposed method, the outer voltage is regulated by PI controllers and the inner current loop is regulated with the help of predicted current equations and Euler approximation. A hybrid control scheme is combined with an indirect LPF power splitting scheme to reduce the delay in control and thereby enhance the dynamic performance of the DC microgrid. The bode analysis is performed to ensure the stability of the voltage control loop, and predictive equations are analyzed for dependence on parameter variation.

The usage of low order LPF in any controller stage adds delay and makes it difficult to get the optimum DC microgrid performance. In addition, the use of constant bandwidth LPF has no control over the charge-discharge rates of the battery. In conventional methods, the cutoff frequency of the LPF is selected based on trial and error, and no precise method has been addressed in the literature so far. Hence, a discrete rate limiter-based hybrid control strategy for HESS in an isolated DC microgrid is proposed to eliminate the phase delay by LPF and uncertainty in the LPF cut off frequency selection. In this work, different operating scenarios such as increment/decrement in PV generation and increment/decrement in load demand are considered for validating the performance of the HESS integrated PV fed DC microgrid control strategy. Further, the proposed con-

troller proves that lower SC voltage operations have a less ringing effect on DC bus voltage.

The proposed methods are analyzed mathematically, and simulation and experimental studies are conducted to validate the effectiveness of the proposed control and energy management strategies. A scaled-down prototype is developed to validate the DC microgrid performance and control scheme. The experimental studies are conducted with the help of the dSPCAE 1104 real-time controller platform. Different operating scenarios such as i) change in PV generation, ii) change in load demand and iii) operation under SC charging are considered for validating the effectiveness of the proposed DC microgrid system. Finally, the simulation and experimental results are compared based on dynamic performance, ensuring better performance than conventional methods.

Contents

List of Figures

List of Tables

List of Symbols

C_0	Output capacitance (μF).
$d_{sc}(k+1)$	Supercapacitor duty at $(k+1)^{th}$ instant.
$d_b(k)$	Battery duty at k^{th} instant.
dv	Error in DC bus voltage.
G_{vib}	Duty to current control transfer function of battery.
$i_{sc}(k)$	Supercapacitor current (A) at k^{th} instant.
K^*	Over all transfer function gain.
L_b	Battery boost converter inductance (H).
L_{sc}	Supercapacitor boost converter inductance (H).
P_L	Load power (W).
P_{pv}	Photovoltaic panel power (W).
$V_{bat}(k)$	Battery voltage (V).
ε_0	Permittivity of free space (Farad/m)
A	Exponential voltage (V).
B	Exponential capacity (Ah^{-1}).
B_{SOC}	Battery state of charge.
c	Molar concentration (mol/m^3).
d	Thickness of Helmholtz layer (m).
$d_b(k+1)$	Battery duty at $(k+1)^{th}$ instant.
$d_{sc}(k)$	Supercapacitor duty at k^{th} instant.
Exp	Exponential zone voltage of battery (V).
G	Error voltage gain factor.
G_{all}	Over all hybrid energy storage system transfer function.
G_{visc}	Duty to current control transfer function of supercapacitor.
$i_b(k)$	Battery current at k^{th} instant.
$i_b(k+1)$	Battery current at $(k+1)^{th}$ instant.
i_{bref}	Battery reference current (A).
I_{pv}	Photovoltaic panel current (A).
i_{ref}	Total reference current.
i_{sc}	SC current.
$i_{sc}(k+1)$	Supercapacitor current (A) at $(k+1)^{th}$ instant.
i_{scref}	Supercapacitor reference current (A).
i_b	Actual battery current (A).

i_b^*	Battery reference current (A).
K_{iib}	Integral term of battery current controller.
K_{iisc}	Integral term of supercapacitor current controller.
K_{pib}	Proportional term of battery current controller.
K_{pisc}	Proportional term of supercapacitor current controller.
L_{pv}	PV boost converter inductance (H).
N_e	Number of electrode layers.
N_p	Number of SC connected in parallel.
N_s	Number of SC connected in series.
P_{bat}	Battery power (W).
P_{sch}	Supercapacitor charging power (W).
PI_v	Proportional integral controller for voltage control loop.
Q	Battery capacity (Ah).
Q_T	Total charge of SC unit.
R	Ideal gas constant.
r	Rate limiter constant.
R_{bat}	Battery internal resistance (Ω).
R_L	Load resistance (Ω).
SC_{EN}	Supercapacitor enable.
T	Operating temperature.
Ts	Exponential voltage (V).
V_0	Output voltage (V).
$V_0(k)$	Output voltage (V).
$V_{0ref}(k)$	Reference voltage (V).
V_b	Battery voltage (V).
$V_{cf}(k)$	Voltage compensation factor.
$V_{cf}(k-1)$	Voltage compensation factor in the previous instant.
V_{pv}	Photo voltaic panel voltage (V).
V_{sc}	Supercapacitor voltage (V).

List of Abbreviations

AC	Alternating Current
ANN	Artificial Neural Network
BW	Band Width
CAES	Compressed Air Energy Storage
CBLPF	Constant Band Width Low Pass Filter
CCM	Continues Conduction Mode
CPL	Constant Power Load
DBP	Droop Based Power sharing
DC	Direct Current
DPM	Deficit Power Mode
EMS	Energy Management Strategy
EPM	Excess Power Mode
ESC	Energy Storage Converter
ESS	Energy Storage System
FBP	Filter Based Power sharing
FC	Fuel Cell
FLC	Fuzzy Logic Controller
FPM	Floating Power Mode
FRSD	Fast Responsive Storage Device
HED	High Energy Density
HESS	Hybrid Energy Storage System
HPD	High Power Density
HPF	High Pass Filter

IZC	Inverted Zero Compensator
LPD	Low Power Density Devices
LPF	Low Pass Filter
MP	Maximum Peak Overshoot
MPC	Model Predictive Control
MPPT	Maximum Power Point Tracking
P&O	Perturb & Observe
PI	Proportional Integral
PM	Phase Margin
PMS	Flexible Ramp Products
PV	Photovoltaic System
RBP	Rule based Power Sharing
RES	Renewable Energy Sources
RHPZ	Right Hand Plane Zero
RL	Rate Limiter
RPG	Renewable Power Generation
SC	Supercapacitor
SISO	Single Input Single Output
SMC	Sliding Mode Controller
SMES	Superconducting Magnetic Energy Storage
SOC	State of Charge
SPM	Surplus Power Mode
VBLPF	Variable Band Width Low Pass Filter

Chapter 1
Introduction

1.1 Background

The present electric power system is continuously evolving due to the energy crisis, global climate change, and grid reliability concerns. The world energy scenario has been moving towards integrating more renewable energy sources in recent days [1]. For example, the national solar mission was launched by the Indian Government to integrate 100 GW of solar energy by 2022 [2]. The entire effort aims to lessen the environmental issues arising from conventional fuel-based power generation. Further, the conventional power system also suffers from long transmission losses, low efficiency, reliability and energy resource scarcity. As a result, it is better to transform the conventional centralized fuel-based power generation into distributed and renewable energy-based generation facilities. Furthermore, the microgrid is intended to alleviate the hassle of grid management systems and improve the grid's flexibility and reliability in line with decentralized on-site generation [3, 4].

The microgrid is an autonomous miniature unit of a power system. The microgrid can be defined as a set of loads and distributed energy sources interconnected within well-defined electrical boundaries that act as a unitary entity concerning the grid [5]. The microgrid can be connected and disconnected from the grid to operate in grid-connected and island modes. Most of the renewable energy sources, loads and power storage devices are inherently DC in nature [6]. This created more scope for research in autonomous renewable energy-based DC microgrid systems. Hexagonal representations of DC microgrid with different sources and loads are shown in Fig: 1.1. The hexagon represents the transmission system, and incoming arrows represent the source connections. The primary sources are photovoltaic plants (PV plants) and wind power generation plants. AC- grid can consider as a backup for the DC system. On the load side, industrial loads, data centres, electric vehicles (EVs), home applications and hospitals are considered separately based on the power level and application.

Figure 1.1: Structure of microgrid and applications.

1.1.1 DC microgrid components

The renewable power generation will be AC or DC, depending on the RES. The power produced by the PV panel is generally DC. At the same time, the power output from wind generation is AC. Due to different RESs nature, the power electronics like AC-DC converters and DC-DC converters are connected in between DC grid and RES [7]. The power converters are in charge of controlling and regulating the RES's power output. Standalone mode and grid-connected mode are the two operational modes of the DC microgrid. In standalone mode, the loads are powered by RES generation and HESS. The grid-connected mode supports the RES power generation from the central grid so that power variations can be limited during operation [8]. The primary components in a standalone DC microgrid are discussed below.

1.1.1.1 Distributed generators

The core energy source of the DC microgrid is distributed generators (DG) [9]. The DGs refer to electricity generation near consumer sites, including renewable energy sources

such as PV and wind turbines and micro sources such as diesel generators. Distributed generators (DG) are the primary energy source for DC microgrids. DGs have significantly risen in recent years as a natural outcome of their successes in reducing pollution, preventing energy crises, improving system performance, and enabling power system transmission, distribution, and demand [10, 11]. Based on the source's controllability, DGs are categorized as dispatchable and non-dispatchable [12]. For example, fuel cell and diesel generators are dispatchable units that may be fully controlled. On the other hand, non-dispatchable units, such as PV and wind generators, are subject to weather conditions and are not controlled [13, 14].

1.1.1.2 Energy storage devices

The ESS plays a crucial role in developing isolated DC microgrid systems by ensuring their durability, reliability, and efficiency [15]. ESS is characterized by its available energy (energy density), power (power density), cycle life, and response time [16]. The Ragone plot for different energy storage devices is shown in Fig: 1.2 to compare the maximum power capability [17]. The battery has a high energy density, allowing it to provide power for a prolonged period. However, the slow response of the battery affects the overall system performance and leads to the deterioration of battery life under sudden changes. Therefore fast responsive storage devices (FRSD) are introduced in different areas along with the battery to meet the transient requirements [18].

FRSD is characterized by its high power density and long cycle life. However, FRSD cannot be used for long term applications due to its fast discharge characteristics. A combination of battery and FRSD can enhance the system's dynamic response and improve the battery cycle life [19, 20]. The available choices for FRSD along with a battery in the hybrid energy storage system (HESS) are flywheel, superconducting magnetic energy storage (SMES) and SC [21]. Due to its size and expanses, the SMES is considered a technology in nascent stages compared to the flywheel and SC [22, 23]. The flywheel has the advantages of high power density, longer life and easy construction. However, it is cumbersome and bulky to handle. Moreover, the flywheel requires complex circuitry for energy conversion and utilization [24, 25]. The SC stands out among the above due to its small size and ease of use. As a result, a combination of battery and SC is popular in DC microgrids and is known as hybrid energy storage system (HESS).

Table 1.1: Comparative study of different ESS

S.No	Storage devices	Energy density (Wh/L)	Power density (W/L)	Response time (ms)	Cycle efficiency (%)	Life time (Years)	Self discharge (%/day)
1	LAB	50-300	10-500	3-20	70-83	5-15	0.1-0.4
2	Flywheel	20-200	5000-20000	>10	80-95	15	70-95
3	SMES	0.5-10	1000-5000	1-10	80-90	20	10-15
4	SC	5-50	5000-50000	<10	80-95	10-15	10-20

1.1.1.3 Power electronic interface and DC loads

The control and regulation of DC microgrid parameters are with the help of a power electronic converter. The PV panel connects to the DC bus through a unidirectional DC-DC boost converter [26]. The power converters used to connect the energy storage devices (ESC) to the DC bus have bidirectional capabilities. The PV control approach employs the maximum power point tracking (MPPT) technique to get as much power out of PV panels [27, 28]. In addition, the DC microgrid voltage and power balance are achieved by the control and energy management of ESC. In an ESC, the discharging occurs during boost operation, and charging is associated with buck operation of ESC. The majority of loads in a DC microgrid system follow resistive nature [29]. The loads can be directly connected to non-controlled loads or power converter based controlled loads. The pulsing DC loads are varying loads that require high transient power. The sudden variation in power generation and load demand leads to the system's instability [30, 31]. A control and management strategy is necessary to mitigate the instability problems and enhance the coordinated operation of renewable energy sources, energy storage devices, power electronic converters and DC loads [32].

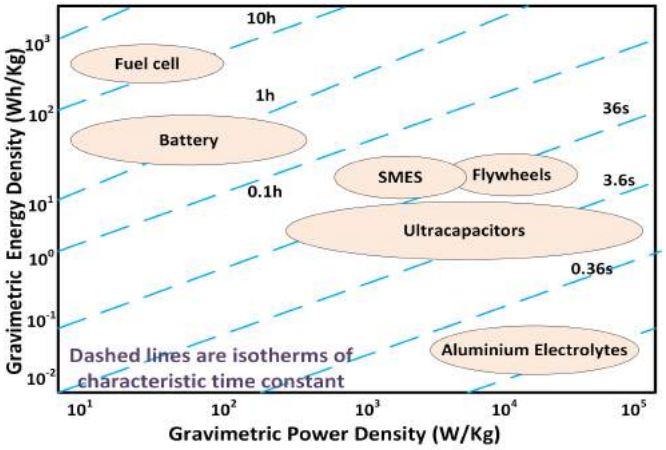

Figure 1.2: Ragone plot for different energy storage systems.

1.2 Aim for the Proposed Work

The uncertainties and associated power balance issues are the significant problems with the incorporation of renewable based power generation. In isolated DC microgrid systems, the power balance and stability are achieved by the integration of energy storage devices along with RES. Therefore, power electronics interfaces are necessary to integrate different ESS, RES, and DC loads into a common DC bus. In addition, the interfacing of RES, ESSs, power electronic converters to the DC microgrid requires control strategies to ensure DC bus voltage stabilization.

Generally, the control strategy for RES are selected to extract maximum power using MPPT algorithms. On the other hand, the battery and SC converters operate based on the load requirement. The HESS controller aims to regulate the battery current, SC current, total HESS current and DC bus voltage based on the reference for achieving power balance by absorbing/supplying the mismatch in RES generation and load demand. The primary level challenge in isolated DC microgrid systems is integrating and operating different RES, ESSs, power electronic converters and DC loads in a stable environment. Hence, the prime objective of this work is to investigate and develop fast and robust control strategies for HESS integrated isolated DC microgrid systems. The research focuses on the design and analysis of isolated DC microgrids, power converters, energy management strategy, stability analysis, simulation study and experimental validation. The other aspect of the thesis includes comparing proposed methods with conventional control strategies based on DC bus voltage regulation, power-sharing scheme, controller design complexity and computational burden.

1.3 Contributions of the Proposed Work

The major highlights of the research work done in this thesis are summarized as follows.

1. An overview of the operation, control and management of HESS in isolated DC microgrid is presented based on a detailed literature study. Different HESS combinations, power electronic configurations and control strategies for HESS in isolated DC microgrids are analyzed. The comprehensive study makes the base for the considered problems in HESS integrated isolated DC microgrids.

2. Initial stage of the thesis contributes to designing and analyzing HESS by combining the effect of LPF and battery for DC bus voltage regulation. The system is modelled using small-signal modelling, and controller parameters are designed from derived trans-

fer functions. The calculated controller parameters can track and regulate the DC bus voltage under different load disturbances.

3. An energy management strategy based on SC voltage is proposed for PV fed isolated DC microgrid to minimize the effect of SC voltage variation. The core of the energy management strategy is the power splitting stage, where a variable bandwidth-based power-sharing is utilized for effective power-sharing between battery and SC.

4. A hybrid control strategy is proposed for HESS by combining the proportional-integral (PI) controller and predictive control. The combined operation reduces the complexity in control parameter tuning and improves the dynamic performance of the DC microgrid.

5. Finally, the thesis contributes a discrete rate limiter based power-sharing scheme is for control of HESS. The rate limiter based control enables control over the charge-discharge rates of the battery and SC. Further, the proposed method can minimize the effect of SC voltage variation in DC microgrid performance.

6. The proposed methods are tested under PV irradiance variation, load variation, SC voltage variation and reference change. Further, a detailed comparison between the proposed and conventional control methods is discussed.

1.4 Thesis Organization

The research work carried out in this thesis is organized into seven different chapters and presented as follows;

The **Chapter 1** describes the background and motivation behind the study, the aim of the work, the research contributions of the work and the thesis outlines are presented.

Chapter 2 presents a comprehensive literature review of the research work in detail. The comparison of different ESSs is summarized. The possible HESS configurations for DC microgrid applications are presented, and different control and energy management strategies for HESS systems are discussed.

Chapter 3 deals with the design and analysis of conventional control of active hybrid energy storage systems. The presented design procedure incorporates the effects of battery, SC and low pass filter on the controller design. The presented method is analyzed using mathematical modelling and validated with simulation and experimental studies.

Chapter 4 proposes a detailed control and energy management strategy to mitigate the effect of SC voltage variation on DC microgrid. The chapter discusses control strategy, controller design, system parameters selection, stability analysis, experimental results and performance of the proposed control scheme over the conventional control scheme.

In **Chapter 5**, a hybrid controller is proposed for HESS integrated DC microgrid. The proposed system ensures fast DC bus voltage regulation and proper power-sharing between the battery and SC. The small-signal linear averaged model of converters are developed to design controller parameters. Finally, the simulation and experimental results are discussed for validation.

In **Chapter 6**, an advanced hybrid controller with a discrete rate limiter is presented to improve the DC microgrid performance. The controller design for HESS by using a discrete model is discussed. The performance comparisons of the proposed and conventional control methods are also presented.

Finally, **Chapter 7** highlights the brief conclusions and the significant contribution of research work and provides scope for further research in this area.

Chapter 2
Literature Review

2.1 Introduction

ESSs play a crucial role in maintaining power balance in renewable power generation and isolated power supply systems. Nowadays, the single ESS combines energy storage with complementary characteristics to get ideal storage characteristics. This section reviews the advantages of energy storage hybridization, different storage configurations for isolated DC microgrids, and HESS control and energy management strategies. The detailed study is as follows.

2.2 Hybrid Energy Storage System and Benefits

As discussed earlier, the RES based power generation is affected by intermittent nature, stability concerns, power quality issues and unpredictable load demand. These issues are mitigated/ controlled with the help of ESSs. However, using a single storage device for handling these problems leads to irregular and frequent charge/discharge cycles, which significantly reduces the life span of ESS [33, 34]. Moreover, there is no ideal energy storage with high energy density (HED) and high power density (HPD). Hence, hybridized energy storage systems are introduced to improve the performance of DC microgrids and enhance the life span of ESS. Many works have demonstrated the advantages of HESS over a single ESS [35–37].

Based on system constraints, the different combinations of ESS can be used as HESS. In general, high power-low energy density and high energy-low power density devices are combined to form the HESS. One energy storage will take care of the short power, and the other compensates for the steady-state power demand. From the Table: 1.1, the common HESS combinations can be obtained as battery/SC, battery/flywheel, battery/SMES, FC/battery,battery/CAES,FC/SC and FC/flywheel [38–41]. It is important to note that the selection of proper HESS depends on hybridization application, costs, space availability and location. Different HESS combinations are summarized in Fig: 2.1. The contribution of HESS in a DC microgrid system is summarized as follows.

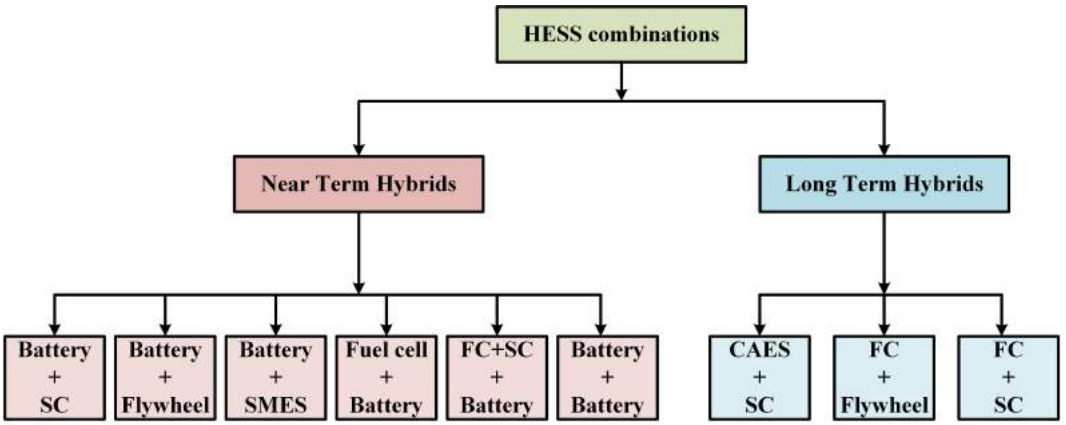

Figure 2.1: Different energy storage configurations for HESS.

2.2.1 DC bus voltage regulation

In isolated DC microgrid systems, fast and accurate DC bus voltage regulation is an important issue, especially during disturbances. In [42], battery and SC are integrated into the DC microgrid using a multi-input converter for fast DC bus voltage regulation and power balance. Furthermore, some works have been addressed to integrate the HESS for DC microgrid operation in grid-connected mode [43, 44]. In the above cases, the main objective is to minimize peak overshoot and settling time of DC bus voltage under various disturbances.

2.2.2 Storage life span improvement

The disadvantage of using single energy storage is the degradation of battery and fuel cell life expectancy when subjected to frequent power variations. Battery lifetime degradation is reduced when repeated charging and discharging are avoided [45]. The HESS structure can improve battery life by minimizing the number of charges and discharge operations involved in the battery by optimizing the battery power profile and preventing battery fluctuations [46, 47]. The authors of [48] presented a power management method for lithium batteries with SCs to extend battery life, with SCs being employed to meet high-frequency demands. It is shown that battery life has increased by 19 % in the study. Another example of hybridization for storage life extension is the FC/SC combination. The fuel consumption and power changes of an FC determine its longevity. Combining FC [49, 50] with high power density storage can extend FC life. To extend the lifespan of FCs, most researchers employed SC/FC hybridization. Using SC, the pressure oscillations and oxygen deficiency are mitigated by minimizing the frequent

charge/discharge cycles in FC [50].

2.2.3 Renewable system intermittence improvement

The ESS is introduced in the literature to mitigate the effect of sudden variation in PV and wind power [51]. The ESS supplies the mismatch in RES power generation and load demand. The use of HESS supplies both steady-state and transient power demand in wind power generation and enhances the performance compared to the use of a single ESS [52]. In wind farms, the SMES and battery are integrated to reduce the large fluctuations of renewable power generation [53, 54]. Control and power balance of wind power generation in grid connected mode using battery-SMES combination is studied using a dual-stage control approach in [53]. Based on grid power demand, the system-level control allocates energy between the battery and the SMES and wind power fluctuations are smoothed using fuzzy logic controller (FLC) with a genetic algorithm. The battery and SC used for mitigating the PV power fluctuations are presented in [55]. Based on the load demand, the battery achieves the power balance in the system. The SC compensates for the transient current demand.

2.2.4 Pulse loads support

High instantaneous power with low average power is required for pulse loads [56, 57]. Thermal and power disturbance problems might arise when a single energy source supplies pulsed loads. When a high power density storage system is integrated into the system, it can provide several benefits, including the reduction of thermal problems, low current stress, and reduction of voltage deviation [58–60]. In [61], the authors proposed the real-time control of battery/SC HESS based autonomous DC microgrid for pulse load applications. The SC Bank is utilised to support the grid and supply the pulsed load for a short period. The results show that employing this control strategy reduces generator frequency variations and enhances system performance.

On the other hand, pulsed loads substantially negatively impact the battery's service life. In [62], investigates the effect of a pulsed load on battery life. The battery life is evaluated under two conditions. The pulsed load is supplied solely by the power battery in the first example, while the pulsed load is distributed as a hybrid system by the battery and the SC in the second. Finally, the hybrid system's lifespan was greatly extended by 17.6 %.

2.2.5 Stability

Voltage stability in a microgrid is defined as the ability of all buses to maintain a steady voltage despite encountering disturbances. The power balance between source, storage and loads indicate this level of stability. The stability of the microgrid can be classified into two categories: grid-connected and islanded [63]. In microgrid applications, energy storage can be used to solve transient stability problems [64–66]. In [67], active damping based approach is presented for DC microgrid to tackle instability concerns caused by constant power loads (CPL). In this method, the energy storage has assigned additional functions, such as adjusting the damping rate of the system to address the problem of instability induced by CPL. The presented method virtually reduces the CPL and increases the resistive loads to reduce the effect of CPL. As a result, CPL's undesirable effect is minimised, and the microgrid stability is enhanced. Based on the publications studied, it is possible to infer that using energy storage devices increases the stability margin of microgrids and that using HESS improves this margin even more than traditional storage.

2.3 HESS Configuration for DC Microgrid

Different configurations are introduced for integrating HPD and LPD into the DC microgrid. The different HESS configurations are illustrated in Fig: 2.2. The system power requirements determine the selection of HESS configuration. There are three basic types of HESS configurations, which are passive HESS configuration, semi-active HESS configuration, and full-active HESS configuration [68, 69].

2.3.1 Passive HESS configuration

Passive configuration is the basic, simple, efficient, and cost-effective connection of two storage devices with the same voltage [62, 70, 71]. Figure 2.2 (a) and (b) show the passive HESS configuration. Battery and SC are directly connected in parallel. Figure 2.2 (a) is the simplest of all configurations and is cost-effective. The power distribution between HPS and HES units is mainly influenced by internal resistances and their voltage-current characteristics, as the storage's terminal voltage is not regulated. However, it lacks control over the ESS operation and requires a high rated battery and SC for high power applications. Figure 2.2 (b) can avoid high-rated ESS requirements by incorporating a DC-DC converter; still, there is no control over the battery and SC voltage. Furthermore, passive configuration demands equal voltage of battery and SC for

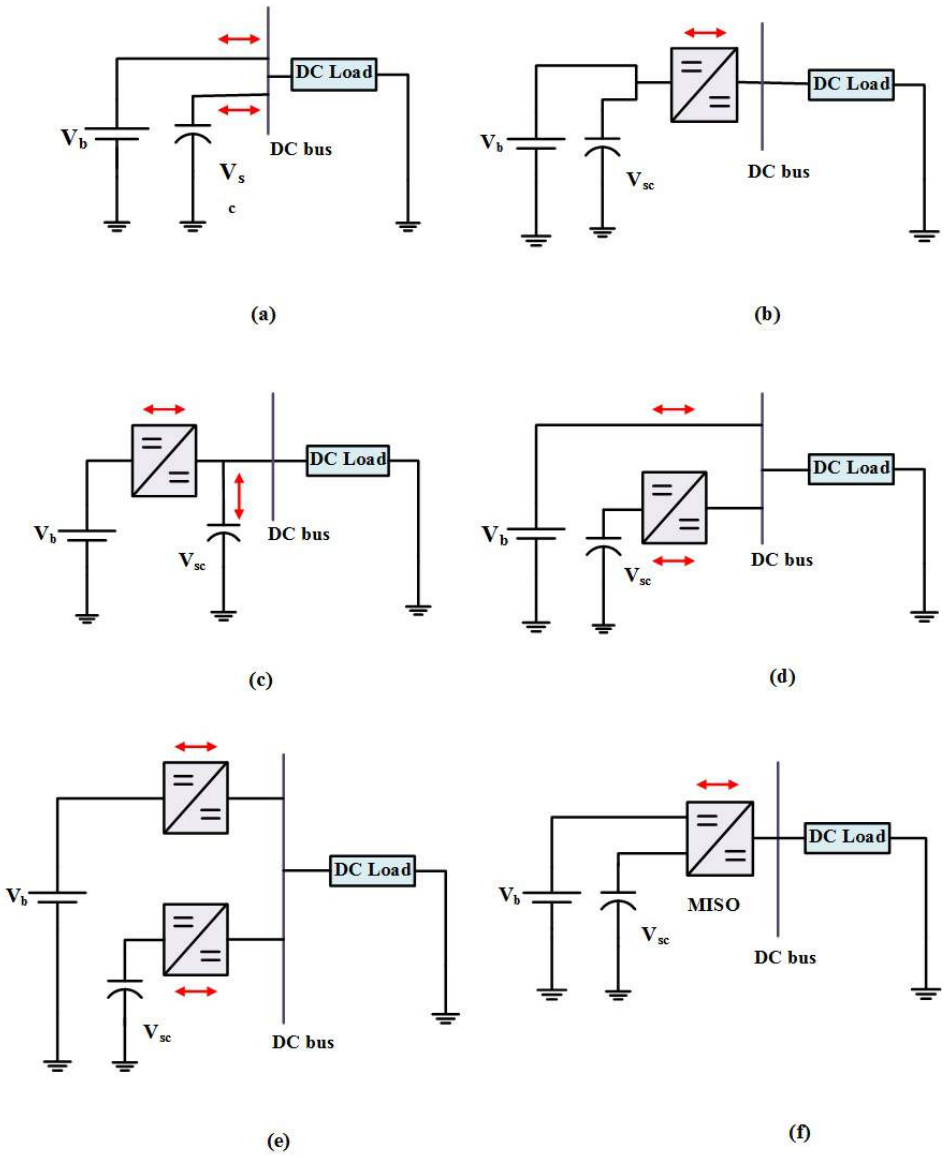

Figure 2.2: Different HESS configurations: (a) & (b) represents passive configuration, (c) & (d) represents semi-active configuration and (e) & (f) represents active HESS configuration

proper operation. As a result, the HPS has a minimal amount of energy accessible and works as a low pass filter for the HESS.

2.3.2 Semi-active HESS configuration

In the semi-active architecture, a power converter is inserted at the terminals of one storage, while the other storage is directly linked to the DC bus [72–74]. Although the addition of a converter increases installation space and costs, this topology gives better

controllability and power supply capabilities than the passive topology. Figure 2.2 (c) and (d) depicts the topologies of various semi-active HESSs. Additionally, the semi-active topology with improved converters in [75] enhances the HESS working range.

2.3.3 Full-active HESS configuration

Active HESS topologies are made up of two or more energy storage devices linked to the system via power electronic converters. Even though the system's complexity, losses, and cost rise, this topology has some advantages. This setup has the advantage of allowing active control over all storage devices. In a fully active HESS, the most frequent arrangement, sophisticated control methods can be employed [43, 44]. For example, in the parallel active hybrid architecture depicted in Fig: 2.2 (e), two converters are used to manage the power of the HPD and LPD. In various studies, multilevel converters have been used as hybrid storage power converters [76–78] as shown in Fig: 2.2 (f). System reliability and power quality can be improved by using a multilevel structure.

Meanwhile, combining numerous energy storage systems into a single converter lowers costs and simplifies coordinating control. Nevertheless, the multilevel converters include many power electronics switches and capacitors, making control challenging. Further, different multi-port converters for HESS were employed [79–81]. Each structure has advantages and limitations, but the active structure has been examined in recent years due to its great potential. When choosing a power electronic converter, different factors need to be considered such as reliability, affordability, efficiency and flexibility.

2.3.4 Comparison between HESS configurations

The HESS structure directly influences the energy management strategy. There is no direct control over the stored power in the passive topology. The output power of one of the storage devices in the semi-active architecture is uncontrollable, and the voltage should be the same as the DC bus. The active topology uses controllers to regulate the DC bus voltage with the expanse of efficiency. Costs, efficiency, controllability, complexity, and flexibility, should be considered while choosing the proper topology. Table. 2.1 compares the HESS topologies from several operating perspectives. The passive topology is simple and inexpensive, but it cannot be controlled. The active topology has the most controllability and flexibility when considering diverse restrictions, such as state of charge (SOC), but it comes at a high cost and complexity. Finally, the semi-active topology allows for limited controllability at a cheaper cost.

Table 2.1: Comparison of passive, semi- active and active HESS topologies

S.No	Topology	Cost	Flexibility	Space requirement	DC bus voltage variation	Control complexity	Applications constraints
1	Passive [62, 70]	Low	Less	Less	More	Low	For low cost and less space systems
2	Semi-active [72, 74]	Medium	Partial	Medium	High for output HPD	Medium	Extended battery life with slight increase in cost
3	Active [79, 80]	High	Full	High	Regulated	High	High dynamic performance and control with trade off in cost

2.4 HESS Control Strategies

One of the most challenging aspects of integration of HESS with DC microgrid is the control strategies. The control strategies aim to achieve fast DC bus voltage stabilization, proper power-sharing between ESSs, improved storage life span, improved power quality, and fast dynamic performance [82–84]. Selecting a suitable controller depends on the type of hybridization, steady-state and dynamic performance, simplicity in implementation and operation, controller response time and control structure. The selection and implementation of suitable HESS controllers can achieve efficient power-sharing and safe operation of HESS [85].

In addition, an energy/power management strategy (PMS/EMS) plays a vital role in deciding the operation of the HESS integrated DC microgrid. The PMS improves the power-sharing between different energy sources at different load conditions and monitor and control the charge/discharge operations of ESSs. The PMS is implemented in literature as a part of the control architecture. The inner layer focuses on DC bus voltage regulation, and the outer layer focuses on charge-discharge rates and limits of ESSs. Depending on the power-sharing scheme of HESS, the control structure and control scheme differ. The basic power-sharing schemes for HESS can be classified into four categories via i) filtration based (FBP) [43, 84], ii) droop based (DBP) [86, 87], and iii) rule-based (RBP) [88–90]. The controller requirement and power balance structure for each controller differ based on the power-sharing scheme. Thus the following section analyses the control structure and implementation of different control methods for these power-sharing schemes.

2.4.1 Control scheme for FBP

The basic active HESS control structure for FBP follows a three-layer structure, as shown in Fig: 2.3. The inner layer consists of two current controllers for battery and SC, respectively, and the outer layer consists of a voltage controller [91]. The middle layer is

the core part of HESS operation, and it generates the battery and SC reference currents based on the total reference current produced by the outer layer. Different controllers can be implemented for the FBP scheme. The core of the FBP scheme is LPF/HPF in the power-sharing stage.

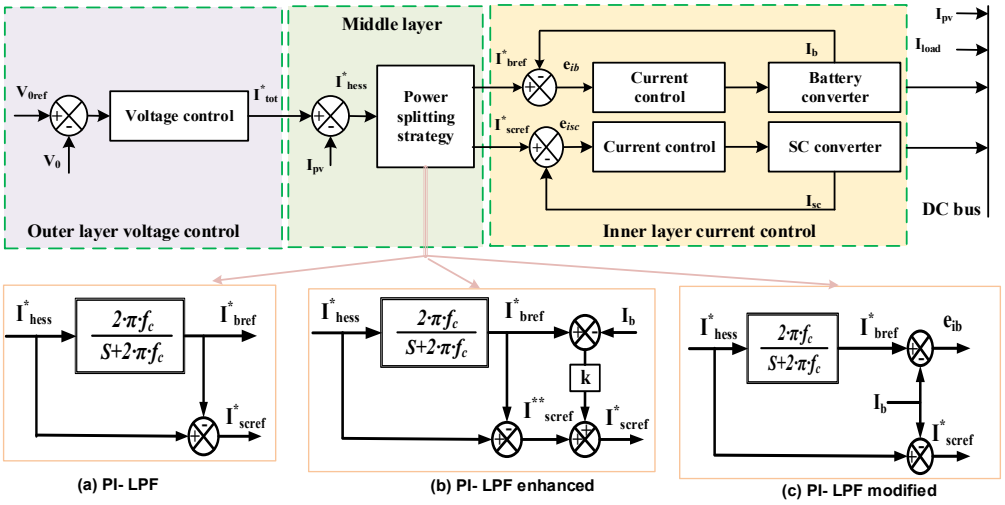

Figure 2.3: Three layer HESS control structure and different power splitting schemes; different power splitting strategies: a) conventional LPF b) enhanced LPF by adding battery error current c) modified LPF based on battery current

2.4.1.1 PI-LPF schemes

As the name suggests, the PI-LPF control scheme uses a PI controller for controlling battery current, SC current and DC bus voltage. In PI-based HESS control schemes, the PI controller regulates the DC bus voltage and HESS currents [92]. The system's performance differs in such systems by utilizing different power splitting methods and PI controller tuning. In Fig: 2.3, the outer voltage controller calculates the required reference current to regulate the DC bus voltage. This reference current is divided into SC current reference (i_{scref}) and battery reference current (i_{bref}) using a splitting algorithm. The LPF based power split strategy is the most common strategy for generating battery and SC current references. The total reference current is passed through an LPF to generate i_{bref} as shown Fig: 2.3 (a) [93]. The SC current reference is the difference between i_{bref} and the total HESS current reference. The addition of uncompensated battery current to the i_{scref} improves the performance of the traditional power splitting

strategy as illustrated in Fig: 2.3 (b) [91, 94]. It reduces the ripple current supplied by the battery and enhances SC utilization. The LPF power splitting strategy is modified to improve the battery utilization by using the battery current to generate i_{bref} and i_{scref} as shown in Fig: 2.3 (c) [95–97]. In all the above schemes, battery current is generated based on LPF. However, it adds delay to the battery reference current calculation. As a result, the SC discharges longer than required, and the battery current takes more time to reach the final state.

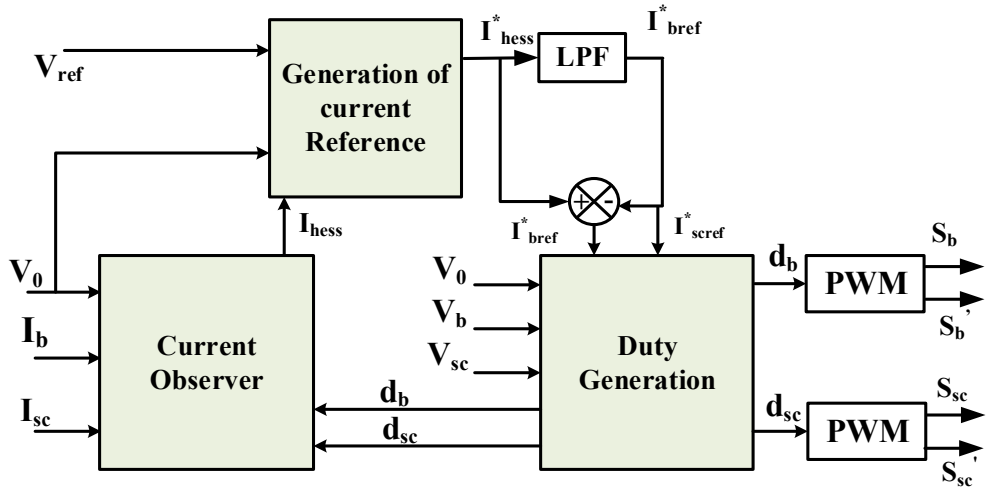

Figure 2.4: Structure of dead beat- LPF control scheme for HESS

2.4.1.2 Dead beat - LPF schemes

Deadbeat control works based on the model of the system. It generates the ratio of duty cycle to minimize error regulation in one control cycle. Thereby, it overcomes the state variable errors as well as effectively maintains the power-sharing between ESS. The additional features of the deadbeat controller are fast dynamic response and high control accuracy. Furthermore, it also acquired the features of conventional controls like simple implementation and more accessible process involvement. In [98], the authors regulated the SC to respond to transient power demand and minimized the stress on the battery to enhance its lifespan. The developed deadbeat controller is shown in Fig: 2.4. In [99], a dead beat control strategy for PV fed DC microgrid is developed. The

output current sensor is added to regulate the DC bus voltage. However, the tight DC bus voltage regulation is difficult with deadbeat control.

2.4.1.3 Hybrid control schemes with LPF

The hybrid control schemes aim to improve the HESS performance by integrating multiple control strategies with the LPF power splitting scheme. One of the recent research approach is integrating sliding mode control for HESS current control and PI control for DC bus voltage regulation [100]. Figure 2.5 shows the conventional diagram for PI-SMC control for HESS [100]. In this control, two SMC controllers regulate the battery and SC current. The use of SMC in the inner layer improves the dynamic performance of the DC microgrid by eliminating the delay caused by PI controllers [101]. Also, the number of parameters required for tuning is reduced with the utilization of inner SMC control. However, there is no proper method for selecting a sliding surface for the optimum performance of a DC microgrid. In PI-based control schemes, the gain

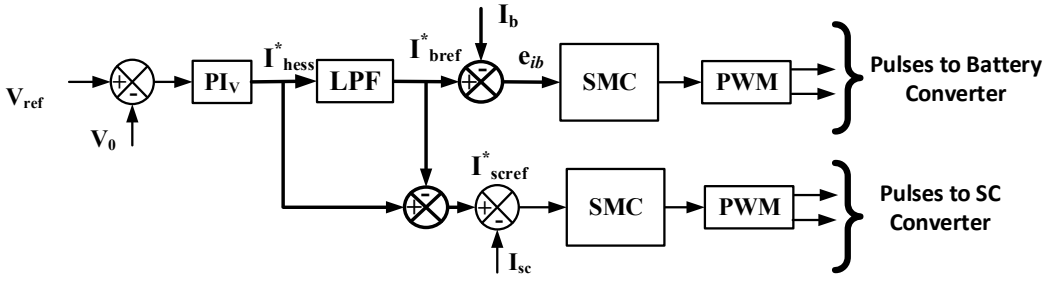

Figure 2.5: Structure of PI- SMC control scheme for HESS

added by the controller is constant in both steady-state and transient periods. The gain is compensated using an inverted zero compensator (IZC) in [102] to reduce the unwanted increment in the transient state. In this work, the battery and SC current are regulated using IZC, and the voltage control loop is regulated with the help of a PI controller. Further, the system analyses the effect of SC voltage variation in DC microgrid performance and proposes an optimization-based design procedure for DC microgrid. The proposed method reduces the initial transient at the time of starting. However, the settling time and overshot are not optimum due to the trade-off in bandwidth and phase margin during design. A PI-hysteresis control strategy is implemented in [24] for motor load applications.

2.4.2 Control scheme for DBP

The droop control methods focus on independent control of battery and SC with a suitable power-sharing in a DC microgrid. The conventional droop control is based on resistive droop [103], which is not directly applicable to HESS. In recent years, researchers developed droop control schemes for HESS in DC microgrid for decentralized control of different sources and storage devices. The major kind of droop control strategies in HESS includes: adaptive droop- based control [104], high-pass filter-based droop control, virtual capacitance droop [105], integral droop (ID) control [106], virtual resistance droop [107], adaptive droop [108], extended droop control strategy [87], virtual capacitance droop with SOC recovery [109], virtual impedance droop [110] and secondary voltage recovery droop [111]. The R-C droop is used in [105] for integrating battery and SC to the DC bus. The R-C droop control act as a filter arrangement such that the battery always gets the steady-state and SC gets the transient reference. In [86], the conventional V-P droop is used to control the battery, and the integral droop is used to regulate the SC. The droop control is extended with SOC charge recovery in virtual impedance droop control [110] and virtual capacitance droop [105]. Compared to normal HESS droop control, the SOC recovery schemes improve the storage performance along with plug "n" play capability. However, the SOC recovery with droop neglects the SC leakage current, limiting system performance. To solve this issue, the authors in [111], proposed a secondary voltage recovery scheme along with SOC recovery for droop controlled SC units in HESS. In this strategy, secondary voltage recovery is used to control the battery and SC to eliminate the effect of leakage current.

2.4.3 Control scheme for RBP

HESS power allocation is performed in RBP based on predefined rules. The state machine, thermostat, and power follower control methods are the three types of RBP schemes [21]. The RBC controller is a straightforward and simple-to-implement system for real-time energy management. Nonetheless, this method's susceptibility to parameter variations is a drawback. In thermostat based RBP, the power-sharing is defined based on the SOC level of HESS. An enhanced method is proposed in [89] to address more constraints for decision making in HESS control. Even though RBP is easy to implement, the parameter dependency limits its implementation.

2.4.4 Intelligent control strategies

Advanced control strategies are introduced to address the complex and nonlinear nature of HESS in literature. The main intelligent control strategies include fuzzy logic control (FLC) [112, 113], artificial neural network (ANN) [114] and model predictive control (MPC) [115]. Due to its simplicity and not requiring an accurate model, the FLC methods are gaining popularity for controlling complex systems. The FLC has been extended for controlling HESS in [116].

The HESS and DC microgrid control are discussed in [113]. The energy storage is managed using FLC. The sudden fluctuations in power demand are diverted to SC using an LPF. A PI controller is used to calculate the energy storage reference currents to regulate the DC bus voltage at the reference. The primary purpose of FLC is to regulate the power of storage devices while keeping the charging and discharging of battery and SC within acceptable limits. In [117], an adaptive FLC- EMS is proposed to meet the power-sharing between the battery and SC. The main objectives of this technique are to improve system efficiency, reduce the battery current variation and improve the SC SOC. However, one key disadvantage of fuzzy logic control systems is that they rely entirely on human abilities and understanding, and fuzzy logic rules must be changed frequently. ANN techniques do not require an exact system model, and their pattern recognition skills make them appealing for RPG and microgrid applications. Earlier, the central focus of ANNs studies is predicting solar irradiation and wind velocity, and few works have focused on the integration of HESS using ANN. However, the tuning and learning processes for ANN-based control approaches require historical data, making implementation complex. An ANN-based control system for grid-connected hybrid ac/dc microgrid with PV modules, a wind turbine generator, a solid oxide fuel cell, and a battery energy storage system are studied in [118]. In this method, the maximum power is extracted from RESs, and power flow is regulated between the primary grid and microgrid. The MPC for DC microgrid can be implemented for HESS power allocation and current reference calculation by considering different constraints [119, 120] or for controlling the power converters by regulating duty signal [121]. Furthermore, a mixture of the two approaches indicated can be used. The MPC control is utilized for power-sharing in a microgrid containing FC/batteries/SC in [120]. In addition, energy storage degradation associated with starting, shutdown, and load fluctuations is researched. The MPC controller block diagram is depicted in Fig: 2.6. A hybrid controller combining damping and MPC presented in [122] improves the system performance compared to

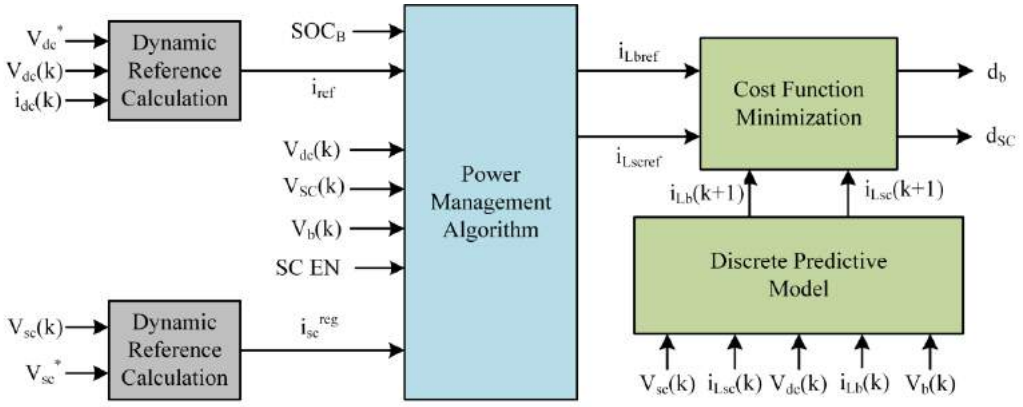

Figure 2.6: Structure of MPC control scheme for HESS

the traditional PI method, and the rate limiter-based controller helps eliminate system delays. However, it requires complex modelling and optimization to control the DC microgrid.

2.5 HESS Power/Energy Management Strategies

The EMS is used to improve HESS performance in both grid-connected and islanded modes of operation. The EMS should keep the power supply stable, reliable, resilient, and good quality in the microgrid. Even during variable RESs generation, the load demand should be met. It should keep the HESS in a safe working range while also extending its operational time. Considering the economic characteristics of the various ESSs, the EMS should give a cost-effective solution to the system. Therefore, the EMS for HESS in the microgrid is separated into two categories based on the mode of operation of the HESS: i) EMS for freestanding HESS operation in DC microgrids and (ii) EMS for grid-connected HESS operation. The following sub-sections explain the EMS for the standalone and grid-connected modes of operation of HESS.

The EMS is separated into two sub-controls: i) primary level control and ii) secondary level control [123]. Secondary level control generates the current sources that keep the RESs and ESSs in power balance. To achieve power balance in the microgrid, the primary level control adjusts the current references generated by the secondary level control. On the performance of the primary level control, the dynamic reaction of ESSs to load and generation variations. Therefore, the primary level of control is crucial to the system's stability. As shown in Section 2.4, the primary level control can be PI-

based control, MPC, or SMC. The algorithms that generate the optimal power references for various units in the system make up the secondary level control in the EMS. The secondary level control considers a variety of system data, including generation forecast, load prediction, SOC estimation, and HESS cost, to offer an ideal current reference. This increases the total microgrid's usage ratio and efficiency [43].

The EMS for the standalone mode of operation of HESS in the DC microgrid has mainly three goals: i) improving HESS performance, (ii) system dependability, and (iii) economic feasibility. Increasing HESS efficiency, boosting power quality, and maintaining microgrid stability are part of the performance optimization process. The microgrid reliability includes extending the lifespan of the ESS, keeping the HESS SOCs in a safe operating region, and protecting the HESS. The cost-effective operation of HESS and scheduling generation and load demand are all part of the economic feasibility [124]. The secondary level control EMS algorithms include deterministic rule-based strategy [125], FLC [126], dynamic programming, genetic algorithms [127], supervised machine learning approach, and particle swarm optimization [128, 129]. The EMS algorithms are selected based on the system requirements and the computational capability of the control units.

The EMS for grid-connected operation can be separated into primary level control and secondary level control, same as the EMS for freestanding HESS operation. The primary level controls in grid-connected mode are RESs control, HESS control, and inverter control [44]. Depending on the system restrictions, the secondary level control generates power references for various units in the system. Depending on grid availability, the EMS also assists the system in switching between grid-connected and freestanding modes.

2.6 Summary

The ESSs are an essential component of the DC microgrid. The intermittent nature of RES and load power balance can be achieved with the help of ESSs. The most commonly used ESDs for DC microgrid is battery considering its less size, cost and high energy density. However, its low power density characteristics increase stress during transient and disturbance periods. Hence, it is essential to incorporate fast responsive devices with the battery to improve the battery life cycle and system performance.

Furthermore, among different HESS configurations, the active configuration provides better control over other energy storage systems. In DC microgrids, different control

strategies are proposed for HESS to improve the power sharing between battery and SC and to regulate the DC bus voltage. Further, EMS are incorporated with DC microgrid to maintain the power balance and control the energy storage devices on the verge of limits. In short, the literature on HESS base DC microgrids mainly focuses on configuration, control strategies and EMS for reliable operation.

Chapter 3
Modelling and Analysis of Fully-Active Hybrid Energy Storage System

3.1 Introduction

In the contest of control and regulation of current and voltage of HESS, the active configuration provides an attractive solution. The conventional control strategy for follows a three-layer control structure that includes inner current regulation, outer voltage regulation and power splitting stage. The LPF based power splitting method is the typical strategy to share the power between the battery and SC. The HESS controller consists of two current controllers for controlling battery current and SC current and a voltage controller for regulating DC bus voltage. The quick regulation of DC bus voltage and current depends on the rapidity of operation of each control loop and the delay imposed by LPF. As discussed in chapter 2, the conventional method considers only the SC characteristics for designing the outer voltage controller, which leads to errors in the calculated parameters.

It is important to note that the controller design is approximated by discarding the battery current loop to reduce complexity. Therefore, when both converters are designed for the same power level, the effect of both converters can be presumed to be the same. However, in most applications, the rated SC voltage is selected more than rated battery voltage to provide better utilization of SC [32]. Thus, it is essential to analyze the performance of HESS by considering both the battery and SC characteristics and the LPF effect. This chapter investigates controller design based on accurate modelling of HESS by factoring in battery converter and SC converter characteristics and the low pass filter effect.

The rest of the chapter is structured as follows. Section 3.2 discuss the HESS- system configuration and modelling. Section 3.3 explains the control strategy and design. Section 3.4 reports the simulation study and results. Section 3.5 deals with hardware implementation and the results, while section 3.6 presents the summary.

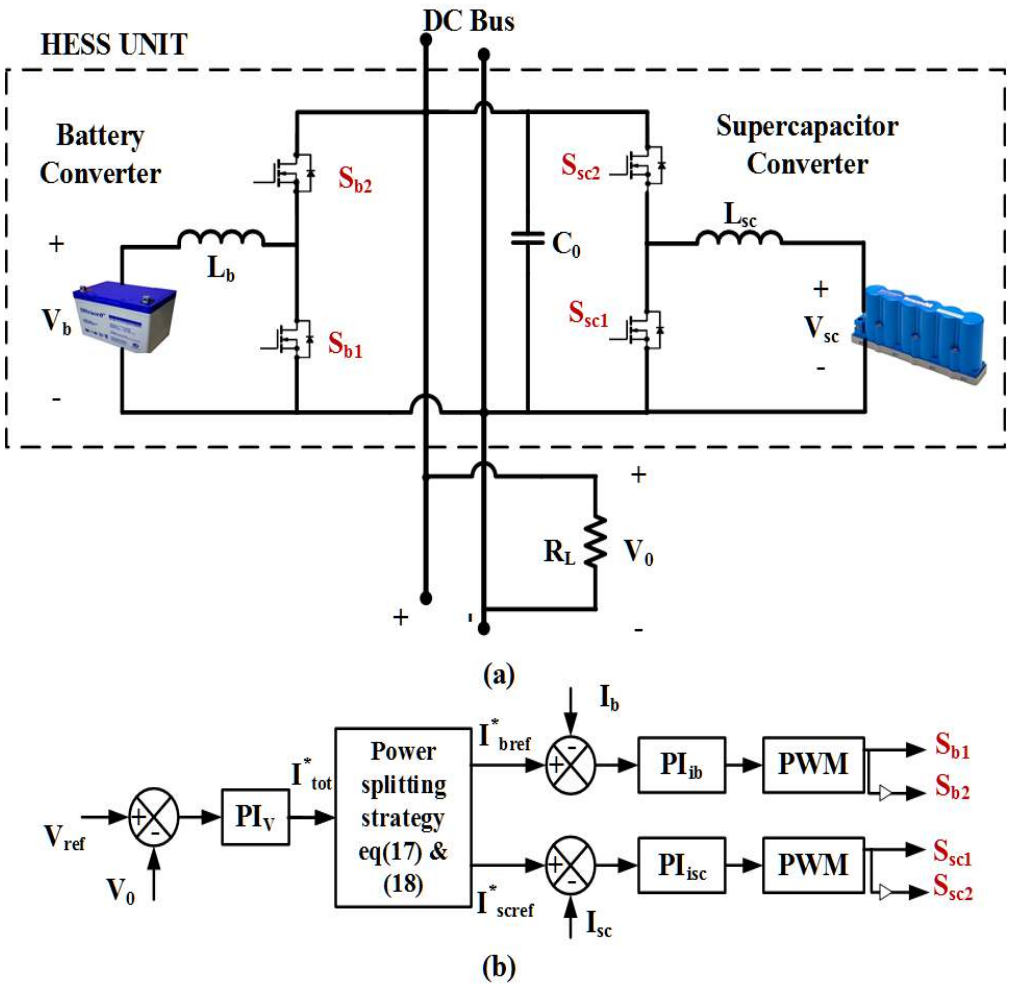

Figure 3.1: HESS: a) active battery- SC configuration b) controller connection of HESS

3.2 HESS- System Configuration and Modelling

In the active configuration of HESS, the storage devices are connected to the DC bus through bidirectional DC-DC converters as shown in Fig: 3.1 (a) [22]. The load represents the DC bus. Battery and SC are connected to the DC bus through a DC-DC boost converter. The diode is replaced with MOSFET switches to achieve bidirectional property for boost converters. Battery converter control is placed so that it is switched on to supply steady-state power. The SC converter is switched to supply transient power. Whenever a change occurs in the DC bus, SC acts faster than the battery so that the stress on the battery is reduced. As a result, the power at the DC bus is maintained constant, and the disturbance is mitigated as fast as possible.

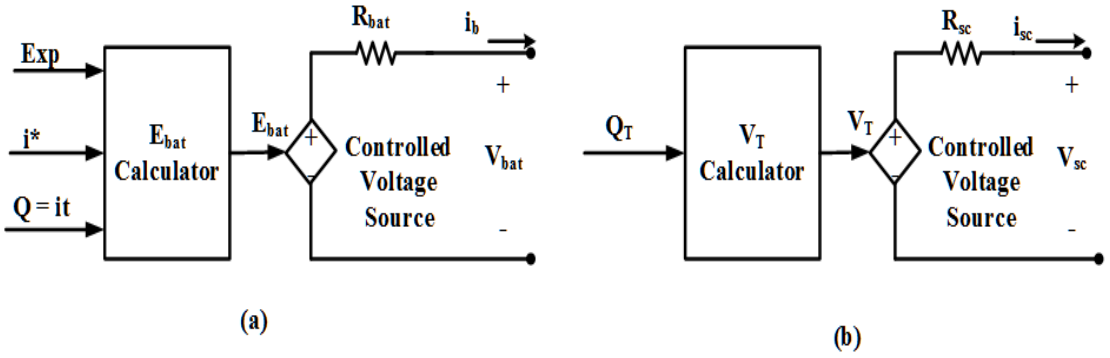

Figure 3.2: Mathematical model of a) lead acid battery b) supercapacitor

3.2.1 Battery energy storage system

The battery plays an important role in the operation of HESS as it provides continuous power to the DC bus. The mathematical model of lead-acid battery is adopted from Mathworks as shown in Fig: 3.2 (a) [130, 131]. Battery operation depends on the SOC of the battery, and the SOC variation of the battery is much slower as compared to SC. For the safety of the energy storage system, SOC is kept in the range of $20\% < \text{SOC} < 80\%$. The battery model are given in equations (3.1), (3.2), (3.3).

$$E_{bat} = E_0 - K\frac{Q}{i_b t - 0.1 \cdot Q}(i_b t + i_b^*) + Exp(t) \tag{3.1}$$

$$V_{bat} = E_{bat} - i_b R_{bat} \tag{3.2}$$

$$\dot{Exp}(t) = B \cdot |i(t)| \cdot (-Exp(t) + A \cdot u(t)) \tag{3.3}$$

Where i_b= battery current (A), i_b^*= filtered battery current (A), Exp is the exponential zone voltage of battery (V), and Q = battery capacity (Ah), R_{bat}= battery internal resistance (Ω), A= exponential voltage (V), B= exponential capacity (Ah^{-1}) and $i_b t$= actual battery charge.

3.2.2 Supercapacitor energy storage system

The SC is considered the connecting bridge between the normal capacitor and batteries. The fast-responding nature with a capacitance of a few hundred farads makes SC suitable for transient applications. The SC model available on Mathworks [132, 133] is used for SC analysis. The SC mathematical model combines the Helmholtz model and the Gouy-Chapman model. SC internal voltage and SOC are given by equations (3.4), (3.5) and (3.6).

The maximum energy stored in SC is given by:

$$E_{sc,max} = \frac{1}{2} C_{sc} V_{sc,max}^2 \tag{3.4}$$

The energy stored by the SC at any instant, $E_{sc}(t)$ is given by:

$$E_{sc}(t) = \frac{1}{2} C_{sc} V_{sc}^2(t) \tag{3.5}$$

The energy and SOC of SC are related to as follows:

$$SOC_{sc} = \frac{E_{sc}(t)}{E_{sc,max}} \tag{3.6}$$

Hence the SOC of SC shows the variation of energy from time to time. Hence SOC is given in terms of charge is shown in equation (3.7) [132]:

$$SOC_{sc} = \frac{Q_{int} - \int_0^t i(\tau) d\tau}{Q_T} \tag{3.7}$$

SC mathematical model is derived from these equations and is shown in Fig: 3.2(b). Where Q_T and V_T are the total internal charge (Coulomb) and voltage (V) of SC and is given by equations (3.8) and (3.9) respectively.

$$Q_T = \int i_{sc}(t) dt \tag{3.8}$$

$$V_T = \frac{N_s Q_T d}{N_p N_e \varepsilon \varepsilon_0 A_r} + \frac{2 N_e N_s RT}{F} sinh^{-1} \frac{Q_T}{N_p N_e^2 A_r \sqrt{8RT \varepsilon \varepsilon_0 c}} \tag{3.9}$$

where, ε= permittivity of electrolyte material (Farad/m), ε_0= permittivity of free space (Farad/m), N_s= number of SC connected in series, N_p= number of SC connected in parallel, N_e= number of electrode layers, R= ideal gas constant, T= operating temperature, c= molar concentration (mol/m^3), Q_T= total charge of SC unit, d= thickness of Helmholtz layer (m) and i_{sc}= SC current.

3.2.3 Energy storage converter system

The HESS system consists of two boost converters, as mentioned earlier. Both converters possess bi-directional properties. Though the design focuses on the boost capability because of right hand zero in the boost converter, it operates in continuous conduction mode (CCM). For the design of converters, inductor ripple current is taken as 5 %, and

capacitor voltage ripple is considered 2 %. The system is designed for 72 W. The voltage across inductor and current through capacitor are given by equations (3.10) and (3.11).

$$L\frac{di_L(t)}{dt}=V_s \tag{3.10}$$

$$C\frac{dv_0(t)}{dt}=\frac{-V_0}{R_L} \tag{3.11}$$

3.2.3.1 Battery converter design

The battery boost converter aims to supply steady-state power to the DC bus. Hence the converter is designed to deliver maximum load power. A 12 V, 7 Ah, lead-acid battery is considered for this application. The advantage of a lead-acid battery is that the voltage drop during discharging is very less. Therefore the converter is designed for a rated 12 V of battery. The converter parameters are derived using equations (3.12) and (3.13) and are derived from equations (3.10) and (3.11).

$$L_b = \frac{V_0 D_b}{\Delta i_{Lb} f_{sw}} \tag{3.12}$$

Where f_{sw} is the switching frequency and D_b represents the battery converter duty ratio. Similarly the output capacitor filter can be obtained by the equation below:

$$C_{0b} = \frac{V_0 D_b}{\Delta v_0 R_L f_{sw}} \tag{3.13}$$

V_0 and Δv_0 are the output voltage and allowable output voltage ripple.

3.2.3.2 Supercapacitor converter design

The design of the SC bidirectional DC-DC converter is similar to the design of the battery converter. However, the design specifications are different. Considering the previous literature, the converter is designed for maximum SC voltage. This method gives a good response at high SC voltage since 75 % of energy stored in a capacitor is available above 50 % of SC voltage. The converter design equations are given by:

$$L_{sc}=\frac{V_0 D_{sc}}{\Delta i_{Lsc} f_{sw}} \tag{3.14}$$

Table 3.1: System parameters for simulation and hardware implementation

S.no	Parameters	Values
1	Battery input voltage, V_b	12 V
2	SC input voltage, V_{sc}	16 V
3	Load resistance, R_L	8 Ω
4	Battery boost converter inductance, L_b	2 mH
5	SC boost converter inductance, L_{sc}	1.80 mH
6	Total output capacitance, $C_0 = C_{0sc} + C_{0b}$	250μ F
7	Output power, P_{out}	72 W
8	Switching frequency, f_{sw}	20 kHz
9	Output voltage, V_0	24 V
10	Nominal power	30 W

$$C_{0sc} = \frac{V_0 D_{sc}}{\Delta v_0 R_L f_{sw}} \tag{3.15}$$

The design values are given in Table: 3.1. The C_0 combines the total effect of both battery output capacitor C_{0b} and SC output capacitor C_{0sc}.

3.3 Control Strategy and Controller Design

The control strategy for HESS focuses mainly on power-sharing between the battery and the SC. The accurate tuning of control parameters decides the operation ranges of the system. This section presents the control strategy, modelling and design of an accurate HESS system and controller tuning. The first step toward the controller design is the small signal modelling (SSM) of the converter system. Based on SSM, the controller is designed by combining the action of both battery and SC converter.

3.3.1 Control strategy

The LPF plays an important role in power-sharing in HESS. The current reference generation with respect to LPF is shown in Fig: 3.3. In the LPF control strategy, the LPF splits the total current reference into high frequency and average components. The cut-off frequency of LPF is selected as 31 rad/sec to reduce system delay [102]. Here *'f_c'*

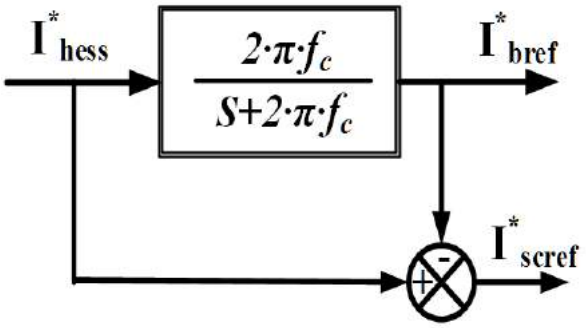

Figure 3.3: LPF based power splitting strategy for HESS

represents the LPF cutoff frequency and relevant equations are given in equations (3.16), (3.17) and (3.18).

$$LPF = \frac{2 \cdot \pi \cdot f_c}{s + 2 \cdot \pi \cdot f_c} \tag{3.16}$$

If the total current in the system is I_{tot}, then reference current for battery and SC is given by

$$I_{Lb,ref} = I_{tot} \cdot \frac{2 \cdot \pi \cdot f_c}{s + 2 \cdot \pi \cdot f_c} \tag{3.17}$$

$$I_{sc,ref} = I_{tot} \cdot (1 - \frac{2 \cdot \pi \cdot f_c}{s + 2 \cdot \pi \cdot f_c}) \tag{3.18}$$

3.3.2 Small signal modeling of boost converters

The first step toward the controller design is the small signal analysis of the converters. The controller parameters are designed using MATLAB/SISO tool with the help of transfer functions derived from small signal analysis. The equations averaged for inductor voltage and current through the capacitor in the boost converter over one switching period are given by equations (3.19) and (3.20).

$$L_x \frac{di_{Lx}(t)}{dt} = v_x - (1 - d_x) v_{cx} \tag{3.19}$$

$$C_{0x} \frac{dv_{cx}(t)}{dt} = (1 - d_x) i_{Lx} - \frac{v_{cx}}{R_L} \tag{3.20}$$

Based on the inductor and capacitor equations, state space model obtained as

$$\begin{bmatrix} \dot{i_L} \\ \dot{v_c} \end{bmatrix} = \begin{bmatrix} 0 & \frac{-(1-d)}{L} \\ \frac{1-d}{C} & \frac{-1}{RC} \end{bmatrix} \begin{bmatrix} i_L \\ v_c \end{bmatrix} + \begin{bmatrix} \frac{1}{L} \\ 0 \end{bmatrix} v_s \tag{3.21}$$

where v_c and v_s represent the instantaneous values of the output capacitor and source voltage. v_s represents either battery or SC voltage depending on controller design. d represents the duty ratio. The output is given in equation (3.22). Since there is no direct feed-forward path, the transition matrix D value will be zero.

$$\begin{bmatrix} i_s \\ v_0 \end{bmatrix} = \begin{bmatrix} 1 & 0 \\ 0 & 1 \end{bmatrix} \begin{bmatrix} i_L \\ v_c \end{bmatrix} + DV_s \tag{3.22}$$

Introducing perturbations to the above equations by replacing $v_c = V_c + \hat{v_c}$, $v_s = V_s + \hat{v_s}$, $i_L = I_L + \hat{i_L}$ and $d = D + \hat{d}$. After perturbation, derivatives of the steady state values of I_L and V_c in state space representation become zero. The resulting small signal equations are:

$$\begin{bmatrix} \dot{\hat{i}}_L \\ \dot{\hat{v}}_c \end{bmatrix} = \begin{bmatrix} 0 & \frac{-(1-D)}{L} \\ \frac{1-D}{C} & \frac{-1}{RC} \end{bmatrix} \begin{bmatrix} \hat{i}_L \\ \hat{v}_c \end{bmatrix} + \begin{bmatrix} \frac{V_c}{L} \\ \frac{-I_L}{C} \end{bmatrix} \hat{d} + \begin{bmatrix} \frac{1}{L} \\ 0 \end{bmatrix} \hat{v_s} \tag{3.23}$$

Based on the equation (3.23), different transfer functions for the converter are derived as follows.

The voltage control transfer functions is:

$$G_{vdx} = \frac{\hat{v}_{0x}(s)}{\hat{d}_x(s)} = \frac{(1-D_x)V_0 - L_x I_{Lx} s}{L_x C_{0x} s^2 + \frac{L_x}{R_L} s + (1-D_x)^2} \tag{3.24}$$

The current control transfer function is calculated as:

$$G_{idx} = \frac{\hat{i}_{Lx}(s)}{\hat{d}_x(s)} = \frac{C_{0x} V_0 s + 2(1-D_x) I_{Lx}}{L_x C_{0x} s^2 + \frac{L_x}{R_L} s + (1-D_x)^2} \tag{3.25}$$

From equation (3.24) and (3.25), output transfer impedance for the converter can be derived and is represented in equation (3.26).

$$G_{vix} = \frac{\hat{v}_0(s)}{\hat{i}_{Lx}(s)} = \frac{(1-D_x)V_0 - L_x I_{Lx} s}{C_{0x} V_0 s + 2(1-D_x) I_{Lx}} \tag{3.26}$$

Where, 'x' indicates 'sc' or 'b' based on converter.

3.3.3 Analysis of accurate design of control system

Based on the SSM, the controller block diagram designed for the purpose is shown in Fig: 3.4. The controller design requires an accurate model of the HESS system as

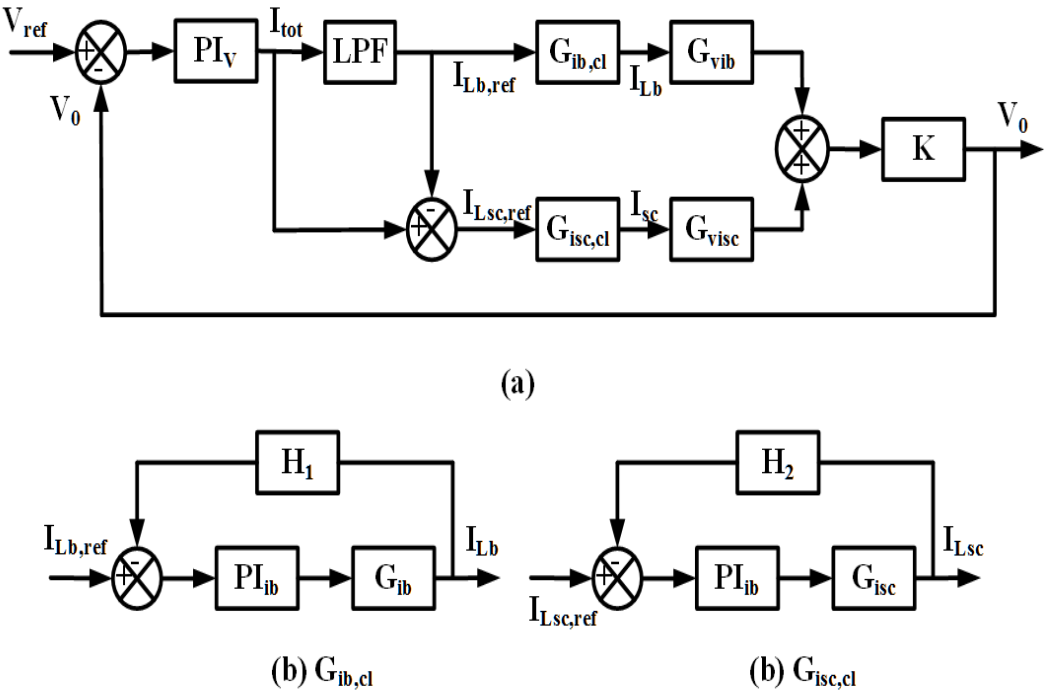

Figure 3.4: Accurate SSM of a) overall system, b) inner battery current loop c) inner SC current loop

the system performance depends on both converter parameters. First, we design the inner current control loop by considering the slow dynamics of the battery and the fast dynamics of SC. Then the voltage control loop is designed to maintain the DC bus voltage constant. Finally, all PI values are tuned with the help of the MATLAB/SISO toolbox.

3.3.3.1 Battery inner current control loop design

The control diagram of the battery inner current loop, $G_{ib,cl}$ is shown in Fig: 3.4 (b). G_{ib} represents the duty to current transfer function and $G_{ib,cl}$ is the overall closed current loop transfer function of battery. H_1= 1 since the system is designed for unity feedback control. As said earlier, the bandwidth of the inner current loop is always made higher than the outer voltage control loop to eliminate switching ripple. The battery current control loop is designed for a lower bandwidth of $\frac{2 \cdot \pi \cdot f_{sw}}{12}$ to prevent the battery from responding to transient currents.

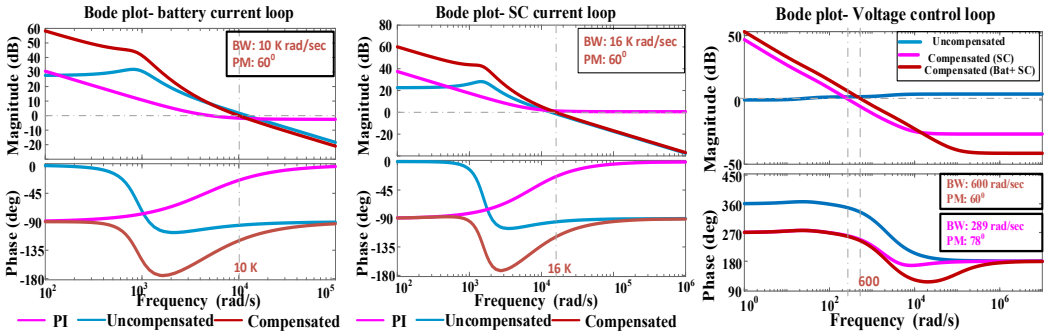

Figure 3.5: Bode plot for different control loops a) SC current loop b) battery current loop c) outer voltage loop

The loop gain of battery current control loop is given by

$$G_{idbl} = PI_{ib} \cdot G_{idb} \cdot H_1 \tag{3.27}$$

and the closed loop current control loop transfer function is

$$G_{idb,cl} = \frac{PI_{ib} \cdot G_{idb}}{1 + (PI_{ib} \cdot G_{idb} \cdot H_1)} \tag{3.28}$$

The PI compensator that regulates the battery current is given by:

$$PI_{ib} = K_{pib} + \frac{K_{iib}}{s} \tag{3.29}$$

K_{pib} and K_{iib} are the proportional and integral gains to regulate battery current. The PI values are tuned for a gain margin of 10 dB and PM of 60^0 [91]. The bode diagram of the corresponding compensated system is shown in Fig: 3.5 (a).

3.3.3.2 Supercapacitor inner current control loop design

The SC current control loop aims to control the charging and discharge of SC current. H_2= 1 since the system is a unity feedback system. It is very pertinent to conclude that the selection of BW decides the operation of SC. The BW is selected higher than the battery current control loop and is less than f_{sw}. The selected BW is $\frac{2 \cdot \pi \cdot f_{sw}}{8}$ with PM of

60^0. The loop gain of SC current control loop is given by:

$$G_{idscl} = PI_{isc} \cdot G_{idsc} \cdot H_2 \tag{3.30}$$

The closed loop current control loop transfer function is:

$$G_{idsc,cl} = \frac{PI_{isc} \cdot G_{idsc}}{1 + (PI_{isc} \cdot G_{idsc} \cdot H_2)} \tag{3.31}$$

The controller for SC current loop is given by:

$$PI_{isc} = K_{pisc} + \frac{K_{iisc}}{s} \tag{3.32}$$

The K_{pisc} and K_{iisc} are the proportional and integral gains of SC current control. The calculated PI_{isc} gains are given in Table: 3.2. It is seen that the fast nature of the SC current loop is reflected in the PI values of the SC current loop since K_{iisc} is much higher than that of battery current loop K_{iib}. The Bode diagram of the corresponding compensated system is shown in Fig: 3.5 (b).

Table 3.2: PI controller parameters and comparison with approximate and accurate model

S.No	Control loop	PI values	PM and BW
1	Inner battery current loop	K_{pib}= 0.744 K_{iib}= 2673	BW= 10K rad/sec PM= 60^0
2	Inner SC control loop	K_pisc= 1.069 K_isc= 7464	BW= 16K rad/sec PM= 60^0
3	Outer voltage loop (Approximate model)	K_{pv}= 0.028 K_{iv}= 220	BW= 289 rad/sec PM= 78^0
4	Outer voltage loop (Accurate model)	K_{pv}= 0.005 K_{iv}= 449.6	BW= 600 rad/sec PM= 60^0

3.3.3.3 Outer voltage control loop design

In the analysis of HESS, the outer voltage control loop require utmost care. This is because the boost converter's right half plane zero (RHPZ) effect can add an initial boost to the system and may lead to instability at starting. Hence, unlike the previous works,

the performance of both converters is considered for the design of the outer voltage control loop. Firstly, the PM and BW for the outer loop cannot be increased simultaneously. Hence the BW is limited to obtaining adequate stability. For the design of the outer voltage controller, the inner current loop gain is considered as unity [87]. The overall loop transfer function for the combined system obtained from accurate modelling is given by G_{all},

$$G_{all} = PI_v \cdot \left(LPF \cdot G_{vib} + (1 - LPF) \cdot G_{visc}\right) \cdot K \tag{3.33}$$

Where K represents the voltage gain of the combined system, and K= 1/2. The total transfer function G_{all} is equal to $PI_v \cdot G_{visc}$ when $G_{vib} = G_{visc}$. This condition is satisfied only when the voltage rating of SC and battery are equal. However, the battery and SC are rated with different voltage ranges in most applications. This affects the overall transfer function obtained and affects the controller parameters.
The outer voltage controller is given by:

$$PI_v = K_{pv} + \frac{K_{iv}}{s} \tag{3.34}$$

In Fig: 3.5 (c), the blue line shows the uncompensated system, and the red line shows the proposed accurate model-based design with PM of 60^0 and BW of 600 rad/sec. The pink line represents the bode plot for PI values with the conventional method acting on the combined system. It is clear that for the combined system, the speed of the loop is reduced considerably when applying the PI values obtained from SC voltage loop alone. The PI values and comparison are shown in Table: 3.2. The voltage control loop values show the variation in parameters due to modelling. It is clear from the PI values that the accurate model is faster than the approximate model. Further from the bode diagram, the accurate model ensures high gain at low frequencies and low gain at switching frequencies, necessary in stability considerations.

3.4 Simulation Results

To verify the control and operation of the battery- SC HESS, simulations were conducted in Matlab/Simulink. The simulation parameters are shown in Table: 3.1. During simulation, SOC limits of the battery and SC were calculated and found to be under the limits. The main aim of HESS is to reduce the stress on the battery and improve system performance. Hence the simulation mainly focuses on the operation of SC to support battery and load performance. To verify the HESS operation, different load disturbances were applied. The detailed study is discussed as follows:

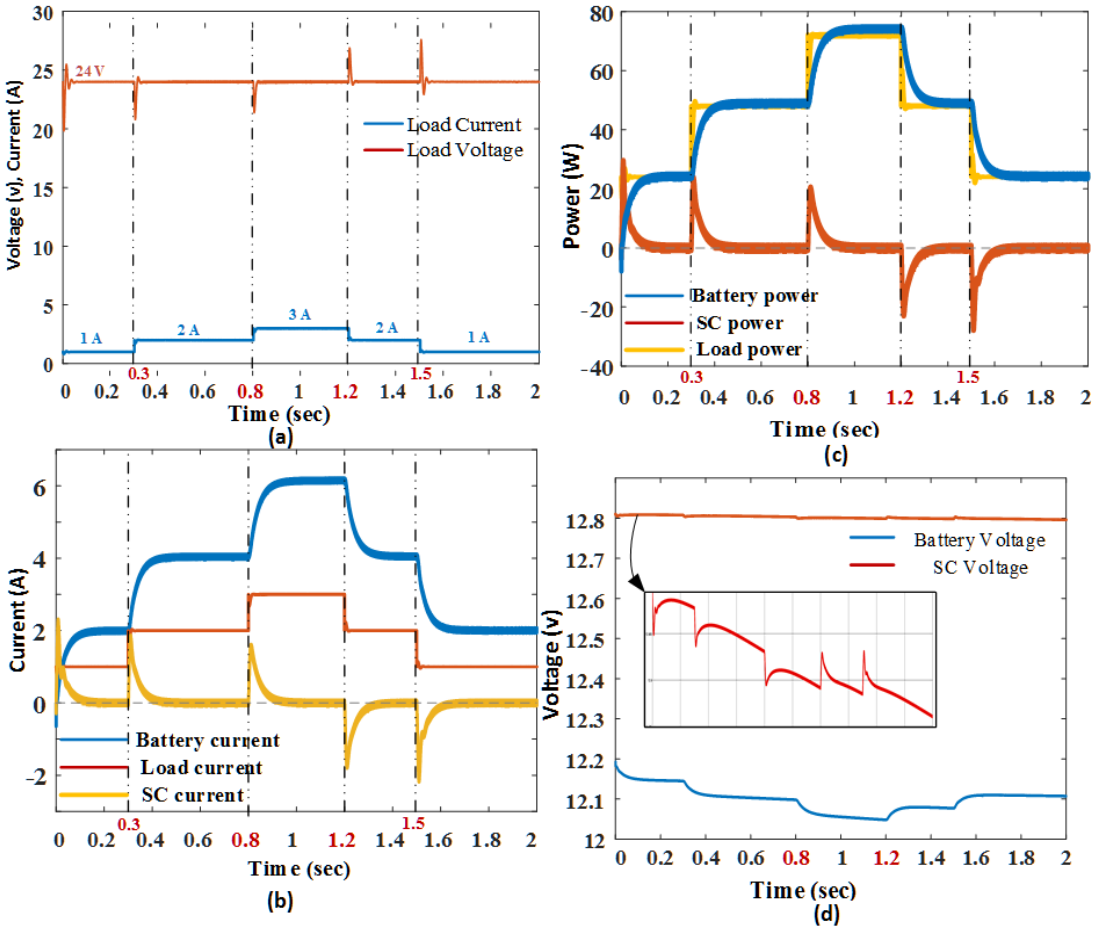

Figure 3.6: Dynamic performance of system during sudden change in load; (a) load voltage and current (b) battery current, SC current and load current (c) DC power, load power and SC power (d) battery voltage and SC voltage.

3.4.1 Performance of system under load change

The HESS is characterized by a fast response to any change in the system. Hence the best way to test HESS is through the load disturbances. Load changes are introduced by adding additional loads to the system to test the system. The load current is increased in steps of 1 A up to 3 A and then reduced in steps of 1 A. The system maintained the DC bus voltage at 24 V, and the load current varies accordingly, as shown in Fig: 3.6 (a). At the time of load increment, battery current increases slowly, and SC discharges to meet the initial transient current.

Further, it is relevant to note that the load current settles faster than the battery current. When the load decreases at t= 1.2 sec and t= 1.5 sec, the SC charges and makes the

battery change the states slowly. The total load current supplied by the battery and SC is shown in Fig: 3.6 (b). The SC supplies current at the transient period, and the average current is zero for steady-state operation. The load power and power delivered by HESS are shown in Fig: 3.6 (c). The variation of SC voltage is also significantly less, which shows that it can supply transient power for extended period. The corresponding voltage waveforms of ESS are shown in Fig: 3.6 (d).

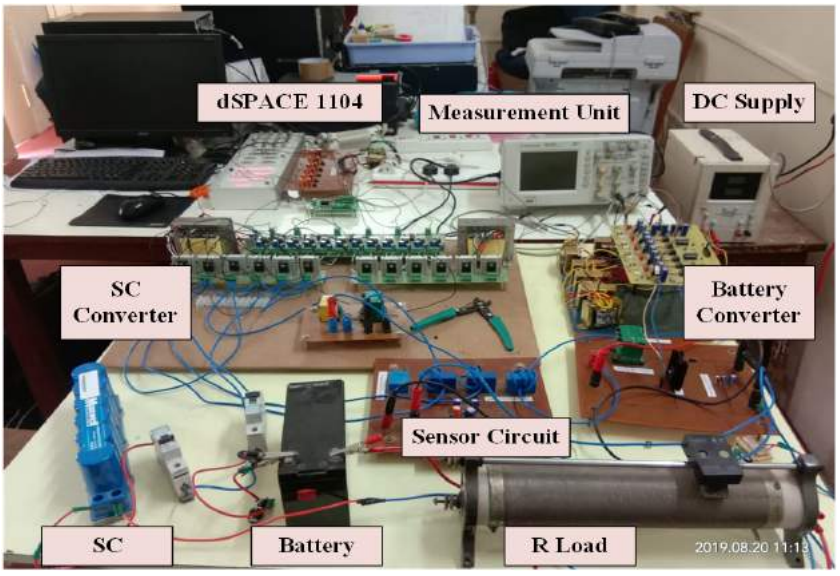

Figure 3.7: Experimental setup for HESS.

3.5 Hardware Implementation and Discussion

The hardware is designed and implemented with the help of the dSPACE 1104 platform and is shown in Fig: 3.7. The PI values obtained from accurate modelling are used for the closed loop implementation of the system. The nominal power is selected as 30W to verify the controller action. The SC operation is verified by introducing source and load disturbance in the DC bus. The load disturbance is created by adding a resistor in parallel to the main load through the controlled switch. The turn-on and turn off of the manual switch created a disturbance, as shown in Fig: 3.8 (a). In hardware development, the SC's current direction is negative for discharging. As a result, SC current waveform shows negative at the time of load increment and positive at the time of load decrement. The waveform clearly shows that load voltage is maintained at 20 V irrespective of the changes in load. During load disturbance, the load current is varied from 0.6 A to 1 A, and SC discharges accordingly. The battery current, load current and SC current are

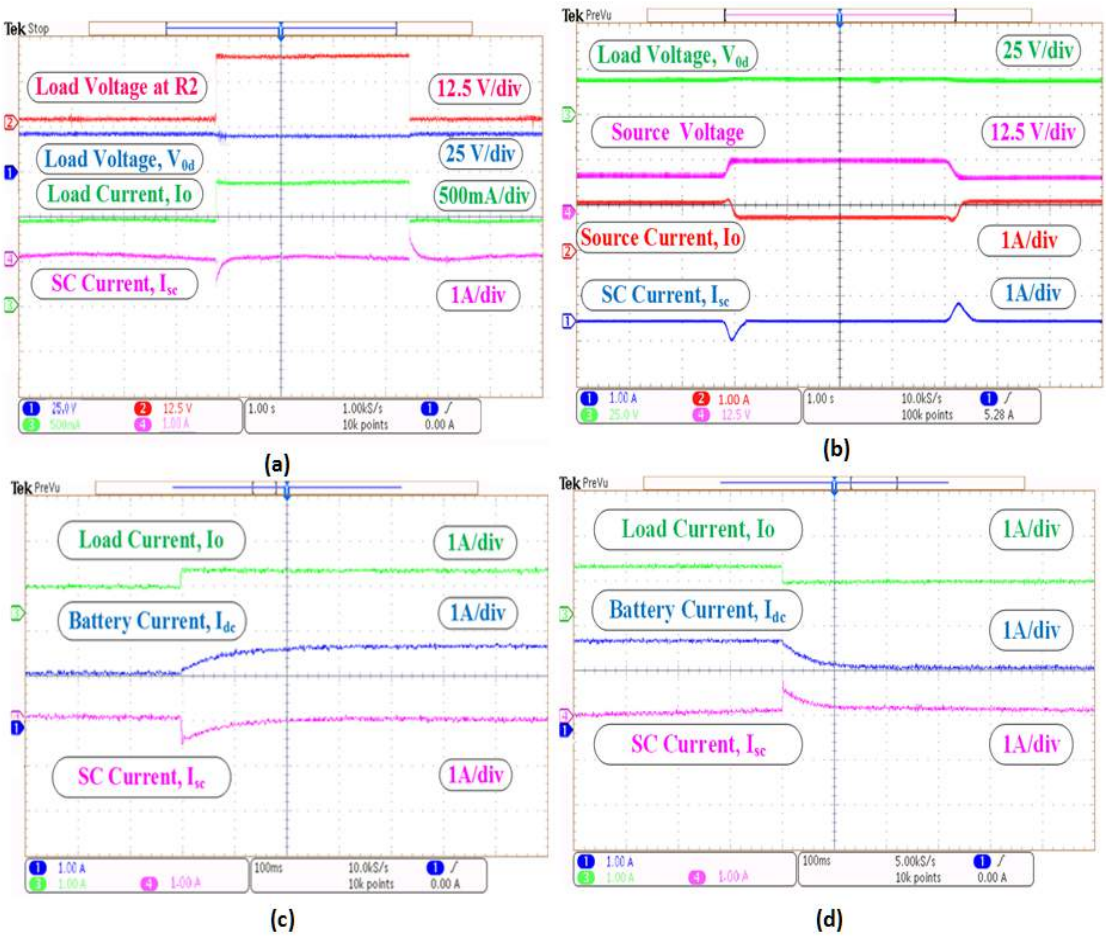

Figure 3.8: Different wave forms during load disturbance a) load voltage, voltage across load disturbance, load current and SC current under load disturbance b) load voltage, source voltage, source current, SC current under source disturbance c) & d) comparison of battery current, SC current and load current under load disturbance.

compared in Fig: 3.8 (c) and (d). The magnified portion of current shows that battery current responds slowly compared to SC current and load current. Here, the load current changes from 0.6 A to 1 A and the battery current changes from 1.2 A to 2 A. The system is analysed with source variation to verify the controller by replacing the battery with a regulated power supply. The corresponding load voltage, source voltage, source current, and SC current are shown in Fig: 3.8 (b). Initially, the source is increased from 10 V to 16 V and reduced to 10 V after some time. It can be seen that the source current is reduced to make the load power constant. Further, SC discharged/charged depends on the transient nature. However, the variation is slower than load variation due to the manual change in source voltage. The experimental study shows that the transient occurs due to source and load variations in the system is absorbed by the SC, and DC bus

voltage is maintained within limits.

3.6 Summary

This chapter presented a complete modelling of battery- SC hybrid energy storage system for DC microgrid applications. The combination of SC with battery is used to improve the system response and to enhance battery life. The efficient operation of HESS depends on the control strategy and the power-sharing between ESS. In the conventional control strategy, the PI-LPF control method regulates the DC bus voltage and HESS current regulation. The selection of PI gains decides the rapidity and accuracy of the system and is calculated based on the system model. This chapter proposes the combined modelling of HESS by considering the low pass filter effect and the effect of battery and SC. The advantage of the proposed method is that it provides enough bandwidth for the outer loop so that faster settling of DC bus voltage is ensured. PM and BW are considered the main constraints for tuning the controller parameters. The inner current loop BW is made higher to achieve a fast response in the system. The outer voltage control loop design involves a trade-off between BW and PM due to the presence of RHPZ. The PI values obtained based on an accurate model show fast response and better stability from frequency domain analysis. The PI values designed are tested under different disturbances in the system. The simulation and experimental results show that the DC bus voltage is maintained constant under all disturbances. The SC voltage waveform shows that it can take sudden disturbances in the system. The proposed method shows that the addition of SC to the battery through active topology improves control over the DC microgrid and reduces the stress on the battery.

Chapter 4
Supercapacitor Voltage based Power Sharing and EMS for DC Microgrid

4.1 Introduction

Integrating batteries accomplishes a highly reliable, efficient, and durable photovoltaic DC microgrid [16]. Supercapacitors boost the dynamics and battery life even further, and such a combination can improve the DC microgrid dynamics. The control and power splitting between the battery and SC plays a crucial role in the operation of the HESS. As discussed in chapter 3, the most common power routing method for HESS is the constant bandwidth low pass filter (CBLPF) based method. The major drawback of the CBLPF based method is that it causes slow dynamics of the control loop and leads to ringing in the DC bus voltage during the significant variation in SC operating voltage [37]. Hence, this chapter address a power management scheme with a variable bandwidth filter for HESS and a power splitting control strategy to eliminate the sluggishness imposed on the battery control loop by LPF.

From the literature study discussed in chapter 2, the issues related to HESS operation are i) The conventional LPF control strategy slows down the system response and demands more energy at lower SC voltages, ii) The operation of DC microgrid with lower SC voltage increases the oscillation in the system and might lead to instability. The DC microgrid requires an energy/power management strategy for (i) identifying the operating modes based on available PV power, ii) maintaining the state of charge of the battery in predefined limits and SC voltage within the operating limits and (iii) to guarantee that PV, battery, and SC power is balanced in each operating modes [84]. Hence this chapter proposes a novel control strategy that eliminates the use of LPF in battery reference current calculation. Further, an EMS is introduced to eliminate the effect of SC voltage variation on DC bus voltage. The proposed energy management scheme uses a dynamic filter for generating the SC current reference that adjusts the filter bandwidth based on SC available voltage. Also, a controlled charging scheme is added along with EMS to regulate the SC voltage conditionally. The advantage of the proposed method is that it reduces the DC microgrid oscillations and enables controlled charge/discharge of SC.

The contributions of this chapter are highlighted as follows:

1. Accurate modeling based HESS controller design is presented for PV-DC microgrid. The controller parameter design procedure considers the LPF effect on HESS control loop.
2. The proposed strategy controls the battery current loop without an LPF, reducing the excessive discharge of the SC unit and delay in the battery loop.
3. The HESS control uses a variable bandwidth low pass filter (VBLPF) for power distribution in the control loop, improving SC utilization and supporting loading for prolonged periods.
4. The proposed HESS energy management strategy effectively reduces oscillations occurring at lower SC voltages.
5. A detailed comparison between the proposed VBLPF and conventional fixed-LPF based HESS controllers are analyzed in the simulation trials at different SC voltages and validated by the experimental outcome.

The rest of the chapter is organized as follows. Section 4.2 describes a summary of proposed DC microgrid system. Section 4.3 presents the power sharing and SC voltage based energy management strategy in detail. Section 4.4 discuss the control parameter design. The simulation study and experimental results are discussed in Sections 4.5 and 4.6 respectively. Finally, section 4.7 summarizes the chapter.

4.2 Configuration of PV-DC Microgrid

The proposed DC microgrid system integrated with HESS is shown in Fig: 4.1. The PV source, battery and SC are connected to the DC bus through DC-DC converters and DC loads are connected directly. The PV panel connects to the DC bus through a unidirectional DC-DC boost converter. The power converters used to connect the energy storage devices to the DC bus have bidirectional capabilities. The PV control approach employs the MPPT to get as much power out of PV panels [44]. On the other hand, the HESS control strategy aims at supporting the DC microgrid under different operating modes such as deficit power mode (DPM), surplus-power mode (SPM), and floating-power mode (FPM) [43]. In surplus/excess-power mode, the PV generation is more than the load power demand, and the ESS stores the additional PV power. In deficit-power

mode, the PV generation is lower than load demand, and ESS discharges the stored power to meet the deficit. In floating mode, the PV generation matches the load demand forcing the ESS to standstill mode. The DC bus voltage regulation and load current sharing are taken care of by the HESS. The battery compensates for the steady-state power variations, while SC absorbs/delivers the transient current at the time of system disturbances. In this chapter, the DC loads are represented with parallel resistances and equivalent dc loads with resistance R_L. In Fig: 4.1, V_{pv}, V_{sc},V_b and V_0 are PV panel, SC, battery, and DC bus voltages respectively. The battery, PV panel and SC currents are represented by variables i_b, i_{pv} and i_{sc} respectively. L_{pv}, L_b and L_{sc} represent filter inductance of PV converter, battery converter and SCESS converter, C_0 is the filter capacitance. S_{pv}, S_{b1}, S_{b2}, S_{sc1} and S_{sc2} are control switches of power converters.

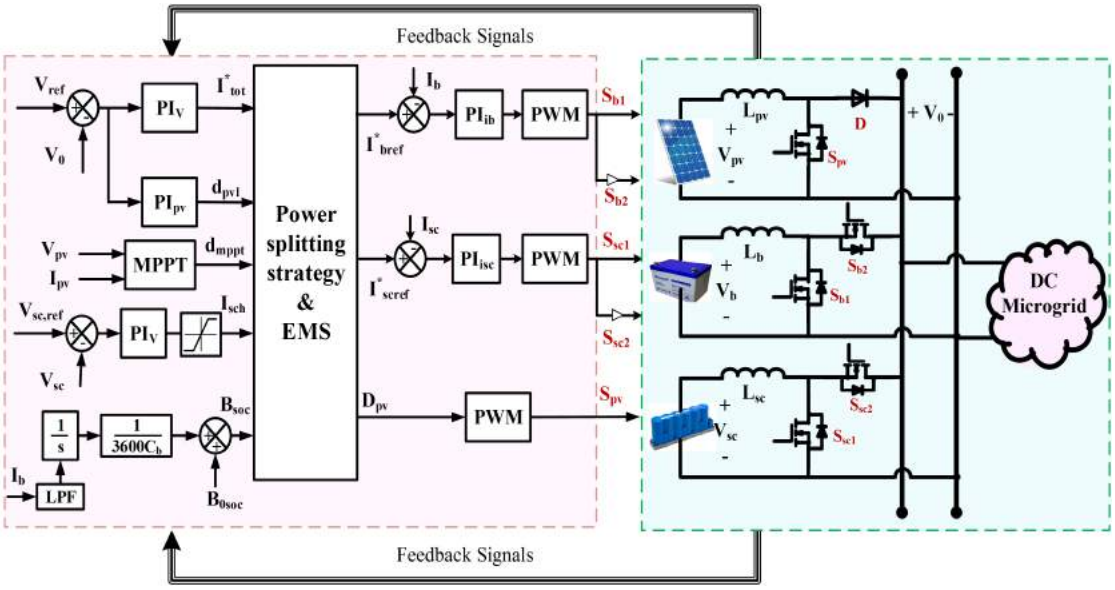

Figure 4.1: The PV- DC microgrid system configuration showing HESS, PV, power electronic converters and control schemes.

4.3 Proposed Power Splitting and EMS

This section discusses the need for a VBLPF in SC operation and designs an EMS for the smooth operation of HESS in PV-DC microgrid. The HESS EMS/PMS aims at keeping the state of charge (SOC) of the battery and SC within the operating limit. The conventional PMS considers battery SOC in the range of 80 % to 20 % and SC SOC in the range of 100 % - 20%. In contrast to the battery, SC voltage varies significantly during operation; at 50% SC voltage, only 25% of the energy is available. Also, SC SOC varies linearly with SC voltage. Hence, SC voltage variation can be considered

a parameter for SC EMS monitoring instead of SC SOC. The proposed LPF power splitting strategies is shown in Fig: 4.2.

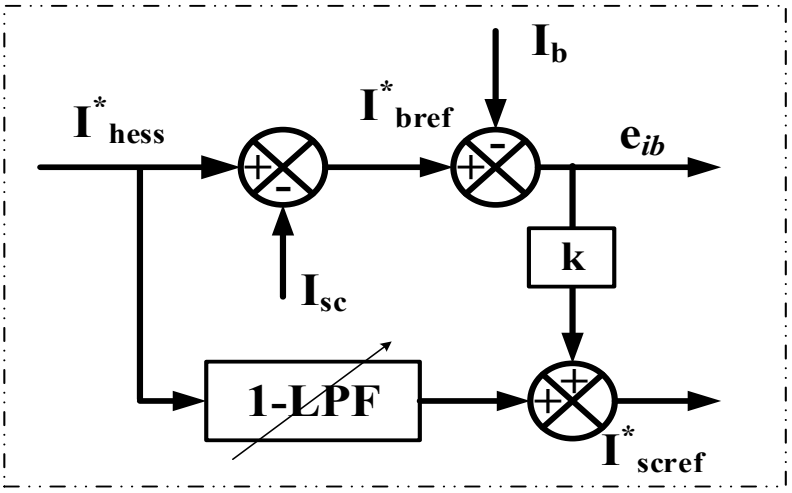

Figure 4.2: Proposed power splitting scheme for HESS.

4.3.1 HESS power splitting strategy

The use of CBLPF always demands constant power from SC at the time of disturbances. As a result, even if the SC voltage is low, the HESS controller will attempt to extract the required energy from it and leads to an oscillatory response from the SC unit, as shown in Fig: 4.3 (a). This oscillatory effect of SC voltage variation can be reduced by selecting the appropriate LPF cutoff frequency. In such cases, the bandwidth of the filter increases as the SC energy reduces. Consequently, it reduces the SC energy demand and the oscillations in the SC current and DC bus voltage as shown in Fig: 4.3 (b). Further, the SC is allowed to discharge more in the range of 100 %-50 % SC voltage to improve the SC utilization. The VBLPF uses a Butter-worth low pass filter with unity gain and variable bandwidth in MATLAB [134]. The filter computes the required bandwidth based on the SC voltage range.

4.3.2 Energy management strategy

The importance of SC-EMS is to ensure proper power balance of DC microgrid under all conditions. In the proposed EMS, VBLPF based energy management for SC proposes along with the battery state of charge (B_{SOC}) management. The EMS decides the

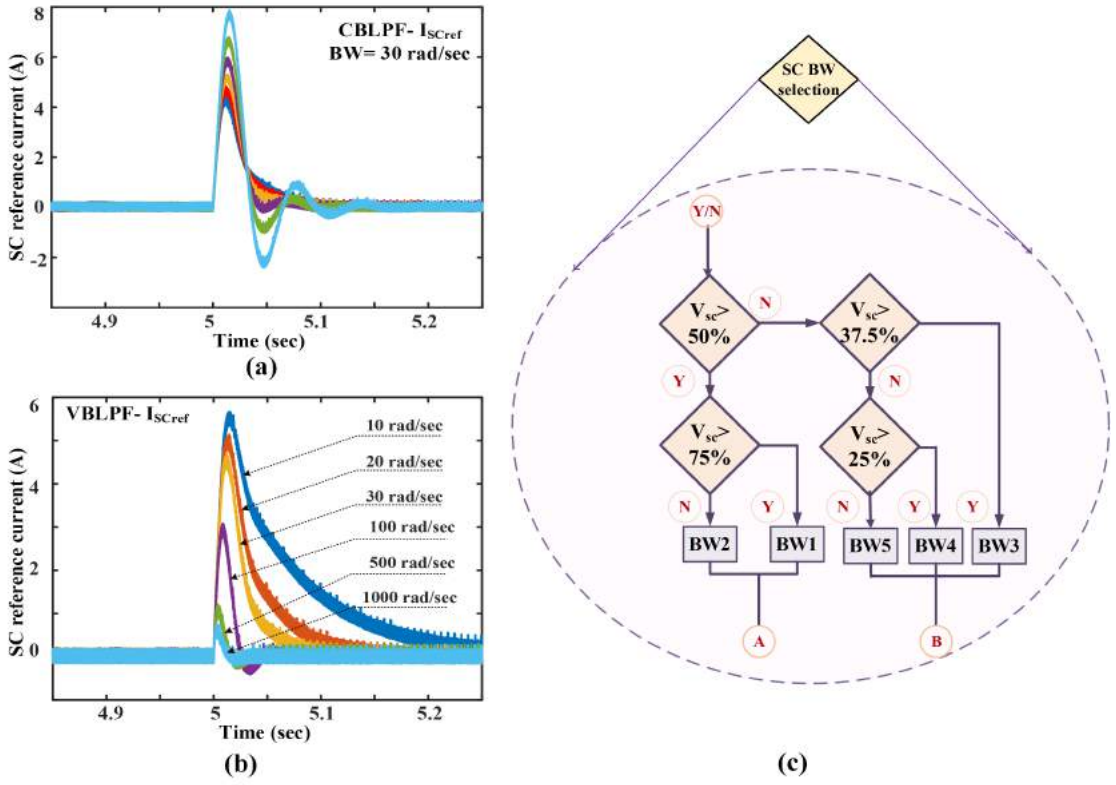

Figure 4.3: a) SC current reference with CBLPF b) SC current reference with VBLPF c) band width selection based on SC voltage.

operating mode based on the I^*_{bref}. The EMS is formed to meet the following operational goals; (i) to assess and decide the operating mode of DC microgrid system based on I^*_{bref}, (ii) to maintain battery SOC B_{SOC} and SC voltage within the operating limits (iii) Allocate charging of SC based on B_{SOC} such that eliminate the current oscillation at lower SOC (iv) to make the battery to respond at the time of steady-state and SC at the time transient state only, and (v) to ensure the power balance between PV, battery and SC at each operating mode. Also, the suggested EMS does not require weather forecasts or load current/power measurements for determining the modes of operation.

The main operating modes in a PV-DC microgrid system are SPM and DPM. The FPM is added with DPM to simplify the operation. Each main mode is divided into four sub-modes based on the available battery SOC as shown in Fig: 4.4. They are (Mode-I) $50\% < B_{soc} < 80\%$ (Mode-II) $20\% < B_{soc} < 50\%$ (Mode-III) $B_{soc} < 20\%$ (Mode-IV) $B_{soc} > 80\%$. In each sub-mode, V_{sc} is monitored and bandwidth selects for operation. The 75 % of stored energy in an SC is available at 50 % of the voltage range. So the VBLPF BW is selected to increase the utilization of SC at high voltage ranges. When

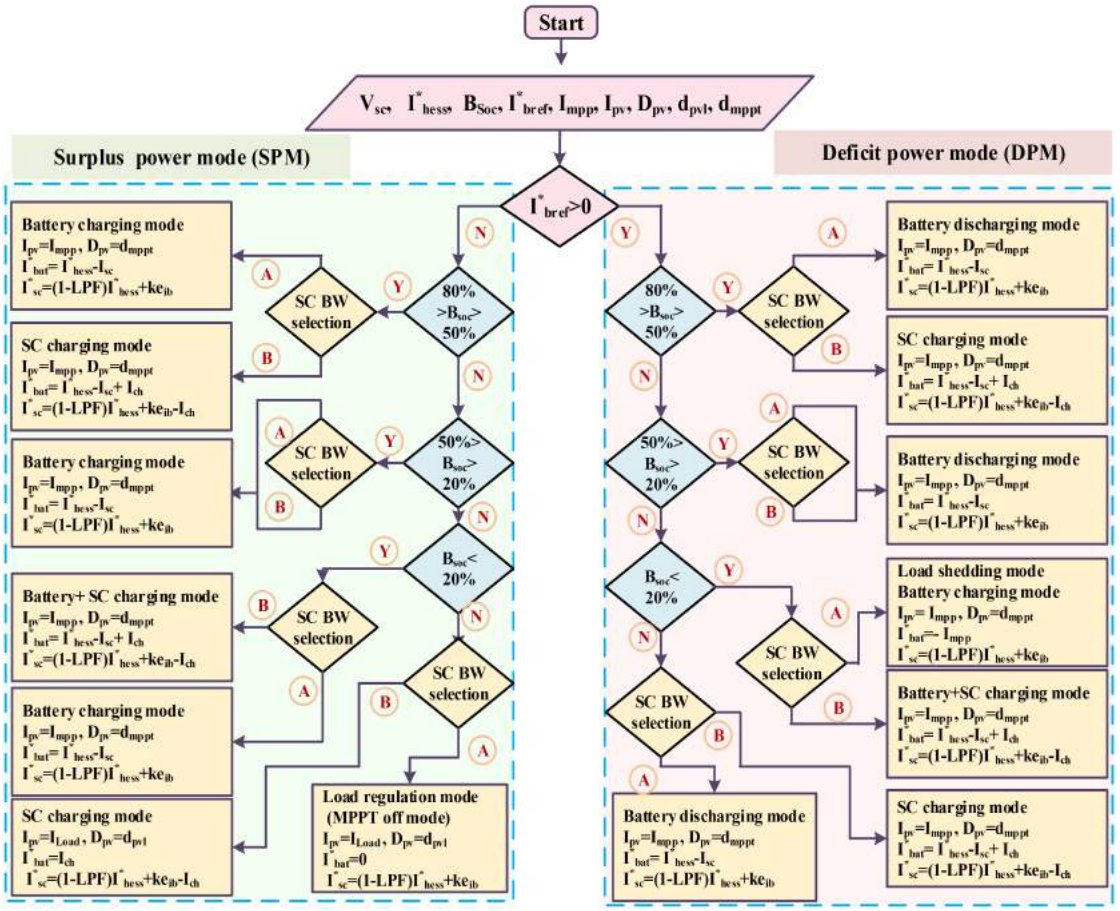

Figure 4.4: Block diagram representation of VBLPF based supercapcitor energy management strategy.

the voltage is between 75 % to 100 %, the LPF BW is BW1= 10 rad/sec, such that SC can supply more current for a longer duration. If the voltage is between 50 % to 75 %, the BW changes to BW2= 20 rad/sec. When the SC voltage reaches 50 % to 37.5 %, the LPF BW changes to BW3= 30 rad/sec. The BW is BW4= 100 rad/sec when the SC voltage is between 37.5 % and 25 %. The BW is BW5= 500 rad/sec for below 25 % SC voltage. Further, the EMS allows the SC to charge from the DC bus based on energy availability. The algorithm for selecting VBLPF bandwidth based on SC voltage is pictured in Fig: 4.3 (c). A detailed EMS for HESS is shown in Fig: 4.4. The following summarizes the operation of the proposed EMS.

1) Deficit power mode, ($I_{bref}* > 0$): In DPM, the PV generation is less than load demand. Hence, the average current ($I_{bref}* > 0$) is greater than or equal to zero. There are four sub-modes to describe the DPM explained as following.

Mode-I $50\% < B_{soc} < 80\%$: In this mode, PV power is insufficient to supply load demand. The battery operates in discharging mode. SC operates with lower BW ranges if the available voltage is more than 37.5 %. SC is allowed to charge in this mode due to battery power availability as shown in Fig: 4.4.

Mode-II $20\% < B_{soc} < 50\%$: In this mode, battery power is limited to supply only the load demand. Therefore SC is restricted from charging as shown in Fig: 4.4.

Mode-III $B_{soc} < 20\%$: The battery and SC cannot support the microgrid during this mode. Hence EMS shifted to load shedding mode and charged the battery. The SC will charge if the SC voltage is less than 50 % as shown in Fig: 4.4.

Mode-IV $B_{soc} > 80\%$: In this mode, the battery is overcharged. This mode shifts the PV control from MPPT to voltage regulation mode to maintain the load voltage. The SC is allowed to charge from the battery if the SC voltage is less than 50 % as depicted in Fig: 4.4.

2) Surplus power mode, ($I_{bref}* < 0$): In SPM,the PV power is greater than load demand. Hence, the average reference current, $I_{bref}*$ is less than zero. There are four sub-modes to describe SPM explained as following. This mode enables the charging of the battery and SC unit.

Mode-IV $50\% < B_{soc} < 80\%$: In this mode, the total PV power is more than load demand. The SC can supply or absorb transients up to 50% of SC voltage and preferred to charge below that range.

Mode-VI $20\% < B_{soc} < 50\%$: If the SC voltage is dropped below 50%, it enables the charging of SC along with battery.

Mode-VII $B_{soc} < 20\%$: If the battery power reduced below limits it need to get charged. This mode sheds the loads and charges the battery. If the SC power is less than 75 %, then SC is kept in charging mode.

Mode-VIII $B_{soc} > 80\%$: In this mode, the battery power reached the upper limit. PV will shift to load regulation mode. SC charges from the supply if the SC voltage is less than 50 %.

4.4 Analysis of PV-DC microgrid Control Strategy

The microgrid control generates the control signals for the PV converter and HESS bidirectional converters. The proposed HESS control strategy is modeled and analyzed using Matlab/Simulink®. The PV is regulated by MPPT and HESS is controlled based on proposed EMS. The HESS controllers parameters are derived using uncompensated loop transfer functions given in Table: 4.1.

4.4.1 PV control strategy

The primary goal of the MPPT algorithm is to obtain maximum power from the PV panel. The most basic and conventional MPPT technique is the P&O method. In this method, the duty ratio is varied in steps based on output voltage to obtain the maximum power point. The flowchart for the P&O method and P-V curve is depicted in Fig: 4.5 (a) and (b). At normal operation, the P&O technique generates the required duty signal (d_{pv1}) for extracting maximum power. Excess power mode with 80 % battery SOC (Mode-IV) causes the PV to switch to load regulation mode. The PV boost converter control signals (d_{pv2}) are generated using PI_{pv}. Where PI_{pv} is the PV voltage controller and is given by,

$$PI_{pv} = K_{ppv} + \frac{K_{ipv}}{s} \tag{4.1}$$

The K_{ppv} and K_{ipv} values are 0.35 and 20 respectively. The proposed EMS select the

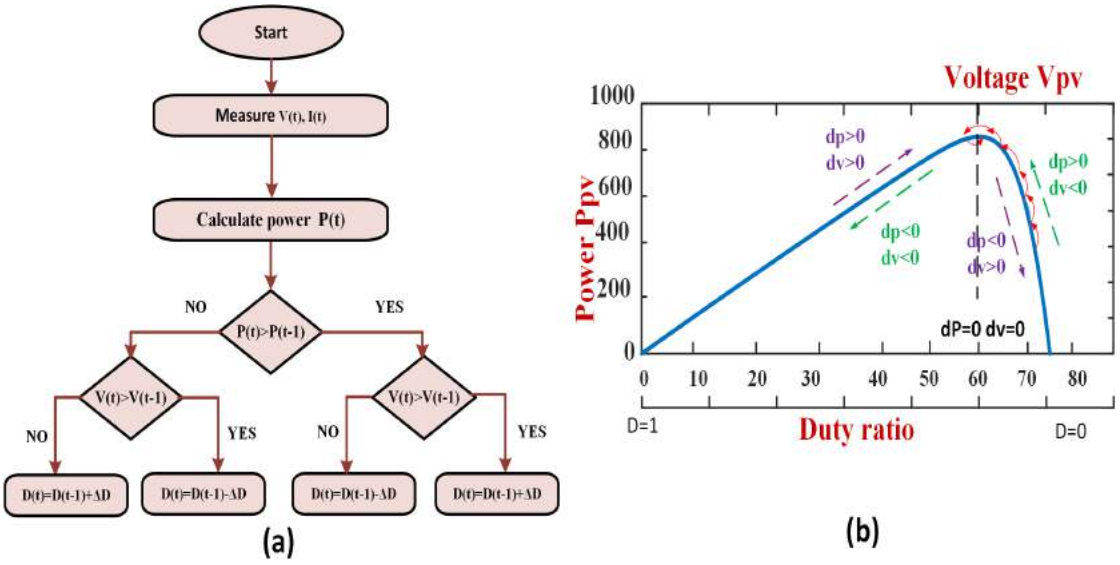

Figure 4.5: PV control strategy: a) P&O MPPT algorithm flow chart b) P-V characteristics with duty.

required duty pulse based on available energy and SC voltage.

4.4.2 HESS reference current generation

In the HESS controller, the reference current generation needs to ensure that the power supplied by HESS and PV must meet the load demand. The power generated by the PV source is independent of the load demand during MPPT mode. Hence the HESS has to supply the deficit power during a reduction in PV generation and store the surplus power during excess PV generation. The relation between HESS and load current can be addressed as follows:

$$i^*_{hess} = i^*_{bat} + i^*_{sc} = i^*_{tot} - i_{pv} \tag{4.2}$$

Where, i^*_{hess}, i_{bat}, i_{sc}, i_{tot} and i_{pv} are the total HESS current reference, battery current reference, SC current reference, total current reference and PV current generated. The battery and SC reference currents are generated based on the proposed power splitting scheme. The average component of HESS reference current is calculated by:

$$i^*_{bat} = i^*_{hess} - i_{sc} \tag{4.3}$$

$$i^*_{sc} = i^*_{hess}(1 - LPF) + ke_{ib} \tag{4.4}$$

where i_{sc},i_{bat}, V_b,V_{sc} and e_{ib} are the actual SC current, battery voltage, SC voltage and battery current error. The gain k is used to limit the current error, and it is given as $\frac{V_b}{V_{sc}}$. The actual SC current is used to calculate the battery reference current. The SC reference current is the sum of uncompensated battery current and the transient part of the total HESS reference current. According to the equation (4.4), the SC current generation varies with SC voltage and VBLPF BW.

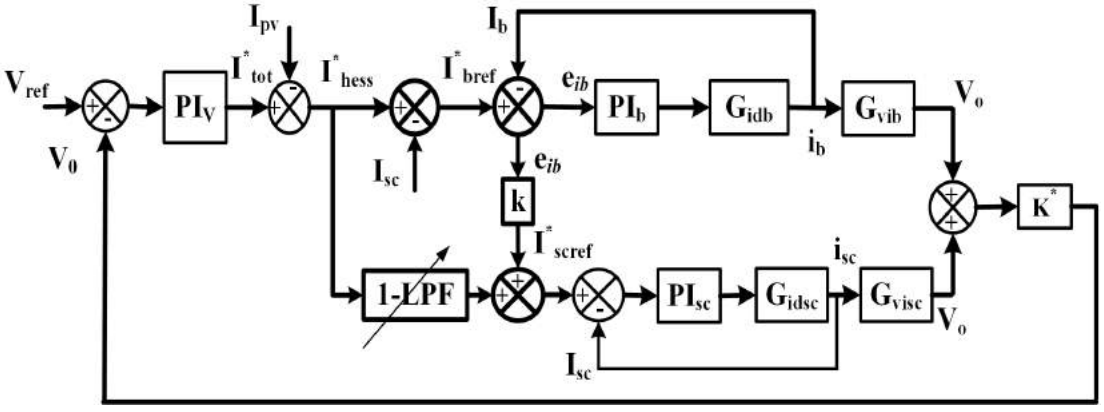

Figure 4.6: Small signal block diagram of proposed HESS control scheme.

4.4.3 Battery current controller

The battery current controller forces the battery current to follow the slow-changing reference current. The controller is designed based on the duty to control transfer function (G_{idb}) of the battery, which is given in Table: 4.1. The block diagram for control system modeling is shown in Fig: 4.6. The battery inductor current is calculated from error as written below:

$$i_b = e_{ib} PI_b G_{idb} \tag{4.5}$$

Where PI_b is the battery current controller and is given by,

$$PI_{ib} = K_{pib} + \frac{K_{iib}}{s} \tag{4.6}$$

The e_{ib} is the battery current error and is given by,

$$e_{ib} = i_b^* - i_b \tag{4.7}$$

K_{pib} and K_{iib} are the battery current PI controller gains. The battery current loop is made

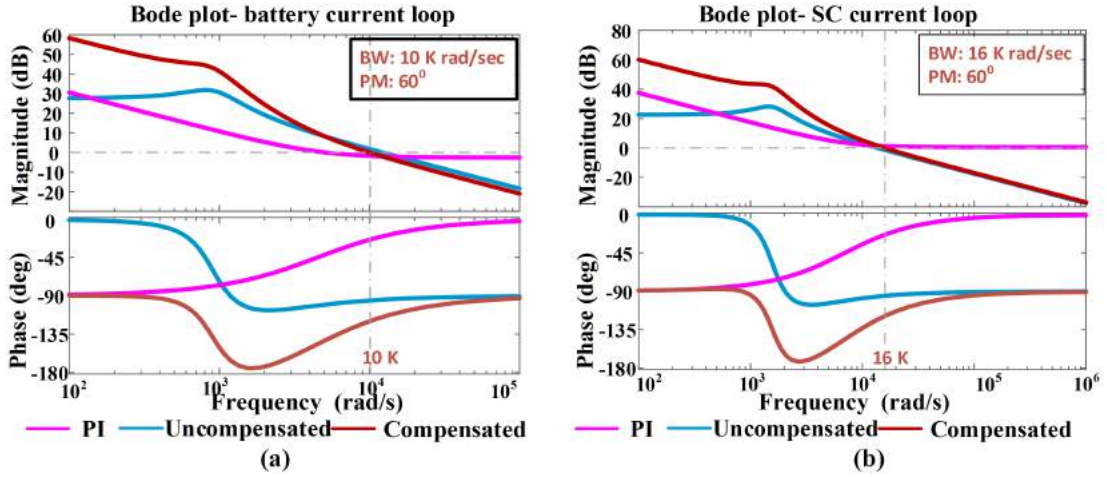

Figure 4.7: Bode diagram of uncompensated and compensated system a) battery current control loop b) SC current control loop.

faster than the voltage control loop and slower than the SC current loop by adjusting the bandwidth. It helps to slow down the battery current during the disturbances. The bandwidth and phase margin of the battery current loop is selected as 10 k rad/sec and 60^0, respectively. The bode diagram of compensated system shows that the controller provides high gain at low frequencies. The low value of integral gain indicates the lower

dynamics of the battery current loop.

Table 4.1: System transfer function and controller parameters

S.No	Control loop	Transfer function	K_p	K_i	B.W (rad/sec)	P.M.
1	Battery current loop	$G_{idb} = \frac{\hat{i}_b(s)}{\hat{d}_b(s)} = \frac{C_{0b}V_0 s + 2(1-D_b)I_b}{L_b C_{0b} s^2 + \frac{L_b}{R_L} s + (1-D_b)^2}$	0.65	220	10000	60^0
2	SC current loop	$G_{idb} = \frac{\hat{i}_b(s)}{\hat{d}_b(s)} = \frac{C_{0b}V_0 s + 2(1-D_b)I_{bx}}{L_b C_{0b} s^2 + \frac{L_b}{R_L} s + (1-D_b)^2}$	0.833	3733	16000	60^0
3	Current to voltage	$G_{vi} = \frac{\hat{V}_0(s)}{\hat{i}_x(s)} = \frac{(1-D)V_0 - LI_x s}{CV_0 s + 2(1-D)I_x}$	0.26	135	600	60^0

4.4.4 SC current controller

The SC current control loop is the fastest in the overall HESS control system. It can deliver/absorb rapid transient power that exists in the DC load bus. The controller design considers the duty to the current transfer function of SC, which is given in Table: 4.1. From the controller block diagram, the SC current calculation is given as:

$$i_{sc} = e_{isc} PI_{sc} G_{idsc} \tag{4.8}$$

Where, e_{isc} is the error in super capacitor current. The SC current controller is represented as PI_{isc} and is written as follows:

$$PI_{isc} = K_{pisc} + \frac{K_{iisc}}{s} \tag{4.9}$$

The faster dynamics of the SC current loop are achieved by the rigorous design of the current controller. The bandwidth is chosen higher than that of the battery current loop and lower than the switching frequency to avoid the unwanted ripple in the output. As a result, the controller bandwidth is 16 krad/sec, and a phase margin of 60^0 is selected. From the bode plot, it is clear that the new compensated system is having high gain at low frequencies and low gain at switching frequencies. Thus, it helps to improve the response at the initial period and reduces the ripple amplitude at switching frequency.

4.4.5 DC bus voltage controller

The outer voltage control loop plays a crucial role in the DC bus regulation. In addition to the delay imposed by LPF, the right-hand zero of the boost converter directly affects the load voltage. Hence the controller parameter selection requires utmost care in the

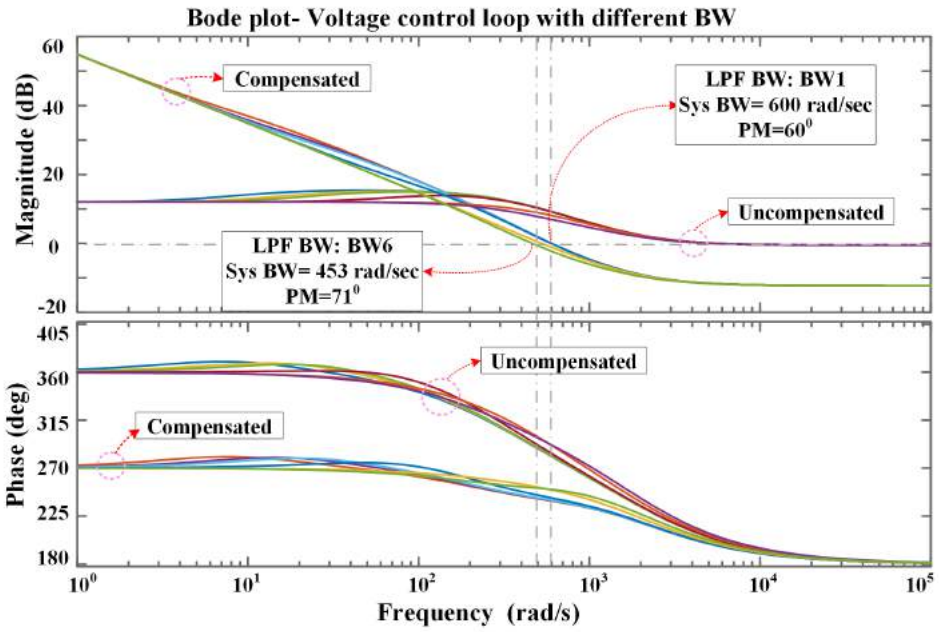

Figure 4.8: Bode diagram of uncompensated and compensated system for outer voltage control loop with different BW.

case of the outer loop controller. The outer loop voltage controller is given as:

$$PI_v = K_{pv} + \frac{K_{iv}}{s} \tag{4.10}$$

The outer voltage controller receives the error between the reference voltage and the actual voltage. To compensate for the corresponding error, the controller generates the total current reference. The outer voltage controller design utilizes the overall transfer function of the system. The outer loop is designed based on the SC control transfer function to reduce complexity in previous works. However, those approaches failed to incorporate battery performance. The combined system model of the proposed control strategy is given as:

$$G_{v,all} = (PI_v G_{vib} + PI_v k G_{visc} + PI_v(1 - LPF)G_{visc})K^* \tag{4.11}$$

Where:

$G_{v,all}$: Overall loop gain of compensated control system

G_{visc}: current to voltage transfer function of SC

G_{vib}: current to voltage transfer function of SC

The‘ gain ’K^*’ is used to obtain the actual output voltage for the model shown in Fig:

Table 4.2: Rating of DC microgrid components

S.No	Components	Specifications
1	PV panel ratings considered	V_{pv}= 61.4 V, I_{pv}= 16.3 A
2	SC unit	V_{sc}= 48 V, C_{sc}=19.3 F
3	Battery unit	48 V, 21 Ah
4	DC-DC converter system	L_{pv}= 3.1 mH, L_b= 2.3 mH, L_{sc}=2.3 mH, C_{0dc}= 430 μF, R_L= 24 Ω
5	Rated output power, P_{out}	1 kW
6	Switching frequency, f_{sw}	20 kHz
7	Load voltage, V_0	96 V

4.6. The inner current loops are faster than the outer voltage loop and its loop gain is taken as unity. The BW of the outer voltage control loop has the lowest value compared to other control loops so that it decouples the slow variation of capacitor voltage from the fast inner current loops. The phase margin and bandwidth of the control loop are 60^0 and 600 rad/sec, respectively. The bode diagram for the outer compensated and uncompensated system with variation in VBLPF BW is shown in Fig: 4.8. From the diagram, an increase in VBLPF BW reduces the system BW and increases the phase margin. At BW= BW6, the control system BW is 453 rad/sec and the phase margin is 71^0, ensuring system stability in all VBLPF BW conditions. The controller parameters are designed using MATLAB/SISO tool. The different control loop, transfer functions, controller parameters, bandwidth and phase margin of each control loop are summarized in Table: 4.1.

4.5 Simulation Study

Extensive simulation studies are performed in Matlab/Simulink®to validate the performance of HESS with the VBLPF control strategy. The simulation parameters of the microgrid system are shown in Table: 4.2. The proposed control and EMS performance are validated under basic operating scenarios such as (i) sudden change PV irradiation and (ii) sudden change in connected load. The Fig: 4.9 depicts the simulation results of various parameters such as V_0, I_l, I_{pv}, I_b and I_{sc}.

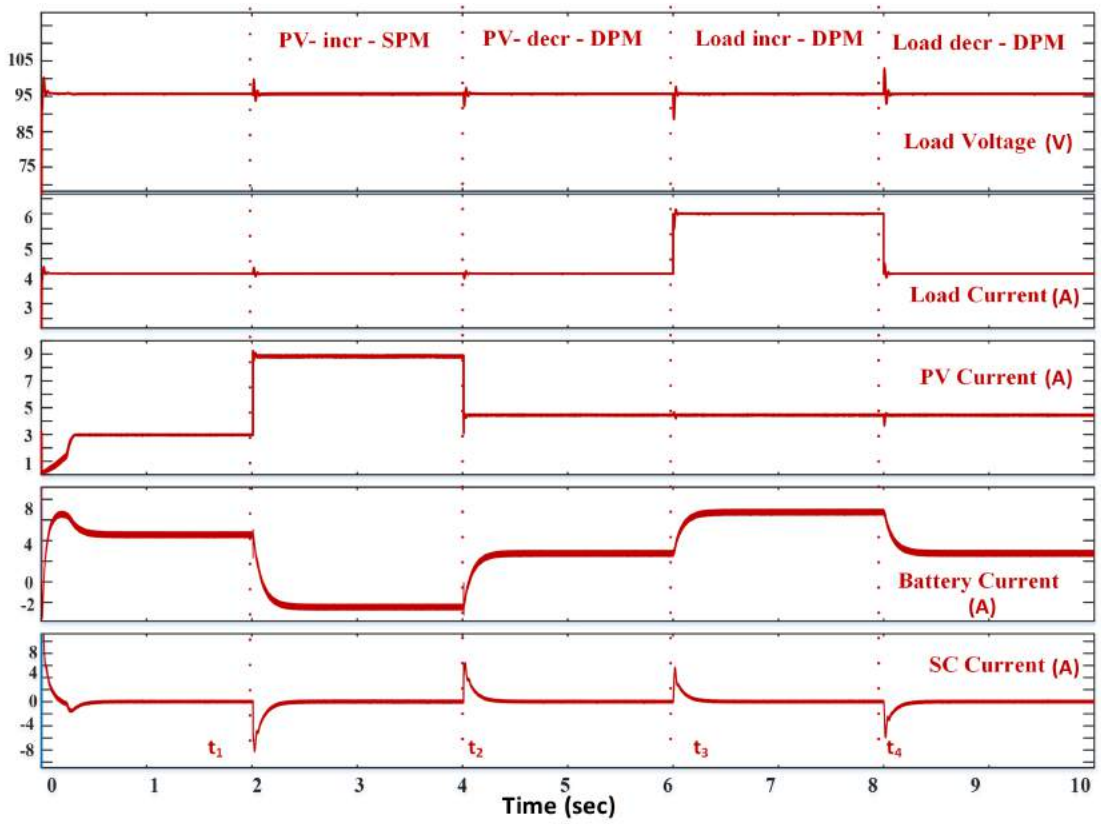

Figure 4.9: Simulation results: system performance during sudden change in source and load: t_1-t_2= PV power increased under SPM, t_2= PV power decreased under DPM, t_3= load increment under DPM, t_4= load decrement under DPM.

4.5.1 Performance under the change in PV generation

The system response under step change in PV power generation is applied at t_1 and t_2 as shown in Fig: 4.9. Initially, the battery and PV together supply the load demand. At t_1, the PV generation is more than load demand (SPM). The surplus power that exists in the DC bus is used to charge the battery. At t_2 instant, the PV generation is reduced to a new lower level with I_{pv}= 4 A. During this period, the battery meets the reduction in load power demand as PV output decreases.The waveforms reveal that the DC bus is regulated within the voltage range and the SC compensates for the rapid power surge generated in the system.

4.5.2 Performance under the change in load demand

The system response under load change is validated by applying step increment in load demand at t_3 and step decrement at t_4. From Fig: 4.9, it is clear that load voltage

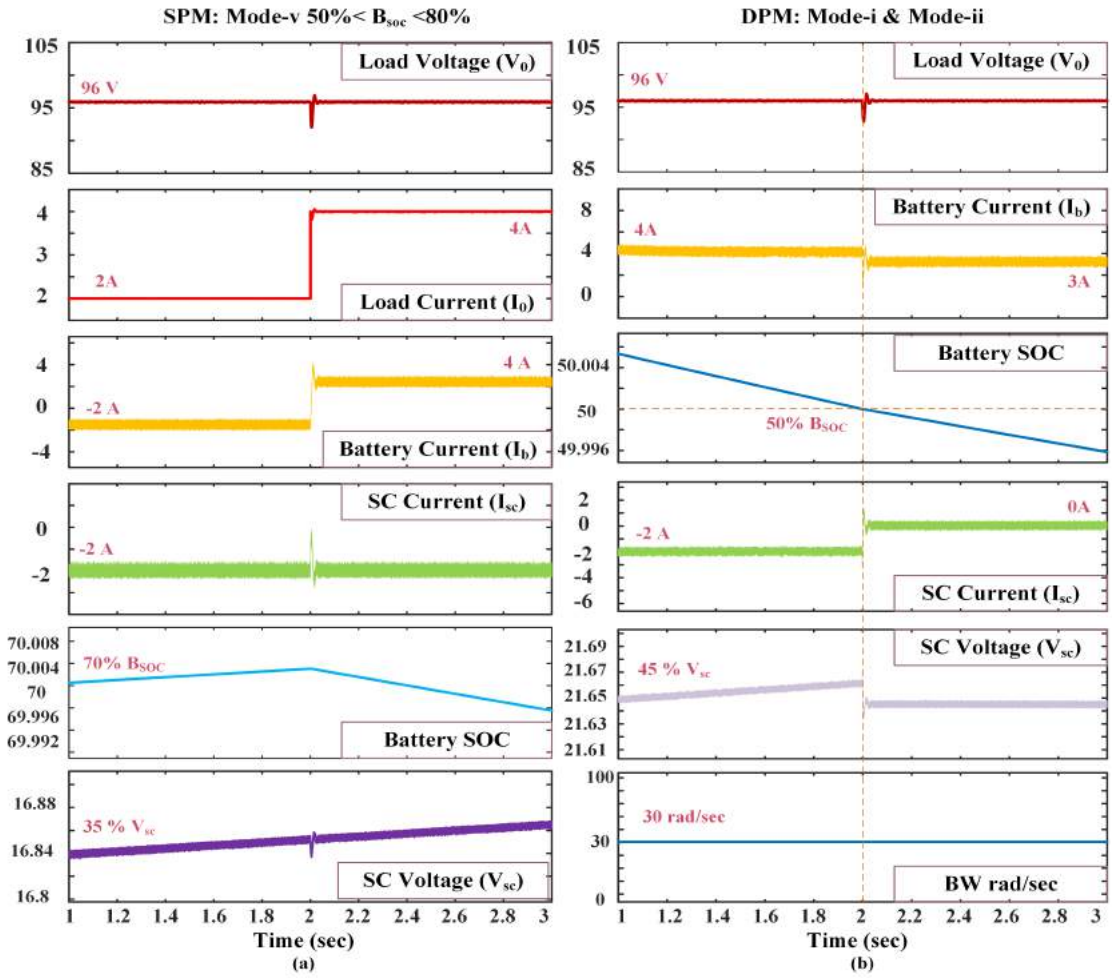

Figure 4.10: Simulation study: performance analysis of EMS at different mode: (a) Mode-I & mode-V (b) Mode-I & Mode-II.

regulates at 96 V in all conditions. The system operates under DPM due to an increase in load demand beyond PV generation. The power difference between load demand and PV generation is used to charge the battery and SC. The SC is fast enough to absorb excess power as the rapid change in battery current is very small. At t_4, the additional load is separated from the DC bus. The power reduction is shared between battery and SC according to the control strategy.

4.5.3 Operation under different DC microgrid operating modes

The system operates under different modes is tested in simulation. The Mode-V, Mode-I and Mode-II are illustrated in Fig: 4.10 to analyze the SC charging and mode shifting in the proposed DC microgrid system. Figure 4.10 (a) shows the Mode-v operation

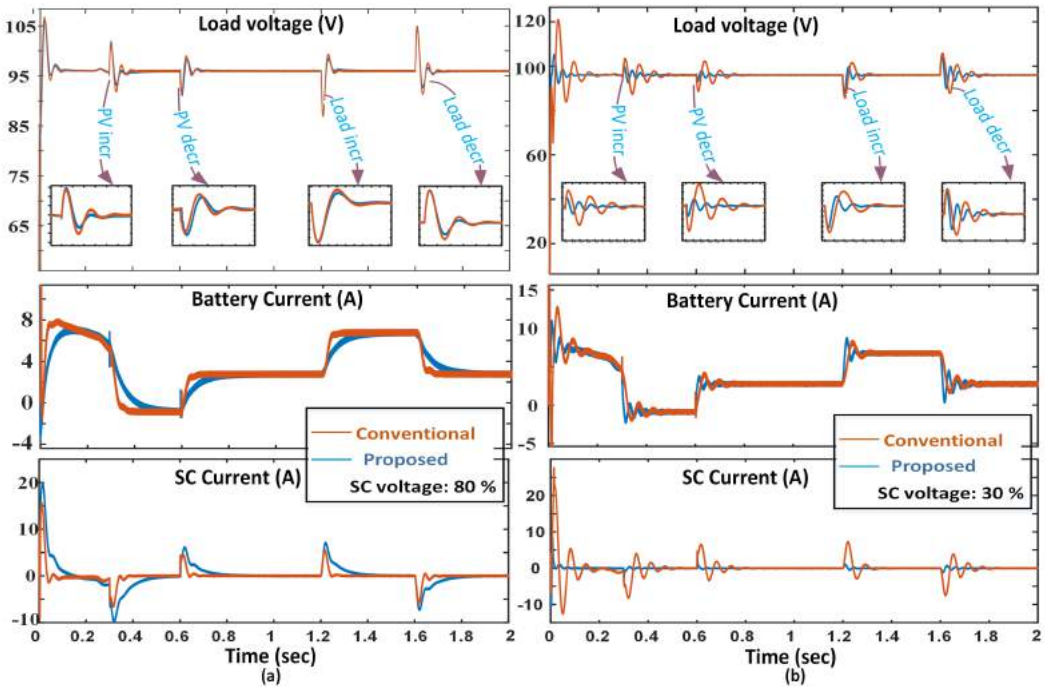

Figure 4.11: Simulation study: comparison of conventional and proposed control strategy with different SC voltages a) load voltage, battery current, and SC current at 80 % of V_{sc} b) load voltage, battery current, and SC current at 30 % of V_{sc}.

under load disturbance. Initially, the SC and battery are charging from PV (Mode-V). At t= 2 sec, the load demand increases from 2 A to 4 A. As a result, the battery shift from charging mode to discharging mode and SC remains in charging (Mode-I) due to the availability of battery power. The corresponding B_{soc}, I_{sc}, V_{sc} are depicted in Fig: 4.10 (a). In deficit power mode, if the B_{soc} went below 50 %, the SC charging stops due to the reduction in available energy. The corresponding battery current, SC current, Battery SOC, SC voltage and BW are shown in Fig: 4.10 (b). In each mode, the battery and SC operating states are wisely selected based on the EMS. It allows the system to operate for a prolonged duration.

4.5.4 Performance comparison of the system under different SC operating voltages

Simulation studies are carried out to compare the performance analysis of HESS control with CBLPF and VBLPF. The conventional and proposed strategies are verified under different DC microgrid conditions. The performance of the system under 80 % of SC voltage and 30 % of SC voltage are shown in Fig: 4.11. According to the literature, the bandwidth of the traditional approach is set to 5 Hz [102]. The system performance

with fully charged SC shows a similar settling time and peak overshoot as depicted in Fig: 4.11 (a). However, the operation with low SC voltage shows an increase in settling time and peak overshoot at load voltage as shown in Fig: 4.11 (b). The conventional method with 30 % SC voltage exhibits the DC bus voltage oscillations for 0.1 sec to 0.2 sec. The maximum peak-to-peak variations for the conventional method are observed at initial transient with 35 V, and the peak is varied between 9 V to 15 V during other system disturbances. On the other hand, the system's operation with VBLPF shows reduced oscillations and faster settling time. The maximum peak-to-peak variation is observed at initial transient with 10 V. All other disturbances create variations less than 10 V. Also, the settling time for DC bus voltage is significantly reduced compared to the conventional method. In the proposed method, the settling time is less than 100 msec for all cases.

The operation of the control strategy is analyzed with similar power splitting strategies presented in Fig: 4.2. The systems are simulated for the same power level and applied the same disturbances for unity. The obtained results are summarized in Table: 4.3. The traditional PI approach shows overshoot of more than 6 % and a settling time between 80 % to 120 %. The battery error compensation allows the system to reduce the maximum settling time by a factor of 50 %. The overall reduction in peak is 3.6 % in [135] compared to the conventional method. The proposed method shows much reduction in peak overshoot. The maximum settling time shows a reduction of 66.6 % compared to the conventional method. It is relevant to note that the oscillations and peak increases in CBLPF methods as SC voltage increases. The use of VBLPF significantly reduces this effect. Compared to other similar topologies, the proposed method analyses the variation of SC voltage in the DC microgrid for all scenarios and uses a VBLPF to mitigate the effect. In summary, the simulation results show faster settling and power sharing at different variations applied in the system. The operation under different SC voltages and modes shows that the system regains its stability after disturbance. Further, the charging of SC has a more negligible effect on DC bus voltage variations and SC can absorb transients during this period. The operation with lower SC voltages shows fewer oscillations for the proposed method compared to the conventional method. The proposed EMS allows the stable operation of the DC microgrid system without disconnecting the SC units during lower SC voltage ranges.

Table 4.3: Comparison between proposed controller and traditional PI control methods

S.No	**References**	**[135]**	**[96]**	**Proposed**
1	%Mp load change	6-8.5%	3.8-5%	3.8-4.6%
2	%Mp PV change	2-3%	1.5-2%	1.5-1.8%
3	Settling time (ms)	60-100	30-50	25-40
4	Power splitting strategy	CBLPF	CBLPF	VBLPF
5	Control strategy	PI	PI	PI
6	EMS	YES	NO	YES
7	Consideration of V_{sc} variation	NO	NO	YES

4.6 Experiment Results and Discussion

Figure 4.12 illustrates the experimental setup of PV-DC microgrid integrated with HESS. It comprises a controlled DC power supply with rating 30 V, 5 A for PV module, battery unit consisting of 12 V, 7 Ah lead-acid battery, and Maxwell SC unit with rating 16 V, 58 F. The converters have a 200 W capacity. Due to source limitation and inductor saturation above 5 A, the nominal operating power is selected as 48 W. The proposed control algorithm and SC energy management are implemented in the dSPACE DS1104 control platform. The test system's performance is analyzed with i) increment in PV generation ii) decrement in PV generation iii) increment in load variation and iv) decrement in load variation. Further, the SC-based EMS is verified experimentally under different SC voltage ranges. The experimental results for wide SC voltage ranges and different power levels are presented to validate the proposed strategy.

4.6.1 Operation with proposed EMS with 50-75 % charged SC unit

In this mode, the SC voltage is less than 75 %. Hence the cut-off frequency of VBLPF is automatically selected as 20 rad/sec. During this period, the SC unit provides almost zero current at steady-state and responds instantaneously to the disturbances. Hence the change in SC voltage is minimal as the PV and battery supply the total load power demand. However, the sudden changes in PV generation or load demand create a power imbalance in the DC bus. The fast action of controllers controls the flow of deficit or surplus power in the DC bus and EMS regulates the power balance in the system. The following section analyses the DC microgrid with 50-75 % charged SC unit operation

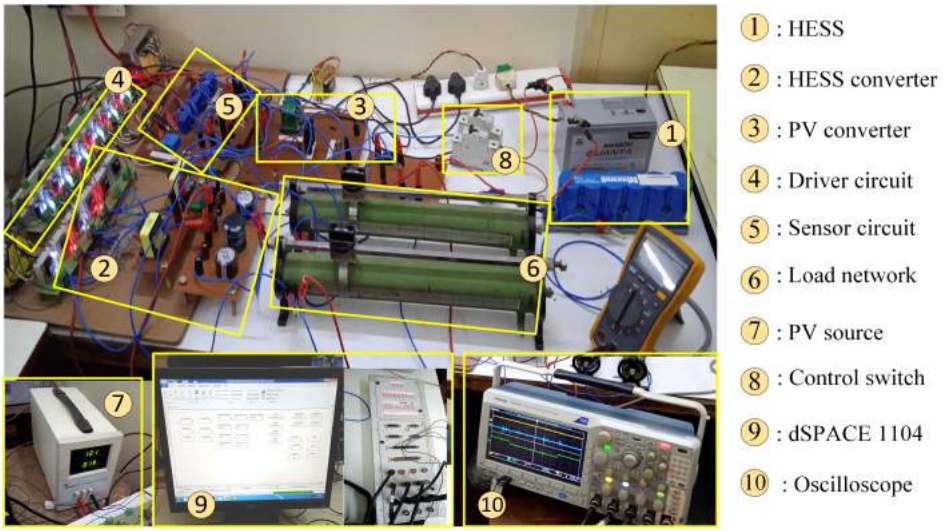

Figure 4.12: Experimental prototype developed for the proposed system.

under different interruptions.

4.6.1.1 Change in PV generation

The experiment is carried out for three different PV generation circumstances as shown in Fig: 4.13(a). Firstly PV generation is made more than load demand. As a result, the excess power in the DC bus charges the battery during the t_0 to t_1 period. The load demand is 1 A and PV current is 3 A. The battery current is negative during the period indicating that the battery is charging from a PV source. At t_1, the PV generation is changed to 1 A. The battery current is increased to 1 A to meet the load demand. It is important to infer from the waveform that the SC supplies the initial current to allow the slow change in battery current. At $t = t_3$, the PV generation increases to 2 A and meets the load requirement. As a result, the battery current gradually decreases to zero, while the SC absorbs the excess current supplied by the battery. Hence, the SC limits the sudden variation in battery current and reduces the stress on battery. In all cases, the EMS balance the power between PV, battery, SC and load, and the DC bus oscillations are mitigated.

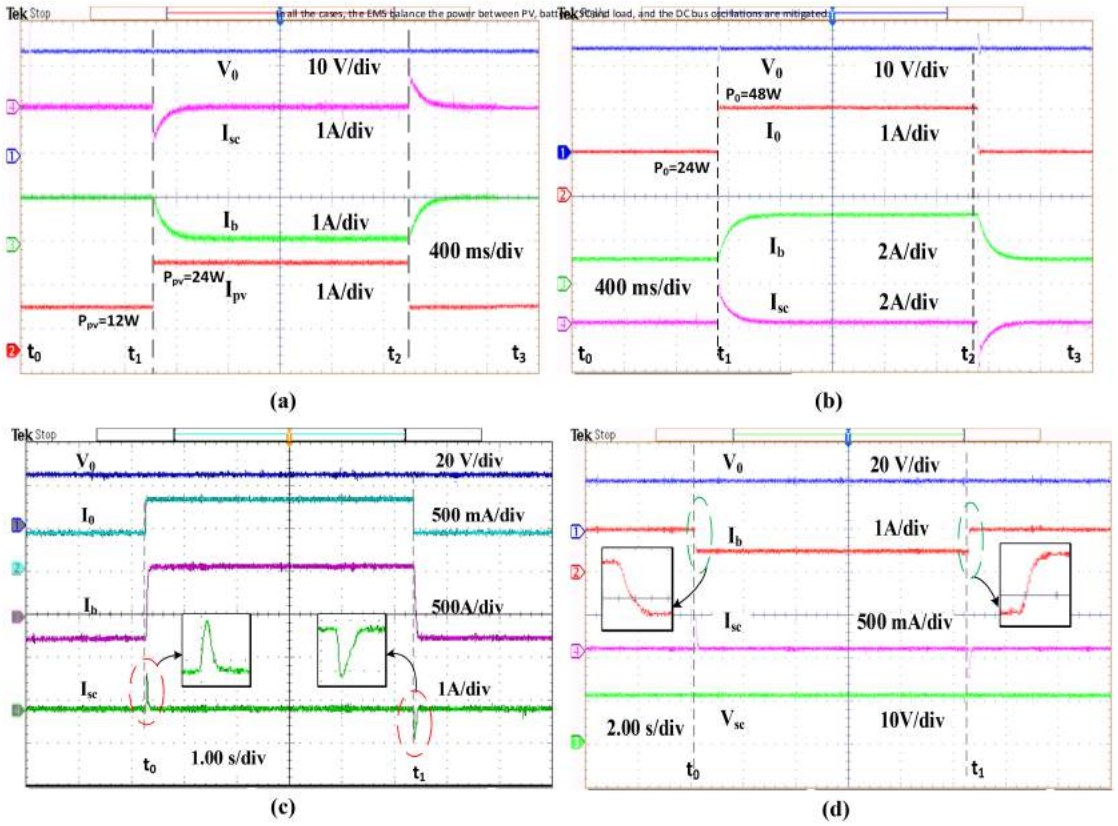

Figure 4.13: Experimental results with 50-75 % SC voltage: a) system under PV disturbance: load voltage, battery current, SC current, PV current b) system under load disturbance: load voltage, load current, battery current, SC current c) load power variation from 12 W to 24 W d) SC voltage and SC current during disturbances.

4.6.1.2 Change in load demand

Figure 4.13 (b) illustrates the operation of DC microgrid under varying load conditions. Compared to PV variations, the load variations introduce more oscillations on DC bus voltage. A 100 % change in load is applied to verify the proposed scheme. The power supplied by PV panel is 12 W, (V_{pv}= 12 V and I_{pv}= 1 A). The required load power at t_0 is 24 W and the battery supplies the remaining 12 W power. This is illustrated in the time period t_0 to t_1. At t_1, the load demand increased to 2 A. To fulfill the load demand, the battery current increases to 3 A. Since the change in battery current is limited, the SC supplies the transient current. At t_2, the load demand reduces to 1 A. The results show that the proposed EMS ensures DC voltage regulation and the power balance achieved between load, PV, battery, and SC based on available power. The proposed strategy is analyzed under different loading conditions. The operation with 7 W and 15 W load

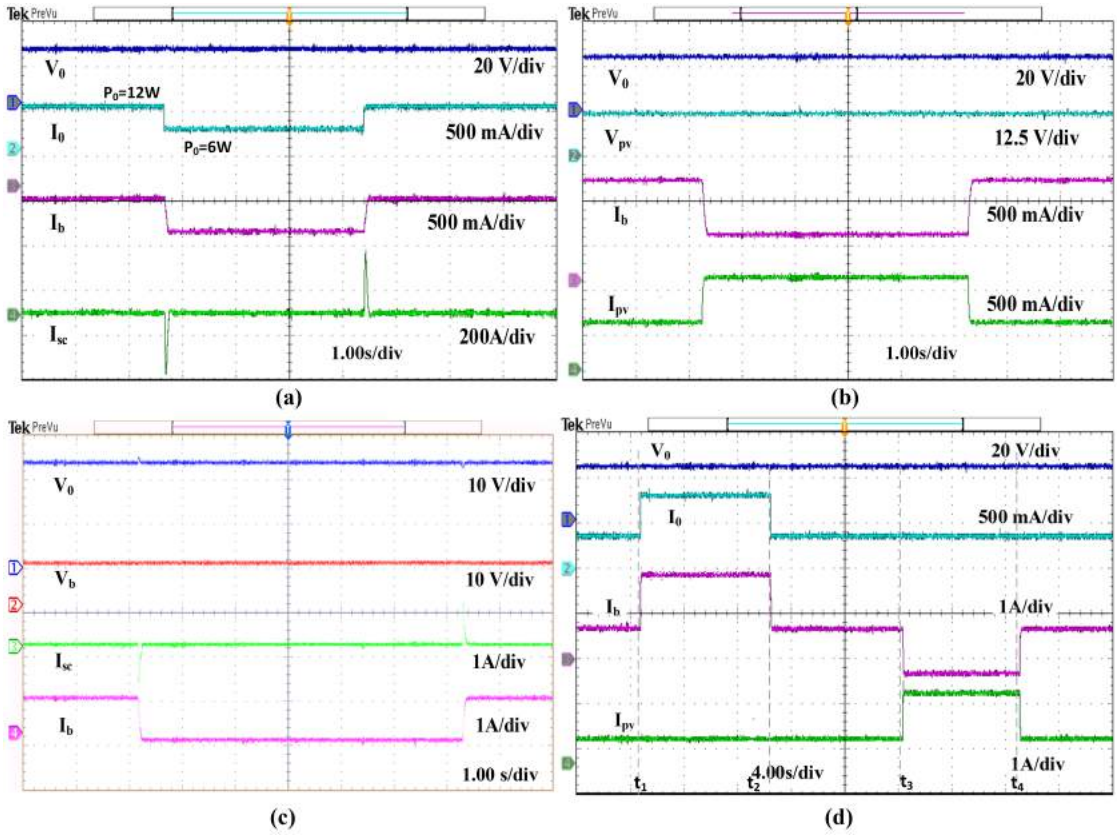

Figure 4.14: Experimental results with 50-75% SC voltage: a) experimental results for 6W to 12W power variation b) PV voltage, PV current, load voltage and battery current during PV variation c) battery voltage, battery current , SC current and DC bus voltage during load change d) system operation under load disturbance and PV disturbance together.

demand is shown in Fig: 4.13 (c). The battery is initially in charging mode and changed to discharging mode after load disturbance. The variation in supercapacitor voltage and current analysis is depicted in Fig: 4.13 (d). The SC voltage is 12 V and the supercapacitor absorbs the transient current of 0.5 A at the time of disturbances. The battery current changes from 1 A to 0.5 A at the time of load reduction. The operation and current sharing during 6 W to 12 W power variations is shown in Fig: 4.14 (a). Further, the PV voltage is maintained at 12 V during operation and battery absorbs the excess power generated during increment in PV generation as shown in Fig: 4.14(b). The DC microgrid operation with measured battery voltage is shown in Fig: 4.14 (c). In the above two cases, the battery and SC voltage is maintained constant irrespective of the disturbances in the system. A summary of DC microgrid operation under different PV generation and load demand is presented in Fig: 4.14 (d). At t_1 and t_2, the load demand

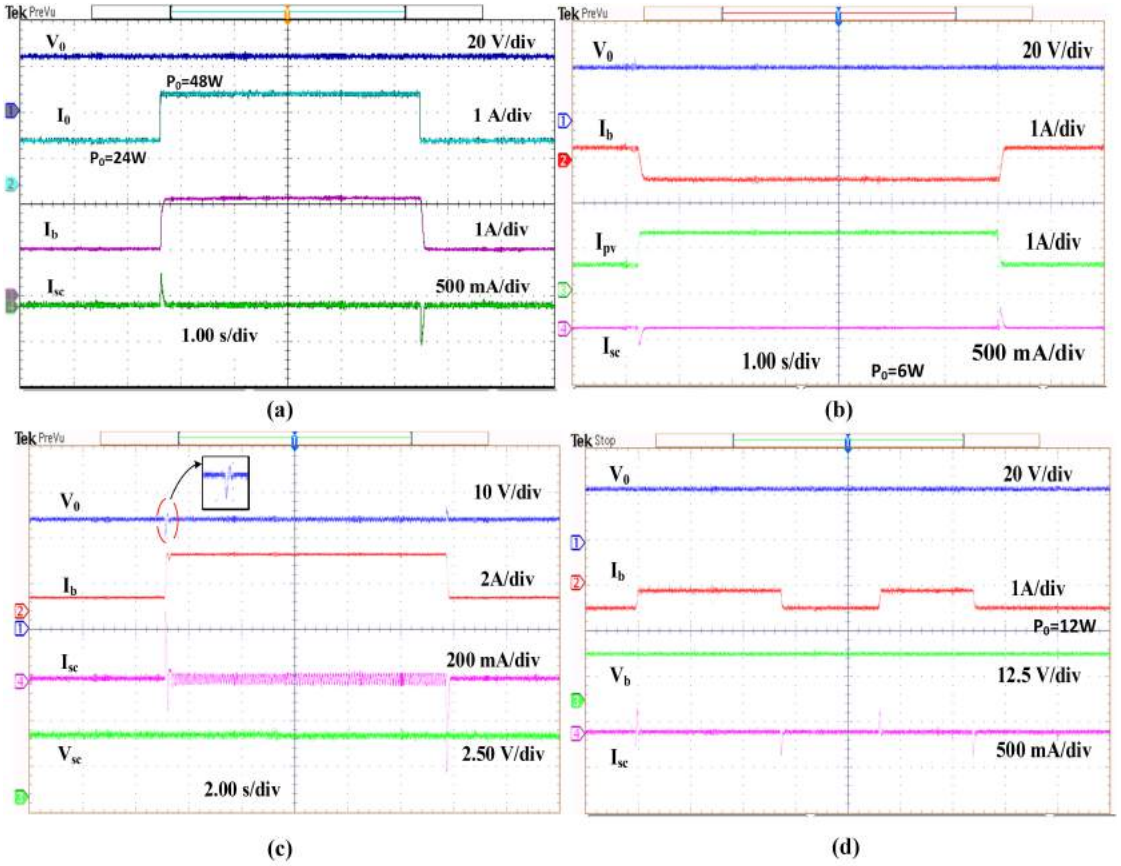

Figure 4.15: Experimental results with 30% SC voltage : a) load voltage, load current battery current and SC current during load disturbance b) load voltage, PV current battery current and SC current during PV disturbance c) oscillations in load voltage and SC current in conventional PI-LPF control strategy d) battery voltage and current during load disturbance.

is varied by 0.5 A. At t_3 and t_4, the PV generation is varied by 1 A. All the excess and deficit power demands are balanced by battery. The SC compensates for the transient power demand. It is significant to note that the DC bus voltage is kept constant at 24 V, regardless of the change in load and source disturbances.

4.6.2 Operation of proposed EMS with 25-37.5 % SC voltage

The proposed control algorithm and SC EMS are verified with lower SC voltage ranges. The cutoff frequency of VBLPF is 100 rad/sec. A 100% load disturbance is applied to verify the system performance with lower SC voltage and VBLPF as shown in Fig: 4.15 (a). The SC is supplying the transient current of 300 mA and the battery is supplying a steady-state current of 2 A. PV current increment and decrement of 0.8 A is applied to the DC microgrid system as shown in Fig: 4.15 (b). The battery changed from discharg-

ing to charging state and SC supplies the transient current with a maximum amplitude of 400 mA. The DC bus voltage is maintained at 24 V irrespective of the variations in load demand and SC voltage.

The system performance is compared with conventional CBLPF control and proposed VBLPF control as shown in Fig: 4.15 (c) and (d). The SC operating voltage is 4.8 V and the battery voltage is 12.2 V. The load demand is increased by 0.5 A and the battery discharges 1 A to meet the load demand. During disturbances, there is an increase in the settling time, and the ringing effect occurs at DC bus voltage due to the application of a CBLPF with lower SC voltage. The increase in the settling time and the ringing effect reduces with the help of VBLPF such that the DC bus voltage settled faster and maintained constant throughout the period. Compared to the conventional method, the proposed method has fewer oscillations in the battery current, supercapacitor current, and DC bus voltage as shown in Fig: 4.15 (d).

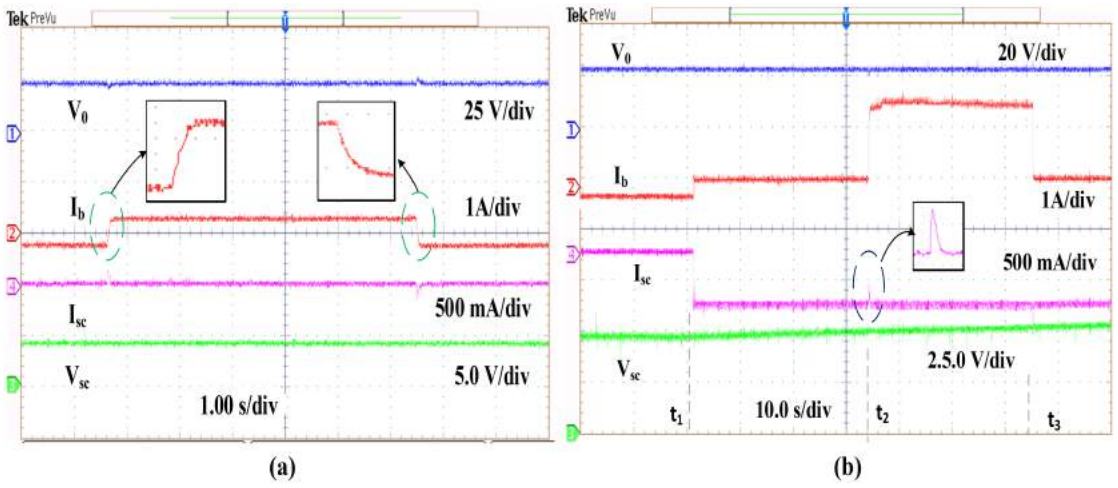

Figure 4.16: Experimental results with 30% SC voltage: a) load voltage, battery current, SC voltage and SC current under proposed control b) charging of SC and DC bus voltage regulation during load disturbance.

4.6.3 Operation with SC charging condition

The charging operation of SC in proposed microgrid conditions is discussed in this section. The SC voltage regulation plays an important role in the HESS energy management strategy. The SC voltage has to charge and discharge based on a particular range of voltage levels. The proposed system operation is depicted in Fig: 4.16 (a). The SC voltage is 4.2 V and the battery is in charging mode during operation. The SC absorbs/delivers

less energy since the SC voltage is less than 50 %. The DC bus voltage has little spikes during disturbances and settles as fast as possible. The charging is depicted in Fig: 4.16 (b). At t= t_1, SC charging is enabled, the SC voltage is seen to be rising and the SC inductor current is seen to be flowing in the negative direction, indicating the charging of SC. At t_2, the load disturbance is applied with battery current demand of 1 A. The load demand is removed at t_2. It is clear from the waveforms that the SC charging is unaffected during disturbances. Further, the battery current is changing smoothly and DC bus voltage has fewer oscillations during operation. The SC voltage is rising from 4.8 V and reached 5.1 V during this period. A summary of hardware studies at different

Table 4.4: A summary of hardware results at different operating points

Load (W)	V_0 **(V)**	I_0 **(A)**	V_{pv} **(V)**	I_{pv} **(A)**	V_b **(V)**	I_b **(A)**	V_{sc} **(V)**	I_{sc}**(Average)** (A)	I_{sc} **(transient) (A)**
48	24	2	12	2	12.2	2	11.8	0	0.8-1
48	24	2	12	2	12.2	2	4.8	0	0.2-0.4
24	24	1	12	1.4	12.2	0.6	11.8	0	0.5-0.7
24	24	1	12	1.4	12.2	0.6	4.8	0	0.2-0.4
12	24	0.5	12	0.5	12.2	0.5	11.8	0	0.3-0.6
12	24	0.5	12	0.5	12.2	0.5	4.8	0	0.1-0.3
6	24	0.25	12	0.3	12.2	0.2	11.8	0	0.2-0.3
6	24	0.25	12	0.3	12.2	0.2	4.8	0	0.1-0.2
SC charging	24	0.5	12	1	12.2	1.4	4.8	-0.5	0.1-0.25

operating points is summarized in Table: 4.4. The analysis presents total power demand and measured voltage and current through the PV, battery, SC and DC loads. With the proposed control method, the effect of variation in SC voltage is limited by regulating the SC reference current using VBLPF. The operation with 73% SC voltage provides more transient current during disturbance. The SC charging current is 0.5 A and transient current during charging is around 0.25 A. In brief, the experimental results agree with the simulation study. The battery and SC share the excess/deficit power that exists in the DC bus. The battery supplies or absorb the average power and SC compensates for the transient power. Hence SC reduces the sudden current stress on the battery and improves the battery life. Further, compared to the conventional CBLPF method, the proposed VBLPF method effectively minimizes the effect of SC voltage variation such as ringing in DC bus voltage and oscillations in battery and SC currents. Hence the VBLPF method effectively manages SC voltage variation and reduces the oscillations thereby improving the battery life during lower SC voltages. Further, the mode shifting due to PV power variation, load variation, and SC charging have less effect on DC bus voltage. The proposed charging scheme shows the charging of SC without affecting DC bus voltage even under disturbances. Hence the VBLPF control scheme provides better

DC bus voltage regulation and SC voltage handling in DC microgrid operation.

4.7 Summary

This chapter proposed a new power sharing scheme with an SC energy management strategy for an isolated PV-DC microgrid with HESS. The proposed control strategy successfully separates the LPF effect from the battery control loop and the VBLPF based EMS leads to better SC utilization at different SC voltage ranges. The developed EMS addresses the DC microgrid in various operating modes and produces a stable and desirable performance. Both the battery and the SC effect on the control loop are considered while modeling the device and designing the outer voltage controller. The HESS is implemented with MPPT controlled PV-DC microgrid and verified for different source and load variations. In contrast to the traditional approach, the simulation and experimental results validate the effectiveness of the proposed system in reducing the oscillations at DC bus voltage and improving the transient and steady-state performances. Several features are illustrated, including quick DC bus voltage regulation, reduced battery current stress, SC charging operation, and mode shift. The system parameters are maintained as per limits during operation, disturbances and mode changes. Furthermore, the suggested EMS eliminates the need for weather forecasts and load current/power measurements, reducing the complexity and number of sensors.

Chapter 5
Hybrid Controller Assisted Voltage Regulation for HESS in DC Microgrid

5.1 Introduction

The goal of a hybrid energy storage system in a DC microgrid is to ensure the regulation of DC bus voltage reference quickly and accurately. The conventional control approaches are challenging to implement with minimal settling time and low overshoot, which leads to significant variations in DC bus voltage [136]. Furthermore, the PI controllers used in conventional strategies add additional phase lag to the control loop and increase the difficulty of parameter tuning. As discussed in literature study, the use of a traditional first-order LPF based power splitting scheme adds delay to the control loop and slows down the system dynamics.

In this contrast, this chapter focuses on a hybrid control strategy for battery-SC HESS that uses a traditional proportional-integral controller for load voltage regulation and simple predictive control for duty calculation. Duty predictive control reduces the tuning burden and provides faster dynamics for HESS current regulation. The proposed predictive control generates the duty in one sampling period, reducing the computational burden. The proposed power splitting scheme for battery and SC is introduced such that it generates battery reference current without the aid of LPF. It reduces the delay in battery reference current calculation and reduces the over-discharge of the battery during the steady-state. A second controller is added to the system as a long-term solution to charge the SC under both steady-state and transient situations. The proposed SC charging strategy did not affect the DC bus voltage regulation and charge/discharge rate of battery current. The vital points of this work can be summarized as follows:

1 The two-stage hybrid controller with a novel power splitting strategy for HESS regulation in PV fed DC microgrid is proposed in this work. While the slow dynamics of the PI controller regulate the DC bus voltage, the discrete nature of duty calculation enables fast dynamics and accurate tracking of battery and SC reference current. The proposed method calculates the required duty in one sample time and reduces the computational burden in the system.

2 The proposed HESS hybrid control follows a simple three-loop structure with external voltage control to regulate DC bus voltage and two predictive control loops for tracking the reference currents. It requires only two parameters to be adjusted for DC bus voltage regulation, reduces the complexity of tuning and settles the DC microgrid faster.

3 In the battery control loop, the proposed power-sharing method eliminates the use of LPF directly. As a result, it ensures accurate battery current tracking and reduces control loop delay.

4 A controlled charging scheme for SC is incorporated to charge SC from the DC bus during regular operation. The Controlled scheme enables charging of SC at regular operation and supplies transient power at the time of disturbances.

5 A detailed controller modelling and analysis are presented to validate the hybrid controller. Further, the controller is tested with simulation ad experimentally for different conditions. In addition, the study is validated by a detailed comparison with the traditional control strategies.

Chapter presented in the following order: Section 5.2 discusses DC microgrid configuration and conventional controller. Section 5.3 explains the proposed control strategy. Section 5.4 and Section 5.5 discuss simulation study and hardware results respectively. Section 5.6 summarizes the work.

5.2 DC Microgrid Configuration and HESS Control Strategy

The proposed autonomous DC microgrid configuration is shown in Fig: 5.1. Three boost converters connect the photovoltaic (PV) panel, battery and supercapacitor to the DC bus. The PV panel converter is a unilateral boost converter based on P&O assisted MPPT control. In HESS, the battery provides the steady-state load power demand, and the SC compensates for the sudden power requirements based on the power decoupling and control strategy. As discussed in chapter 2, the HESS control for the DC microgrid follows a three-layer structure. In the three-layer structure, the outer layer controls the regulation of DC microgrid voltage and generates the reference current. The inner layer determines the control signal/ duty signal based on error in battery and SC currents. The middle layer of the HESS control scheme derives the battery and SC reference currents from the total HESS reference current provided by the outer layer.

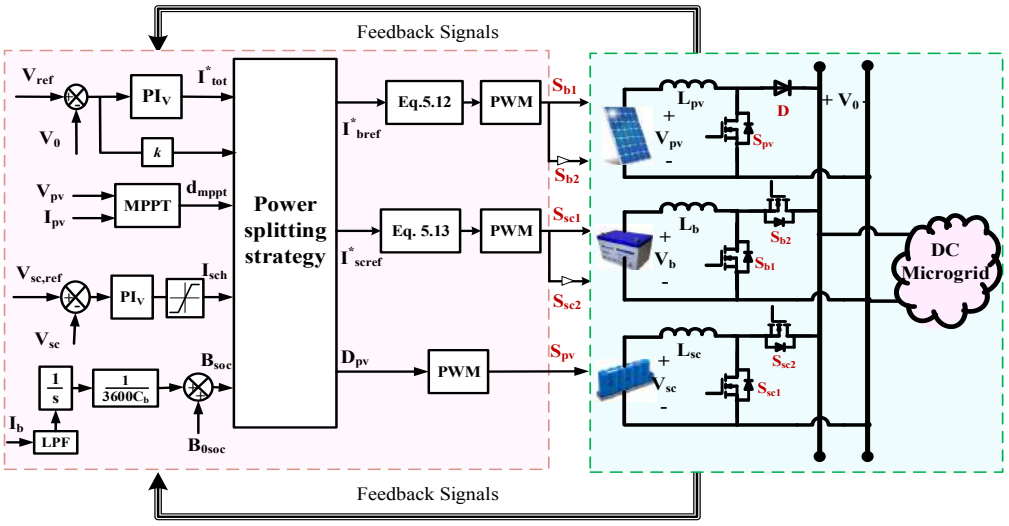

Figure 5.1: Configuration of PV fed DC microgrid and control structure.

5.3 Proposed Control Strategy

The DC microgrid control has two parts via PV module control and HESS control. The PV module uses P&O MPPT technique to extract the maximum power from solar panels. The HESS requires separate controllers to regulate DC bus voltage and power balancing. The traditional HESS control strategy follows a dual loop structure with PI controllers. However, it is demanded to tune three PI controllers with six parameters to obtain optimum performance. On the other hand, the hybrid controller combines the ability of traditional PI controllers with the speed of prediction control, as shown in Fig: 5.2. The PI controller is designed to regulate the DC bus voltage, and the predictive control is used to control the HESS currents. The battery and SC current reference are generated using an LPF decoupling strategy. The primary function of the HESS control strategy are i) generation of total HESS current reference from DC bus voltage error, ii) transient and steady state power allocation between battery and SC iii) generation of modulating signals for power converter based on prediction and iv) control of SC voltage and battery state of charge regulation.

5.3.1 Control of PV module

This work uses the basic P&O MPPT technique to control PV panels. In the P & O algorithm, the duty signal is controlled in steps to reach the maximum power point.

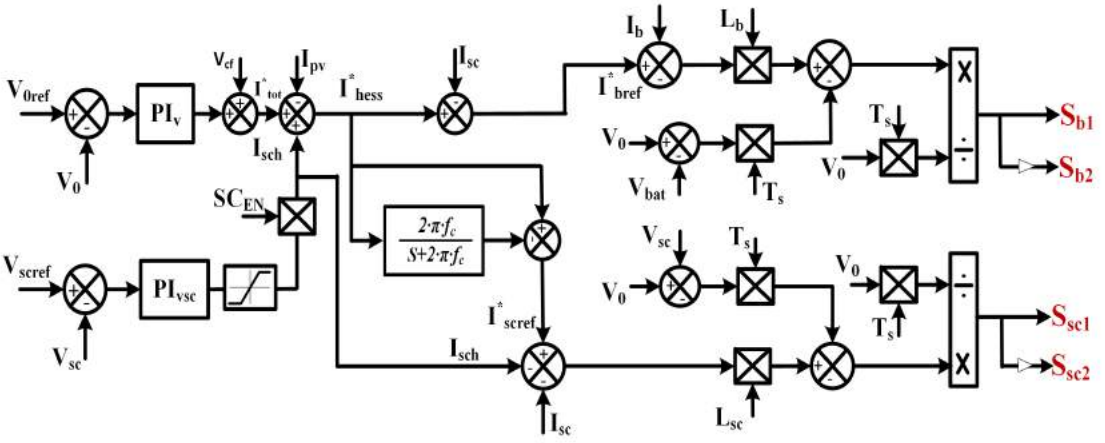

Figure 5.2: Block diagram of proposed hybrid controller with SC charging scheme.

First, the PV power (δP_{PV}) and PV voltage (δV_{PV}) variations with previous samples are recorded and then compared to produce the duty pulse for the next instant [27].

5.3.2 Power balance and reference generation

The total DC microgrid current reference is generated by outer voltage controller (PI_v) based on error in DC bus voltage. The proposed power sharing strategy decides the reference current for battery and SC. The total power balance in the system can be written as:

$$P_L(t) = P_{PV}(t) + P_{bat}(t) + P_{sc}(t) = P_{avg}(t) + P_{tr}(t) \tag{5.1}$$

Where $P_{PV}(t), P_{bat}(t), P_{sc}(t), P_L(t)$ are the PV power, battery power, SC power and load power. $P_{avg}(t)$ and $P_{tr}(t)$ represents the average and transient power exist in the load bus. The sudden power demand is compensated by the SC and the average power is balanced by PV and battery. The charging of supercapcitor is controlled by SC_{EN}. Under SC charging, SC_{EN} made unity. $P_{sc,ch}(t)$ is the charging power of SC.

$$P_{PV}(t) + P_{bat}(t) = P_L(t) + P_{sch}(t) \tag{5.2}$$

$$P_{sch}(t) = -P_{sc} \tag{5.3}$$

The $P_{sch}(t)$ is positive during charging and negative during discharging. The total HESS

current reference including SC charging current can be given as:

$$i^*_{hess} = i^*_{bref} + i^*_{sc} = i^*_{tot} - i_{pv} + V_{cf} + i_{sch} \cdot SC_{EN} \tag{5.4}$$

Where, V_{cf} is the voltage compensation factor used to improve the dynamic performance of microgrid. It can be represented in discrete form as

$$V_{cf}(k) = G * dv + V_{cf}(k-1) \tag{5.5}$$

Where $dv = V_{0ref} - V_0$ and G is the voltage compensation gain. G is selected in such a way that G= 0 for dv $>$ 1 and a small positive number less than 1 for dv $<$ 1. The feedback of the previous state allows reducing the error in DC bus voltage. The total HESS reference current is split into the battery and SC reference current using the power splitting strategy.

$$i^*_{hess} = i^*_{bref} + i^*_{scref} \tag{5.6}$$

Where,the total current reference is i^*_{tot}, SC current reference is i^*_{scref}, battery current reference is i^*_{bref} and total HESS current reference is i^*_{hess}. The average battery current component of HESS current by considering charging is calculated by:

$$i^*_{bref} = i^*_{hess} - i_{scref} \tag{5.7}$$

$$i^*_{scref} = i^*_{hess}(1 - LPF) \tag{5.8}$$

The LPF with cutoff frequency f_c is given by:

$$LPF = \frac{2 \cdot \pi \cdot f_c}{s + 2 \cdot \pi \cdot f_c} \tag{5.9}$$

The main aim of LPF in the proposed method is to generate supercapacitor reference current. A high value of f_c leads to poor operation of supercapacitor unit. Also, a low value of f_c leads to sluggish response in the control system. Hence based on literature and simulation, the f_c is selected as 5 Hz [91].

5.3.3 HESS current control and duty signal generation

The duty calculation is a simple method to get the required duty to regulate the DC microgrid. To regulate the HESS currents, the inductor equations are used to calculate the duty. The battery and SC inductor current average equations can be given as:

$$\frac{L_b(di_b(t))}{dt} = V_{bat}(t) - V_0(t)(1 - d_b(t)) \tag{5.10}$$

$$\frac{L_{sc}(di_{sc}(t))}{dt} = V_{sc}(t) - V_0(t)(1 - d_{sc}(t)) \tag{5.11}$$

After expanding equations (5.10) and (5.11) using euler's difference law [30], rearranging for modulating signals $d_b(k+1)$ and $d_{sc}(k+1)$;

$$d_b(k+1) = \frac{T_s(V_0(k) - V_{bat}(k)) + L_b(I^*_{bref} - I_b)}{T_s V_0} \tag{5.12}$$

$$d_{sc}(k+1) = \frac{T_s(V_0(k) - V_{sc}(k)) + L_{sc}(I^*_{scref} - I_{sc})}{T_s V_0} \tag{5.13}$$

The d_b and d_{sc} signals are compared with a sawtooth waveform of period T_s, to get the duty pulses for the SC and battery converter. The prediction based duty calculation determines the required modulating signal in one cycle, which reduces the computational burden and improves the dynamics of the control system. The overall block diagram of the proposed PI- predictive hybrid controller with SC charging scheme for HESS is shown in Fig: 5.2.

5.3.4 DC bus voltage control

The outer voltage controller computes the total DC microgrid reference current concerning the error in DC bus voltage. The RHPZ that appeared in the boost converter model results in unwanted oscillations in DC bus voltage [24]. Thus the PI controller design requires extra care in selecting the bandwidth for the outer voltage control loop. The outer voltage controller computes the required current reference from the voltage error. The SISO tool in MATLAB [23] and the overall transfer function without the controller are used to tune the PI controller parameters. The phase margin of 60^0 and bandwidth of 700 rad/sec are selected to ensure stable voltage regulation [24]. The designed values are k_p= 0.25 and k_i= 160.

5.3.5 Supercapacitor voltage control

To control the SC voltage, an additional voltage controller is added. The charging is active only if $SC_{EN} = 1$. During operation, the SC voltage varies from 100 % to 0 % depending on the power requirement. However, the useful energy varies nonlinearly concerning the reduction in voltage. For example, 75 % of useful energy is dissipated when SC voltage reduces to 50 %. Hence the lower limit of SC operating voltage is set at 50 %. Below 50 %, the SC_{EN} enables to charge of the SC unit. The SC charging current (I_{sch}) is added to the i^*_{tot} such that the sudden change in system current is split between battery and SC as shown in Fig: 5.2. The charging current is decided by the SC voltage control PI and saturation limit. The PI values selected as K_{psc}= 0.2 and K_{isc}= 5. The new HESS reference current for HESS considering SC charging current is given by:

$$i^*_{hess} = I^*_{tot} - I_{pv} + I_{sch}SC_{EN} \tag{5.14}$$

The new SC reference current is given by:

$$i^*_{scref} = i^*_{tot} - i^*_{bat} - I_{sch}SC_{EN} \tag{5.15}$$

5.3.6 Analysis of effect of parameter variation

This section analyzes the effect of parameter variation on calculated duty. Figure 5.3 shows the average value of calculated duty for battery and SC converter. From equations (5.12) and (5.13), the duty mainly depends on converter filter inductance, battery voltage, and SC voltage. The calculated duty is plotted against each parameter by considering other parameters are at 80%. The variation in calculated duty with respect to converter inductance is shown in Fig: 5.3 (a). The plot shows that the reduction in inductance increases the duty to supply the required current. Further, an increase in inductance than the designed value has less effect on duty. It is important to note that the duty increases to the upper peak as the SC voltage lowers. Sometimes this may lead to duty saturation in a practical scenario. Hence, fixing the lower limit of SC voltage during operation is important. The charging of SC is added to address this issue such that SC charging enables below 50 % of SC voltage. The SC converter duty variation against SC voltage variation is plotted in Fig: 5.3 (b). The calculated SC duty varies between 0.6 to 0.96. Below 50% of SC voltage, the duty is increased above 0.8. Because, at lower SC voltage, it requires high duty to regulate the load voltage. On the other hand,

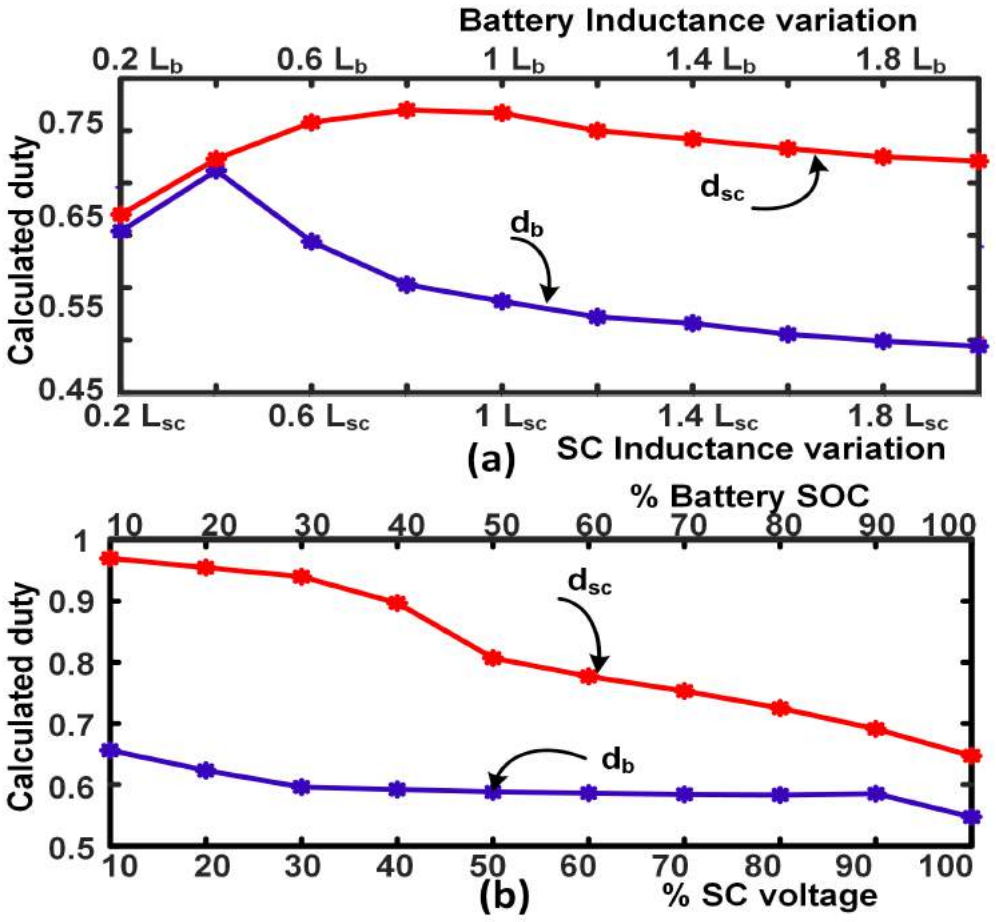

Figure 5.3: Variation in calculated battery and SC duty signal with respect to a) converter inductance variation b) battery SOC variation and SC voltage variation.

the battery voltage will be almost constant irrespective of the SOC. Hence, the variation in calculated duty is limited to 0.55 to 0.65 as battery SOC varies, as shown in Fig: 5.3 (b).

5.4 Simulation Results

This section presents the simulation results of the proposed scheme by considering two test cases. The control system and system model are created using simulink blocks in MATLAB. With the ultimate objective to exhibit the ampleness of the proposed strategy, it is tested and differentiated from traditional methods. The lead-acid model of 48 V, 28 Ah is utilized as a battery. The switching frequency used for circuit operation is 20 kHz. The PV module is selected at a maximum peak voltage of 61.4 V and 1 kW of power. MOSFET switches are selected to provide the bidirectional capability for the

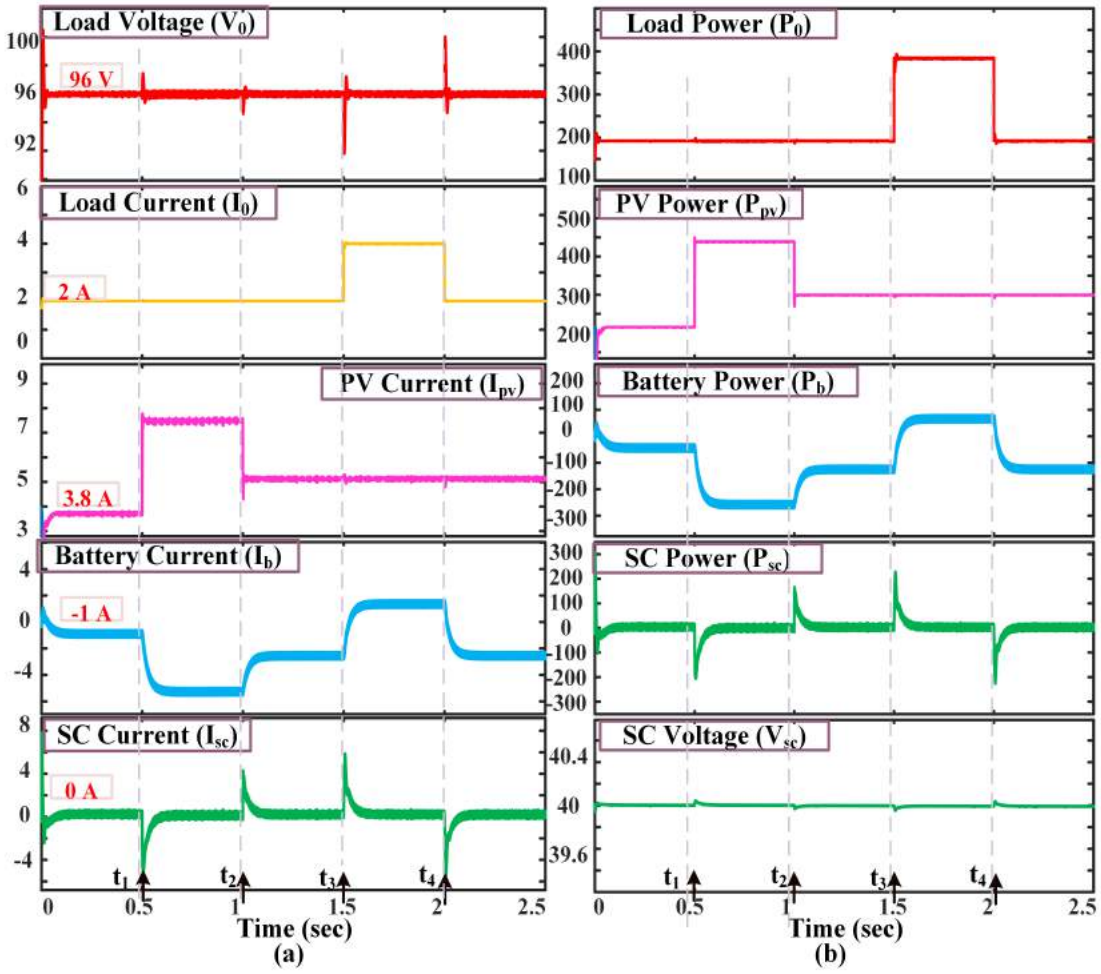

Figure 5.4: Simulation results: a) DC bus voltage, load current, PV current, battery current and SC current b) load power, PV power, battery power, SC power, SC voltage.

boost converter. The simulation parameters are presented in Table: 5.1. The proposed approach simulation results for two test cases are examined below.

5.4.1 DC bus stabilization: step variation in PV generation

The PV generation is disturbed to verify the operation HESS. Figure 5.4 shows the waveform for simulation under different instances. Initially, PV supplies load demand and the additional PV power is stored in the battery. SC current is zero during this period. At t= 0.5 sec, the PV generation increases from 3.8 A to 7.6 A. Battery charges from the excess power supplied by the PV. The SC absorbs the sudden excess power created in the DC bus. At t= 1 sec, the PV current reduces to 5.2 A due to reduced irradiance. The battery absorbs the excess power during the period. The load current

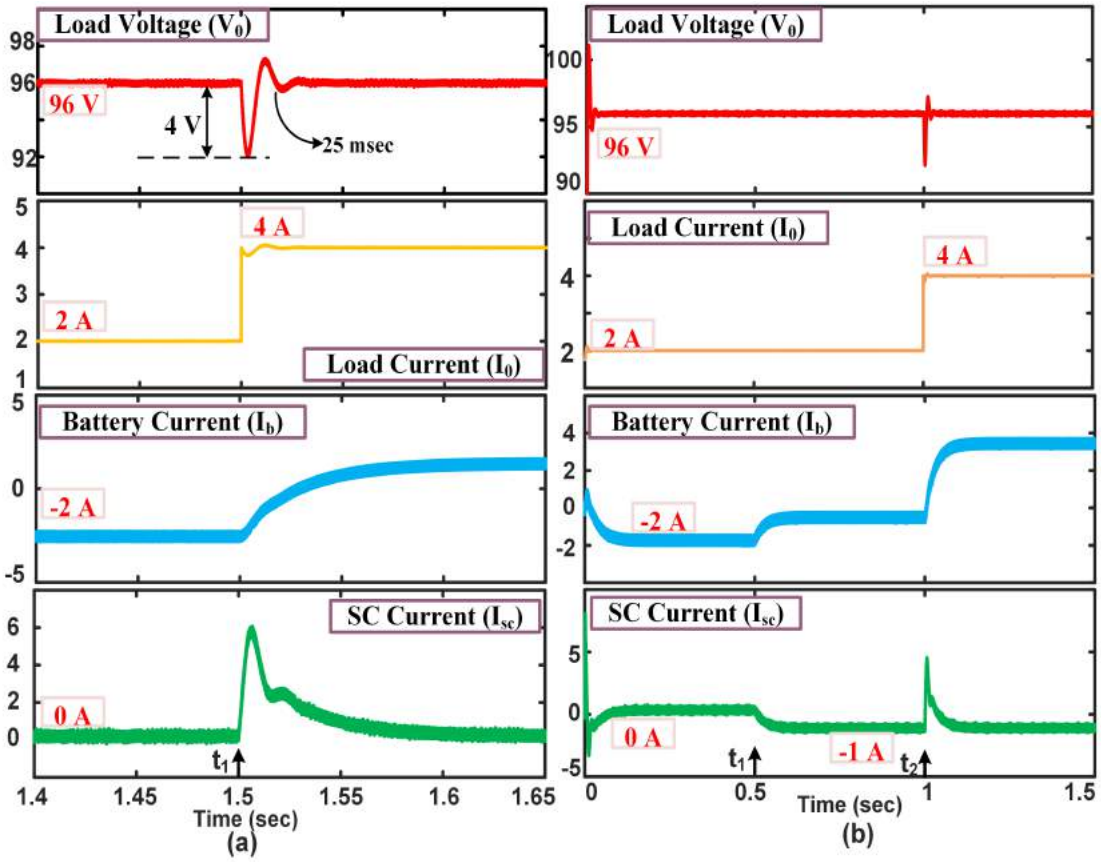

Figure 5.5: Simulation results: a) enlarged portion of load disturbance b) controlled charging of SC under load disturbance.

Table 5.1: Rating of DC microgrid components considered for simulation study

S.No	Parameter	Values
1	PV panel ratings considered	V_{pv}= 61.4 V, I_{pv}= 16.3 A
2	SC unit	V_{sc}= 48 V, C_{sc}=19.3 F
3	Battery unit	48 V, 21 Ah
4	DC-DC converter system	L_{pv}= 3.1 mH, L_b= 2.3 mH, L_{sc}=2.3 mH, C_{0dc}= 430 μF, R_L= 24 Ω
5	Rated output power, P_{out}	1 kW
6	Switching frequency, f_{sw}	20 kHz
7	Load voltage, V_0	96 V

during this period is 2 A. The time taken by the DC bus voltage to settle back to the original voltage is approximately 20 msec. Also, the battery and supercapacitor currents reached the new steady-state value of 150 msec.

5.4.2 DC bus stabilization: step variation in load demand

The connected load across the DC bus is varied using a controlled switch. Load demand increases by 2A in t = 1.5 sec and returns to the previous state in t = 2 sec. Since PV generation is constant, the HESS forces provide the excess load demand and battery current increases from -3 A (charging) to 2 A (discharging). The SC supplies the sudden power requirement, thereby facilitating a smooth change of battery current. The 100 % change in the load current fluctuates the DC bus voltage by 4.166 %. The disturbance is mitigated within 30 msec and enables faster settling of DC bus voltage. Load power, PV power, battery power, SC power, and SC voltage are shown for different cases in Fig: 5.4 (b). A enlarged portion of load increment is shown in Fig: 5.5 (a). At the time of disturbance, the battery change to discharging state from charging, and SC absorbs the transient power. The maximum peak ripple voltage is 4 V and the settling time is approximately 25 msec.

Further, the duty variation during load disturbance is analyzed to understand the duty calculation technique. The calculated duty of battery and SC are given in Fig: 5.6 (a) and (b). The battery shows consistent duty compared to SC. However, since SC supplies the transient and ripple power, its calculated duty has more variations during the disturbance. In summary, the DC bus oscillations due to PV variations are limited compared to load variation. Further, the battery and SC share the average and transient power during disturbances.

5.4.3 DC bus stabilization: SC charging

The charging process starts once the SC voltage is less than 50% of the rated voltage. The controller mentioned in Section 3.3 operates when the $SC_{EN} = 1$. The charging of the SC is shown in Fig: 5.5 (b). At t= 0.5 sec, SC_{EN} made unity and the SC starts charging. The charging does not affect the rate of change of battery current, and the fluctuation in DC bus voltage is negligible. At, $t = t_2$, 100% load disturbance is applied. The battery provides the additional current required by the load, whereas SC provides instantaneous power without deviating from charging.

5.4.4 Comparison with traditional methods

The proposed hybrid control strategy is compared with traditional PI control strategies and similar topologies. A summary of the comparison is presented in Table: 5.2. The similar three-level control strategies and proposed power splitting scheme with PI con-

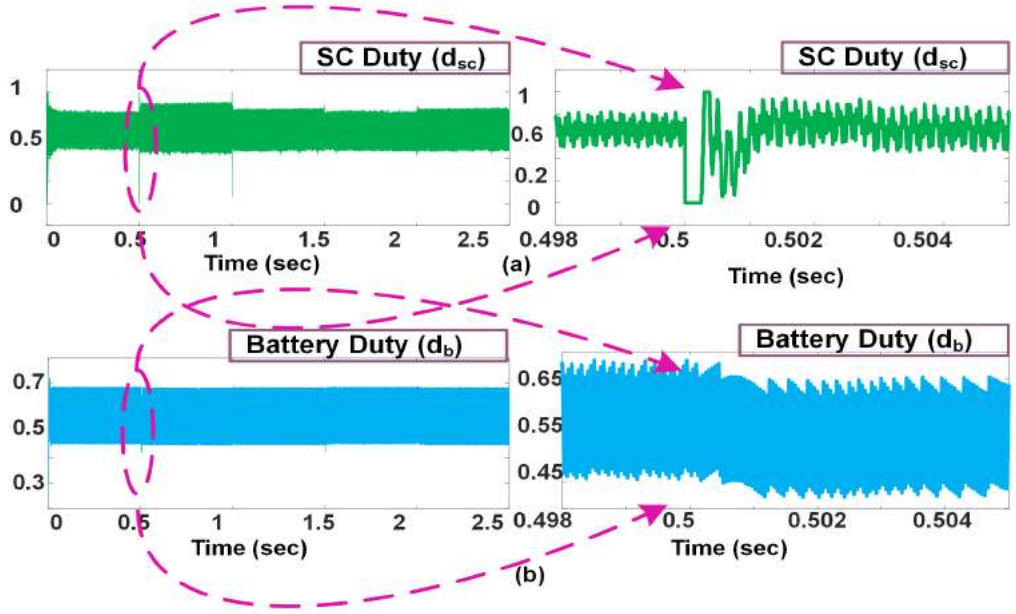

Figure 5.6: Simulation results of calculated duty PV disturbance a) SC converter duty signal b) battery converter duty signal.

troller and hybrid control strategies are compared to verify the effectiveness of the proposed method. All control strategies are simulated and compared for same power level. The traditional control strategy [135] with LPF shows high peak variation and settling time compared to other methods. The second method utilizes the power splitting strategy based on battery current as shown in Fig: 2.3 (c) [96]. This method reduces the peak overshoot below 5% and settling time below 50 msec. The proposed power splitting strategy with PI controllers shows settling time below 40 msec and peak overshoot below 5%. However, the above cases require three PI controllers, and their simultaneous tuning becomes complex for implementation. The use of prediction and PI together reduces the lag effect on the control system and improves the DC bus voltage control dynamics. As a result, the proposed method shows a 43 % reduction in peak overshoot and a 62 % reduction in maximum settling time compared to the conventional approach [135]. Also, the proposed system has less the 4.2% peak overshoot and 30 msec settling time.

5.5 Hardware Implementation and Discussion

A low-power hardware prototype has been developed to test the proposed hybrid controller for the PV DC microgrid depicted in Fig: 5.7. The dSPACE DS1104 real-time

Table 5.2: Comparative study of hybrid and conventional control strategies

Parameters	**[135]**	**[96]**	**PI+LPF [137]**	**Proposed**
%Mp load change	6-8.5%	3.8-5%	3.8-4.6%	3.6-4.2%
%Mp PV change	2-3%	1.5-2%	1.5-1.8%	1-1.5%
Settling time (ms)	60-100	30-50	30-40	20-30
Control strategy	PI	PI	PI	Hybrid
SC voltage regulation	No	No	Yes	Yes
No. of tuning parameters	6	6	6	2

platform is used to develop the controller for this experiment. A regulated power supply is manipulated as a PV source in this experiment [96]. A boost converter is employed to control the PV currents. The battery and SC rating is 12 V, 7 Ah lead-acid type, and Maxwell BMOD0058 16 V, 58 F. The function of the HESS microgrid is tested in several scenarios. The nominal DC bus voltage is selected as 24V. The details of the prototype are listed in Table: 5.3. The total hardware operation can be divided into four modes via mode-I: load increment, mode-II: load decrement, mode-III: PV increment, and mode-IV: PV decrement. The proposed approach in hardware results for different modes are explained as follows.

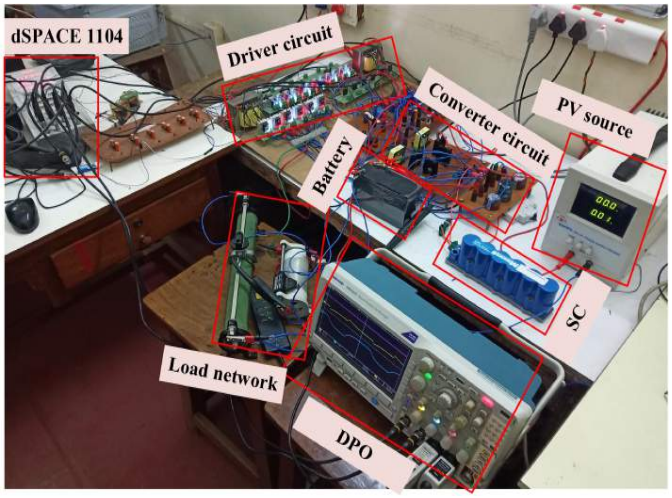

Figure 5.7: Experimental setup for HESS assisted PV-DC microgrid.

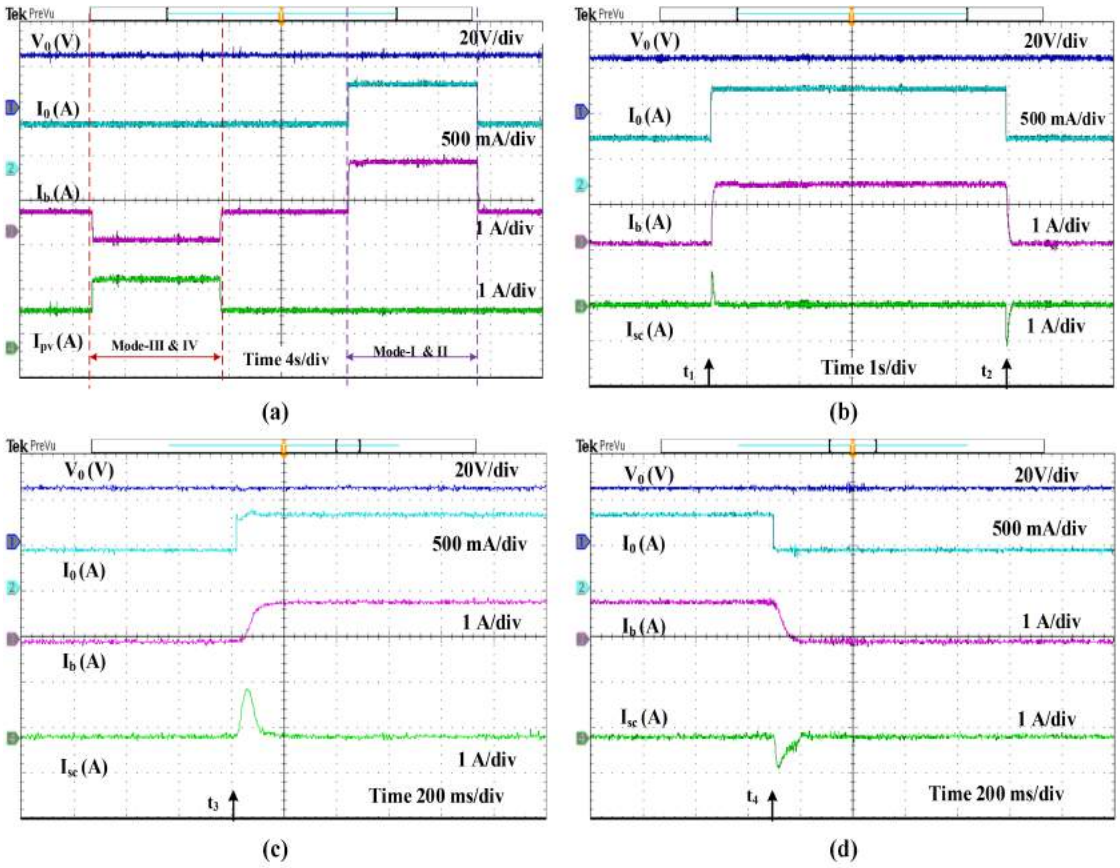

Figure 5.8: Experimental results: a) DC bus voltage, load current, PV current, and battery current during mode-I, II, III & IV b) DC bus voltage, load current, battery current and SC current during load disturbances c) enlarged view of mode-I d) enlarged view of mode-II.

Table 5.3: Rating of hardware setup

S.No	Component	Specifications
1	Manipulated PV source with DC supply	V_{pv}= 12 V,I_{pv}=2 A
2	supercapacitor unit	V_{sc}= 16 V, C_{sc}=58 F
3	Battery	V_{sc}= 12 V, 7 Ah, lead acid
4	DC-DC converter system	L_{pv}= 4.1 mH, L_b=2 mH, L_{sc}=2 mH,C_0=440 μF
5	Nominal power for Hardware, P_{out}	24 W
6	Switching Frequency, f_{sw}	20 kHz
7	Load Voltage, V_0	24 V

5.5.1 Change in connected load

Here, the load variations are created by connecting two rheostats in parallel through a mechanical switch. The overall system performance tested with load and source disturbances are demonstrated in Fig: 5.8 (a). The PV current is changing from 0.9 A to 1.7 A and load demand varied from 0.5 A to 1 A. During load disturbance (mode-I & II), the PV generation is constant and battery current increases to meet the load demand. The load voltage, battery current, SC current and load current during load disturbance are shown in Fig: 5.8 (b). Initially, the PV supplies the load demand and the battery current is 0 A during this period. The load changes from 0.5 A to 1.1 A and the battery current changes from 0 A to 1.2 A. The enlarged portion of load increment and load decrement are shown in Fig: 5.8 (c) and (d). It is clear from the results that the DC bus voltage has fewer oscillations during load disturbance. In addition, the battery provides only average power, and the SC compensates for transient power. The DC microgrid at different operating points are summarized in Table: 5.4.

Table 5.4: A summary of microgrid operation

Mode	**Load Power (W)**	V_0 **(V)**	I_0 **(A)**	V_{pv} **(V)**	I_{pv} **(A)**	V_b **(V)**	I_b **(A)**	V_{sc} **(V)**	I_{sc}**(Average) (A)**	I_{sc} **(transient) (A)**
I& II	24	24	1	12	1	12.2	1.2	11.8	0	0.8-1
I& II	12	24	0.5	12	1	12.2	0	11.8	0	0.8-1
III& IV	12	24	0.5	12	1.4	12.2	-0.4	11.8	0	0.5-0.7
III& IV	7.2	24	0.3	12	1.3	12.2	0.7	11.8	0	0.8-1
SC charging	16	0.7	12	1.2	12.2	1.2	8	0	-0.5	0.4-0.5

5.5.2 Change in PV generation

When the PV generation changes, the HESS charge or discharge load depends on the demand. A summary of increase and decrease in PV generation is shown in Fig: 5.9 (a). Initially, PV generation is more and battery current shows negative due to charging. At t_1, PV current reduces from 1.1 A to 0.6 A. As a result, the battery changes from charging to discharging with 0.3 A. At t_2, PV current increases to 1.1 A and again increases to 1.5 at t_3. During this period, the battery starts to charge as the PV generation exceeds the load demand. At t_3, the battery charger with a current of 0.6 A. In all PV changes, the SC compensates for the transient current and the battery balances the average current. At t_4, The PV current changes from 1.5 A to 0.6 A forcing the battery to discharge more power. The battery current changes to 0.3 A and SC supplies transient current with the peak of 1 A. A further enlarged portion of PV disturbance are shown in Fig: 5.9 (b), (c) and (d). It is clear from waveforms that the DC bus voltage has

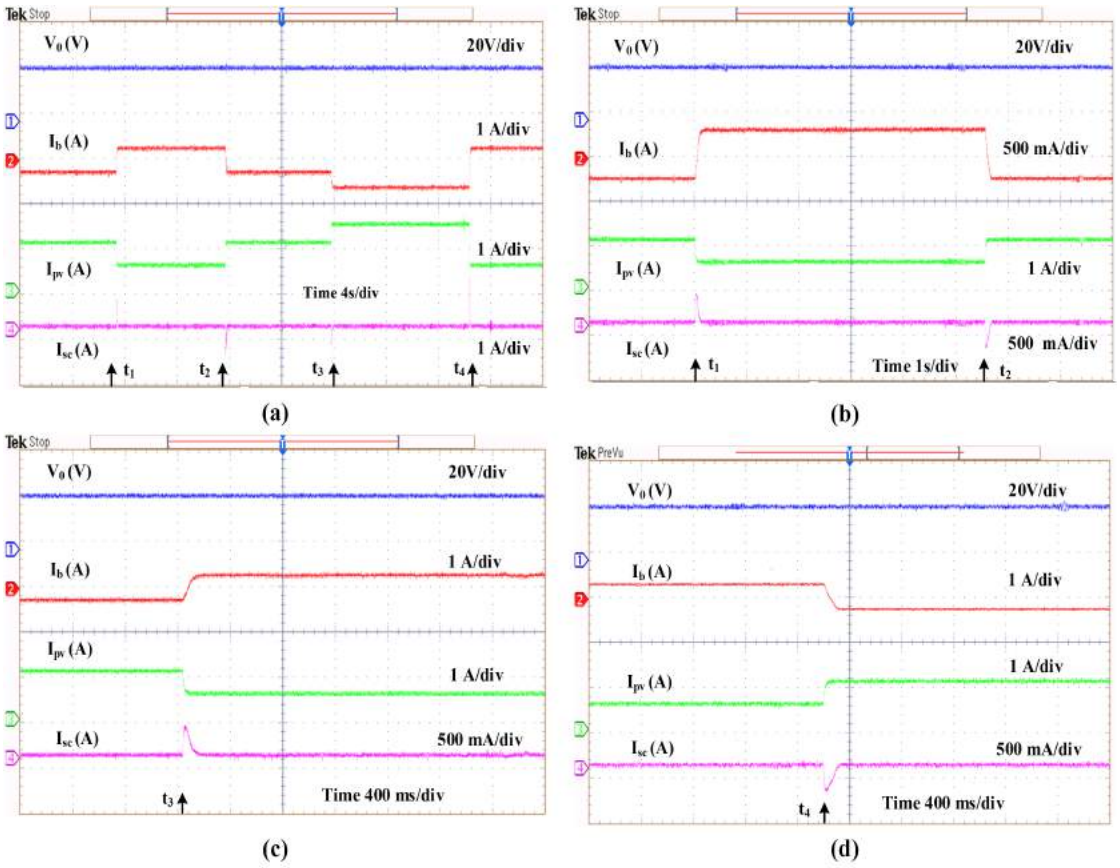

Figure 5.9: Experimental results: a) DC bus voltage, PV current, SC current, and battery current during PV disturbance (mode-III & IV) b) DC bus voltage, PV current, battery current and SC current during PV disturbances c) enlarged view of mode-III d) enlarged view of mode-IV.

minimal variations during oscillations and SC absorbs the transient power according to the control strategy.

5.5.3 Charging of SC

To verify the SC charging scheme, SC_{EN} is made unity at t_1. Initially, the battery is charging from the DC bus with -0.4 A, SC current is 0 A, SC voltage is 8 V and DC bus voltage is constant at 24 V. At t_1, the SC started charging from DC bus with 0.8 A as shown in Fig: 5.10 (a). The battery current changes to 0A to support SC charging. At t_2, load disturbance is applied to verify the charging of SC during disturbances. As a result, the battery current increases from 0 A to 1.2 A, and SC provides the transient current with a peak amplitude of 1 A. The DC bus voltage has a minimal dip during the load disturbance. In summary, the SC can support t battery during charging and supply

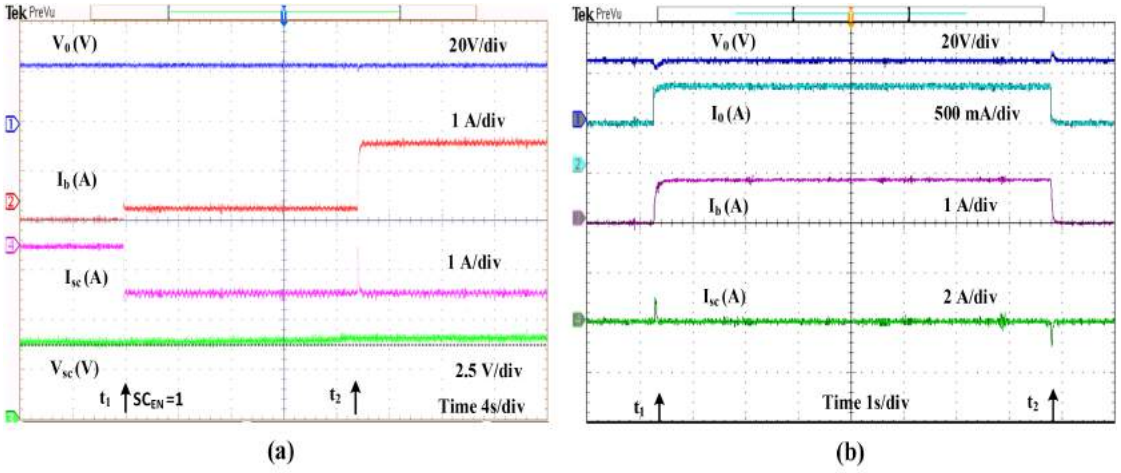

Figure 5.10: Experimental results: a) DC bus voltage regulation with SC charging b) DC bus voltage, battery current, load current and SC current with conventional PI-LPF control strategy.

the transient power without affecting the DC microgrid operation.

5.5.4 Comparison with conventional PI method

The conventional PI-LPF based control of HESS has a simple structure compared to the proposed hybrid controller. The proposed method requires a minimum of five sensors to implement the hardware whereas the conventional requires four sensors to implement it with SC charging scheme. On the other hand, the simulation study shows that the conventional system has more DC bus oscillations during load disturbances and takes more time to reach the steady-state than the proposed method. Figure 5.10 (b) shows the experimental waveforms for conventional PI-based DC microgrid. Initially, the battery is charging from the DC bus and the load demand is 0.4 A. At t_1, the load demand is increased by 100 %. The load voltage shows a variation of 1.8 V to 2 V, whereas the proposed strategy shows voltage variation less than 0.5 V. It is clear from the waveforms that the DC bus voltage peaks are more in the conventional method compared to the proposed hybrid control strategy.

5.6 Summary

This paper presents a hybrid controller for HESS with a new power-sharing strategy for an isolated PV fed DC microgrid. The proposed controller combines a PI controller for DC bus voltage regulation and predictive control for HESS current tracking. Further, the power splitting scheme is incorporated with the controller and can generate battery ref-

erence current without the direct aid of LPF. This feature improves the DC microgrid's dynamic power-sharing and DC bus voltage regulation along with the discrete control.

Initially, the DC microgrid system and the hybrid controller are designed and analyzed for possible variations in the system. The calculated duty for the battery has a minimal dependency on parameter variation. On the other hand, the computed duty signal for SC tends to reach upper saturation at less than 50 % SC voltage. Hence, a charging controller is incorporated to charge the SC while operating at lower SC voltages. The steady-state and dynamic performance of the autonomous microgrid is assessed by offline simulation and verified experimentally using a laboratory prototype. The proposed system offers a 43 % decrease in peak overshoot and a 62 % decrease in maximum settling time compared to the traditional PI-LPF control technique.

Finally, the experimental studies are conducted to validate the performance of proposed controller performance. It is clear from the experimental results that the DC bus voltage has fewer oscillations during operation, HESS balances the power demand in the DC microgrid, and SC compensates for the transient power. To sum up, the proposed hybrid controller integrated autonomous DC microgrid able to achieve 1) fast dynamic voltage regulation, 2) proper power-sharing of battery and SC during steady-state and transient period, 3) smooth charging of SC below 50 % of SC voltage, and 4) reduces the complexity in modelling and parameter tuning for implementation. According to the findings, combining PI with predictive control improves the dynamics and assures proper power-sharing of HESS in an isolated DC microgrid.

Chapter 6
Controlled Power Sharing of HESS in PV Fed DC Microgrid

6.1 Introduction

This chapter presents a hybrid control strategy to improve the control and power-sharing of a hybrid energy storage system used in an isolated DC microgrid. While the photovoltaic panel is the primary energy source, the battery and SC work together to meet the additional power requirements [81]. A modification to the traditional filter method for dividing the average and transient HESS current components is done by replacing the LPF with a discrete rate limiter to ensure proper power splitting and smoother battery discharge. The rate limiter integrates power balance into the system and allows for the integration of battery discharge rates, eliminating the problems caused by the unintentional selection of the cut-off frequency. In addition, the HESS current outputs are no longer affected by low-order LPF phase delay.

A two-level hybrid controller with internal duty prediction control and external PI voltage control is proposed in this chapter. Two independent duty prediction controls are used to control the battery converter and the SC converter. The proposed duty prediction control of converters relies on basic modeling equations and generates the control signals in one iteration. This helps to reduce the computational burden and enables fast settling of DC bus voltage. The coordinate operation of predictive control and PI control depends on the power-sharing between battery and SC. The rate limit unit is introduced to split the current components using a more explicit term that directly indicates the permissible battery charge/discharge rates and eliminates the lagging behavior in LPFs. Further, the combination of duty prediction with the rate limiter ensures rapid dynamic response of the SC while effectively achieving proper reference tracking on slow dynamic battery current. An additional controller is added to the system as a permanent solution for charging of SC. Unlike many other SC charging schemes, the proposed method does not affect the DC bus voltage regulation and charge/discharge rate of battery current. The DC microgrid system is simulated and tested experimentally with various source and load variations to test the effectiveness of the proposed architecture.

The main contributions of this chapter include,

1 An improved two-stage hybrid controller with a rate limiter for HESS power decoupling in PV DC microgrid is proposed in this work. The discrete nature of duty prediction enables faster dynamics, and the rate limiter provides controlled decoupling of HESS reference current.

2 A simple SC charging method is implemented for the regulation of SC voltage. The proposed method charges the SC without affecting the DC bus voltage and rate of change of battery current.

3 In addition, the proposed rate limiter-based power decoupling method balances the DC bus power in single iteration. Hence it reduces the delay imposed by the LPF on the control loop and reduces the burden in computation.

4 Unlike a battery, the reduction in SC voltage results in the ringing of DC bus voltage. The proposed control method mitigates the effect of SC voltage variation on DC bus voltage and battery current.

5 The proposed system mitigates the effect of variation in PV generation and load demand effectively with minimal voltage variation and settling time.

This article has been organized as; section 6.2, Configuration and control of PV-DC Microgrid. Section 6.3 discusses the proposed HESS power sharing and control strategy for HESS. In section 6.4 shows the simulation results and case studies using MATLAB/Simulink. In section 6.5, hardware results are presented to validate the simulation results. Finally, section 6.6 summerizes the work.

6.2 Proposed HESS Power Sharing and Control Strategy

The specific DC microgrid system integrated with HESS is shown in Figure 6.1 as discussed in chapter 5. The proposed control strategy combines the simplicity of conventional PI controllers and the fastness of prediction control strategies. It uses the PI control strategy to regulate the load bus voltage. A power splitting-based energy management algorithm is introduced to split the total HESS power demand into the battery and SC reference current. The inner current controller predicts the required duty pulses

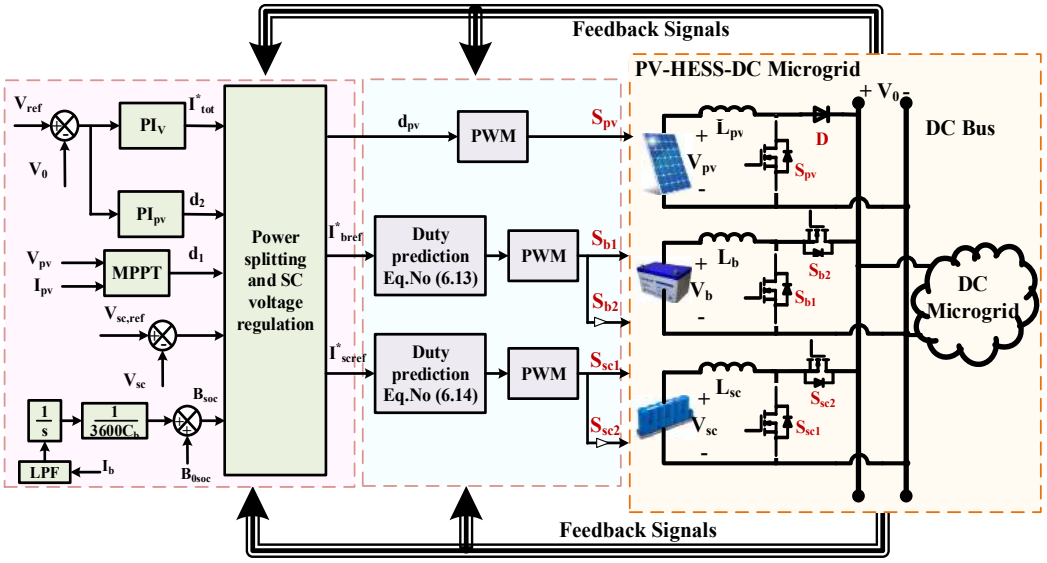

Figure 6.1: The PV- DC microgrid system configuration showing HESS, PV, power electronic converters and control schemes.

based on error current. The predictive control calculates the values in a single iteration and reduces the complexity of optimization and tuning. Equations (6.9) and (6.10) provide the dynamic model of the converter utilized for predictions, whereas equations (6.13) and 6.14 represent the duty prediction, as obtained in section 6.2.1. Further, a part of the error voltage is added to the HESS current reference to reduce the steady-state error associated with predictive control. The proposed HESS control system has three parts.

a Generation of HESS current reference from error DC link voltage.

b A Power management algorithm consists of power balancing and power splitting between battery and SC.

c Modulating signal prediction utilizing battery and SC inductor currents, as well as a dynamic DC/DC converter model that assures the lowest DC bus voltage.

6.2.1 HESS reference current generation

The reference current generation needs to ensure that the power supplied by HESS and PV must meet the load demand. The power generated by the PV source is independent

of the load demand. Hence the HESS has to supply the deficit power to load during PV generation reduces and need to store the surplus power during PV generation exceeds load demand. The system is given by:

$$P_{PV}(t) + P_{bat}(t) + P_{sc}(t) = P_L(t) = P_{avg}(t) + P_{tr}(t) \tag{6.1}$$

Where $P_{PV}(t), P_{bat}(t), P_{sc}(t), P_L(t)$ are the PV power, battery power, SC power and load power. $P_{avg}(t)$ and $P_{tr}(t)$ represents the average and transient power exist in the load bus. The total average power is supplied by battery and PV together. The transient power occurs during starting, and disturbances are supplied and absorbed by the SC unit. The total power in the DC bus can be given by;

Under steady state condition

$$P_{bat}(t) = P_L(t); P_{sc}(t) = 0 \tag{6.2}$$

The power sharing during SC voltage regulation mode (SC_EN =1) is given by

$$P_{PV}(t) + P_{bat}(t) = P_L(t) + P_{sc}^{ch}(t) \tag{6.3}$$

$$P_{sc}^{ch}(t) = -P_{sc} \tag{6.4}$$

During charging of SC, $P_{sc}^{ch}(t)$ is positive and it is negative during $P_{sc}^{ch}(t)$ discharging mode. The SC_EN = 1 is enabled when V_{sc} discharged to lower limits. From the power balance equation, battery reference current can be written as:

$$i_{bref} = \frac{V_{dc}}{V_b} i_{ref} + i_{sch} \tag{6.5}$$

At transient conditions, the discharge of i_{bref} is limited by rate limiter. The rate limiter is designed in such a way that it modifies the i_{bref} based on the previous state. The algorithm used for splitting the total current to steady-state and transient current is shown in Fig: 6.2, $'r'$ is the limiting value for the battery current discharge rate. If $i_{bref}(k+1)$ denotes the i_{bref} for next sampling instant and $i_{bref}(k)$ denotes the i_{bref} value for the previous instant and the absolute difference between these two is greater than r then $i_{bref}(k+1)$ is modified as;

$$i_{bref}(k+1) = i_{bref}(k) \pm r \tag{6.6}$$

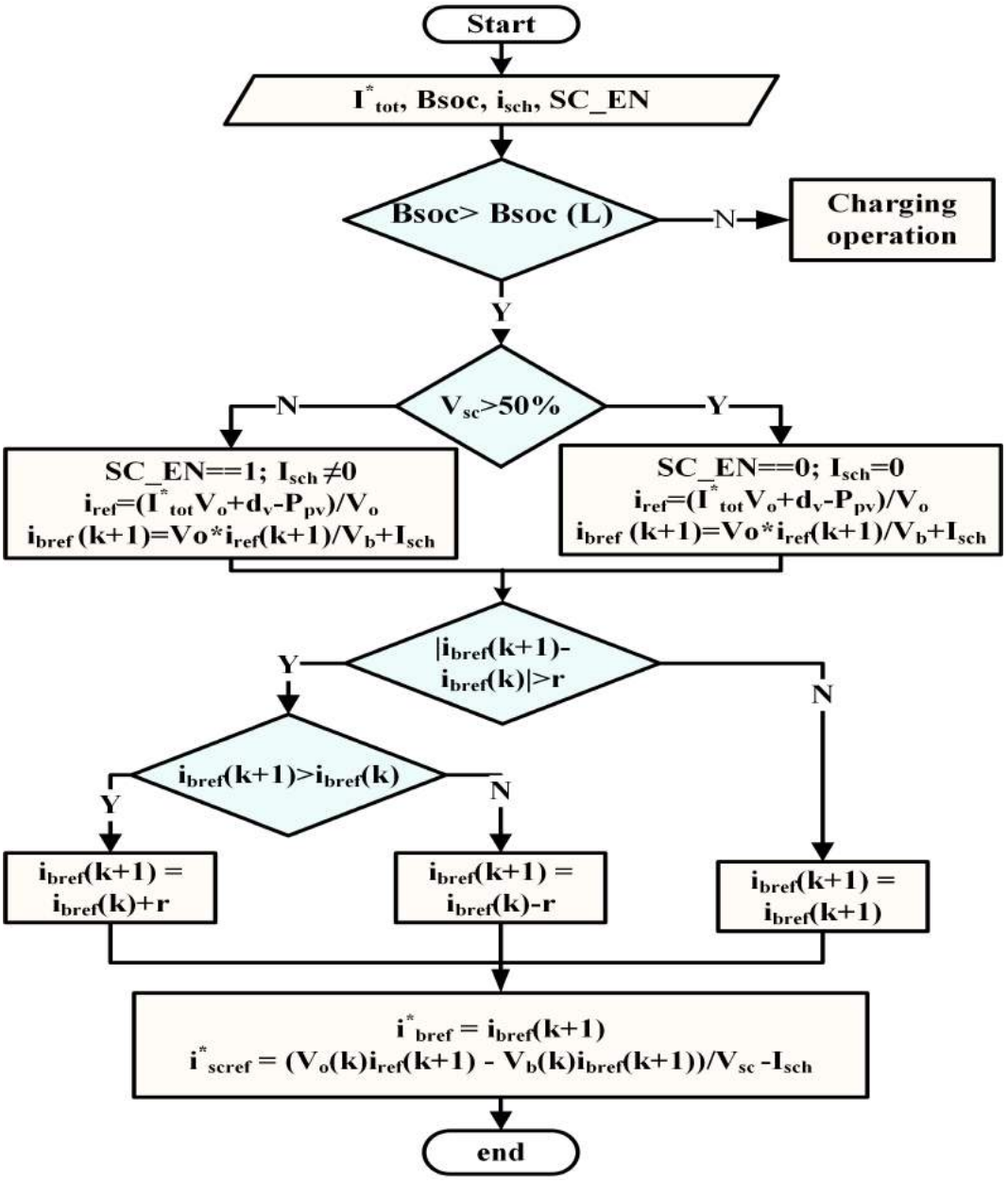

Figure 6.2: Schematic representation of rate limiter based reference current generation by considering SC charging.

The SC should supply the remaining i_{ref} current during this interval to maintain the power balance in the system.

$$i_{scref}(k+1) = \frac{i_{ref}(k+1)V_0(k) - V_b(k)i_{bref}(k+1)}{V_{sc}(k)} \tag{6.7}$$

6.2.2 Outer voltage controller design

The outer voltage control loop plays a crucial role in the DC bus regulation. The right-hand zero of the boost converter directly affects the load voltage. Hence the controller parameter selection requires utmost care in the case of the outer loop controller. The outer loop voltage controller is given as:

$$PI_v = K_{pv} + \frac{K_{iv}}{s} \tag{6.8}$$

The outer voltage controller receives the error between the reference voltage and the actual voltage. The controller generates the complete current reference for the corresponding error. The outer voltage controller design utilizes the overall transfer function of the system. The PI parameters for the outer voltage control loop are designed using the method given in reference [91]. The phase margin and bandwidth of the control loop are 60^0 and 600 rad/sec, respectively. The designed values are k_p= 0.25 and k_i= 160.

6.2.3 HESS current control and duty pulse generation

The average voltage balance equation for inductors is developed to calculate the modulating signals based on reference current, battery, and SC inductor currents. The duty signals are calculated with help of average model bifurcation using Euler approximation [138]. The averaged equation for L_b is given by,

$$\frac{L_b(di_{bat}(t))}{dt} = V_b(t) - V_0(t)(1 - d_b(t)) \tag{6.9}$$

For L_{sc}, the current equation is

$$\frac{L_{sc}(di_{sc}(t))}{dt} = V_{sc}(t) - V_0(t)(1 - d_{sc}(t)) \tag{6.10}$$

After expanding equations (6.9) and (6.10) using Euler's difference law [138];

$$\frac{L_b(i_b(k+1) - i_b(k))}{T_s} = V_{bat}(k) - V_0(k)(1 - d_b(k)) \tag{6.11}$$

$$\frac{L_{sc}(i_{sc}(k+1) - i_{sc}(k)}{T_s} = V_{sc}(k) - V_0(k)(1 - d_{sc}(k)) \tag{6.12}$$

From the perspective of model bifurcation, equation ((6.11)) and ((6.12)) can be rearrange to obtain modulating signals d_b and d_{sc}. Also, the $i_{sc}(k+1)$ and $i_b(k+1)$ indicates the reference target for SC and battery current. In other words, the $i_{sc}(k+1)$ and

$i_b(k+1)$ can be written as I^*_{scref} and I^*_{bref}. The signals at k^{th} sampling instants indicates the actual measured signals in the system.

$$d_b(k+1) = \frac{T_s(V_0(k) - V_b(k)) + L_b(I^*_{bref} - I_b)}{T_s V_0} \tag{6.13}$$

$$d_{sc}(k+1) = \frac{T_s(V_0(k) - V_{sc}(k)) + L_{sc}(I^*_{scref} - I_{sc})}{T_s V_0} \tag{6.14}$$

By comparing d_{bat} and d_{sc} with a sawtooth waveform of period T_s, the duty pulses S_{bat} and S_{sc} can be generated. As a result, the HESS regulates the power demand their operating characteristics. The duty predictive control computes the d_{bat} and d_{sc} in real-time within one cycle. That helps the HESS respond quickly to PV and load variations and improves the dynamic performance of the overall system. The overall block diagram of the proposed PI- predictive hybrid controller for HESS is shown in Fig: 6.1.

6.2.4 Supercapacitor voltage control

The SC voltage regulation is achieved by adding an additional PI controller. The controller is active only when the SC_EN= 1. Unlike a battery, SC voltage can vary from 100 % to 0 % during operation. The 75 % of the stored energy in a SC is available at 100 % to 50 % voltage range. Further decaying in SC voltage leads to adverse effects on the DC bus voltage [43]. Hence the lower limit of SC voltage is fixed at 50 % as shown in Fig: 6.2. The SC charging reference current is added to the total reference current and subtracted from the SC current such that a sudden change in battery current is eliminated. Corresponding total HESS current reference and SC current reference are as follows.

$$i_{ref} = \frac{I^*_{tot} V_0(k) + dv(k) - P_{pv}(k)}{V_0(k)} + I_{sch} \tag{6.15}$$

$$i_{scref}(k+1) = \frac{i_{ref}(k+1)V_{dc}(k) - V_b(k) i_{bref}(k+1)}{V_{sc}(k)} - I_{sch} \tag{6.16}$$

Where $dv(k)$ is the compensating factor added to reduce the steady state error. $dv(k)$ is given by;

$$dv(k) = m(V_{ref} - V_0(k)) + dv(k-1) \tag{6.17}$$

The error constant 'm' is a small positive integer chosen to reduce the error in DC bus voltage and helps the HESS current to reach the correct steady state value.

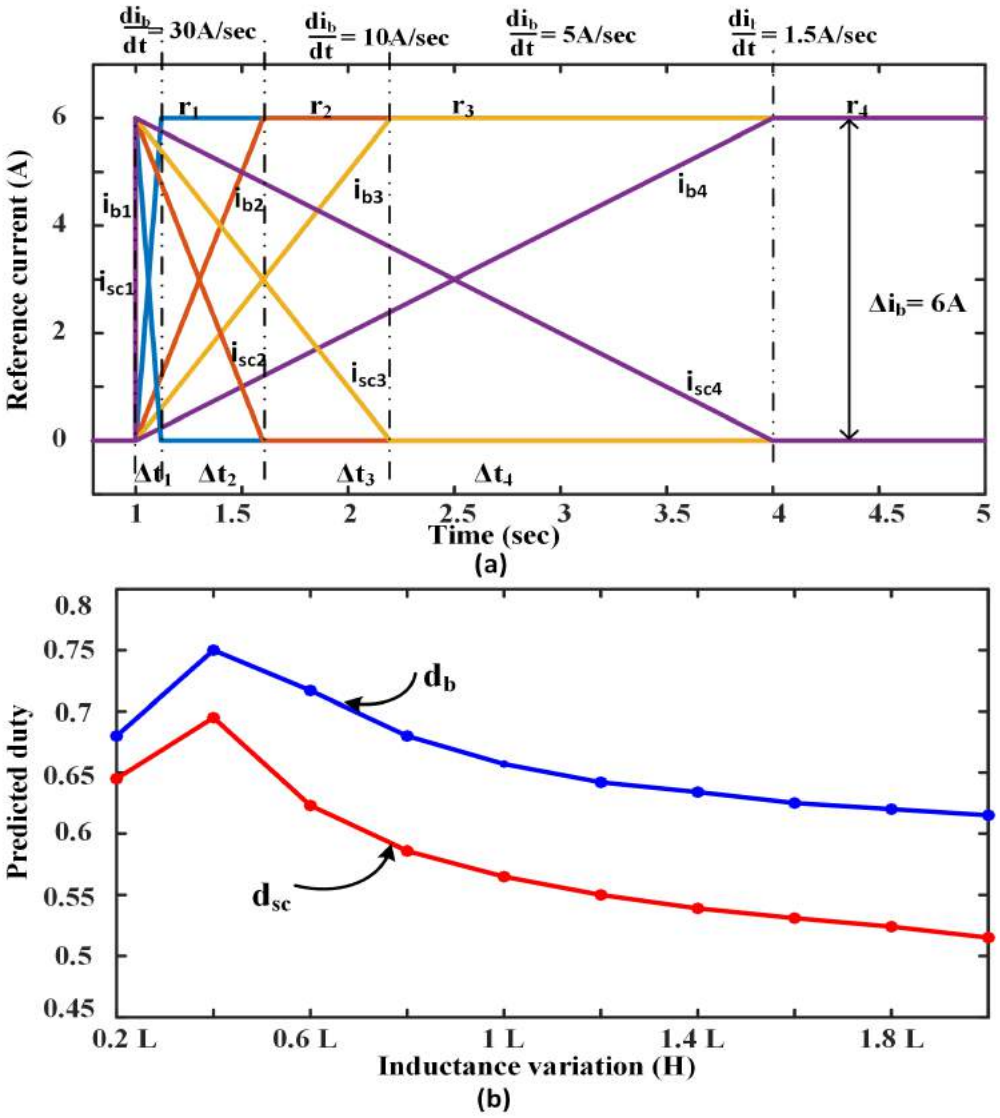

Figure 6.3: Analysis of effect of variation in parameters a) selection of rate limiter constant and battery rate of discharge b) dependency of predicted duty on inductor parameter variation.

6.2.5 Analysis of effect of parameter variation

The operation of the proposed controller is mainly affected by the prediction accuracy and rate limiter constant (r). The rate limiter effect on the battery and SC reference current generation is depicted in Fig: 6.3 (a). The load disturbance considered here is the same for all cases and is applied at 1sec. The required average current is in 6 A. With high 'r' value indicates fast settling of battery and SC current. As the 'r' value decreases, it takes longer for the battery current to reach its final state. Further, the

Table 6.1: Rating of DC microgrid components considered for simulation study

S.No	Component	Specifications
1	PV panel	V_{pv}= 60 V, I_{pv}=14.7 A
2	Supercapacitor	V_{sc}= 48 V, C_{sc}=19.3 F
3	DC-DC converter	L_{pv}= 3.1 mH, L_b=2.3 mH, L_{sc}=2.3 mH, C_{0dc}=430 μF
4	Output power, P_{out}	1 kW
5	Switching Frequency, f_{sw}	20 kHz
6	Load Voltage, V_0	96 V

final reaching time depends on the HESS current to be supplied. The duty prediction depends mainly on the variance in the inductor rather than the capacitor. The variation in predicted battery and SC duties based on variation in inductor values are presented in Fig: 6.3 (b). The predicted duty is higher at lower inductor values, which allows the inductor to store more power. On the other hand, the variance in duty after the specified inductance value is modest, which indicates that the increase in inductance has little effect on the duty prediction.

6.3 Simulation Results and Case Studies

To verify the proposed system, an extensive simulation study is conducted in MATLAB/Simulink®. The simulation parameters used for the study are developed based on basic converter modeling given in [139] and the selected parameters are shown in Table: 6.1. From Fig: 6.3, the 'r' value is selected as 20 A/sec. The DC microgrid system performance with proposed control structure is verified under four scenarios via, (i) increment in PV generation (scenario-I, at t= t_1) (ii) decrement in PV generation (scenario-II, at t= t_2) (iii) increment in load demand (scenario-III, at t= t_3) (iv) decrement in load demand (scenario-IV, at t= t_4).

6.3.1 System operation under disturbances

The simulation results are presented for validating the operation system variables at disturbances and power balance among the different devices. The system parameters such as V_0, I_0, I_b, I_{sc} and I_{pv} under various scenarios are shown in Fig: 6.4 (a). The system power sharing at different instants is shown in Fig: 6.4 (b). Initially, the PV generation and load demand are equal. Therefore, the HESS current is almost zero

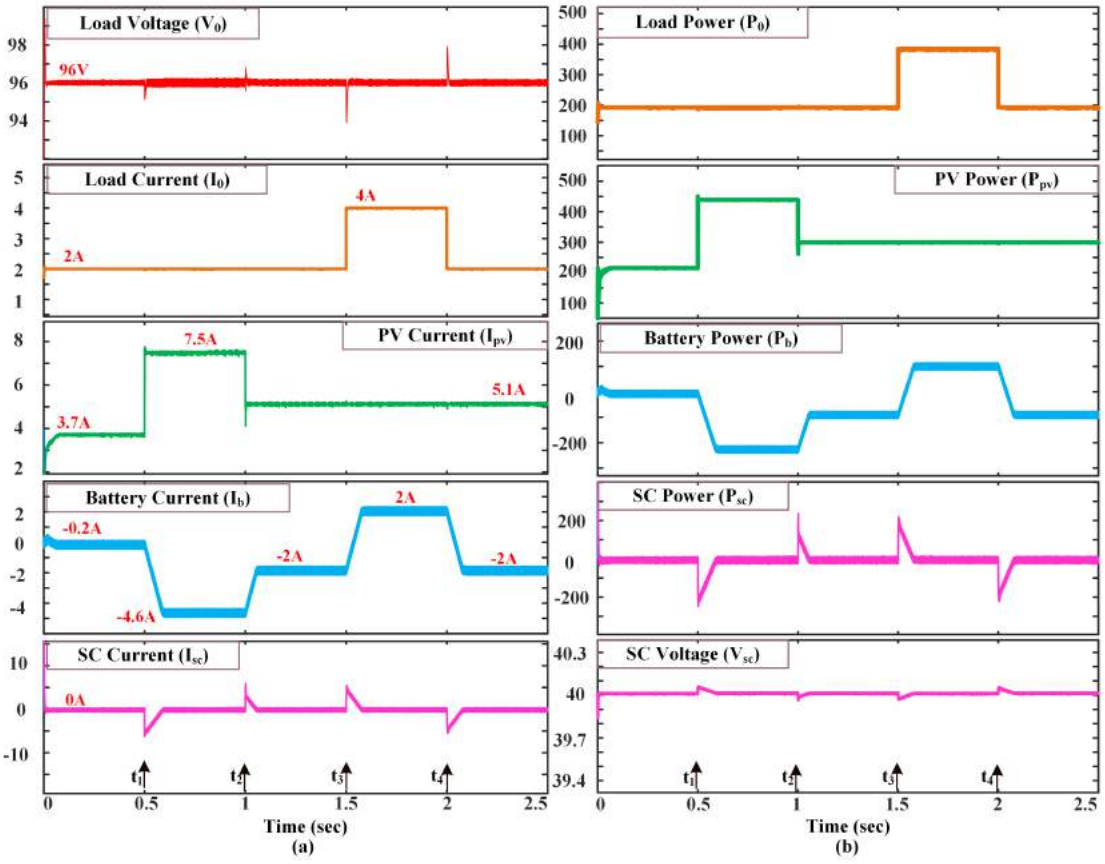

Figure 6.4: Simulation results: a) system parameters under different source and load variation; load voltage, load current, PV current, battery current, SC current b) power supplied, dissipated and absorbed by PV, load, battery and SC respectively.

during this period. At t= t_1, the increase in PV generation from 200 W to 450 W causes the injection of extra power to the system. The battery absorbs the excess steady state power, and the SC absorbs the transient pressure. The load voltage dip (2 %) at the time of disturbance and regains its actual value in 7 milliseconds. In conventional control strategies, the rise occurs after the dip. The proposed system is settled before a further rise in voltage. The system regulates the increase in 100 % load demand at t= t_3 with reduced load bus variations. From Fig: 6.4 (a), it is clear that DC bus voltage maintained constant at 96 V in all scenarios with a small disturbance at the time of disturbance, the change in battery current is slower, and the SC is compensating the transient current. The total load power demand is shared between the PV, battery, and SC. The SC supplies power only at the time of disturbances that make the SC voltage almost constant during steady state operation, as shown in Fig: 6.4 (b).

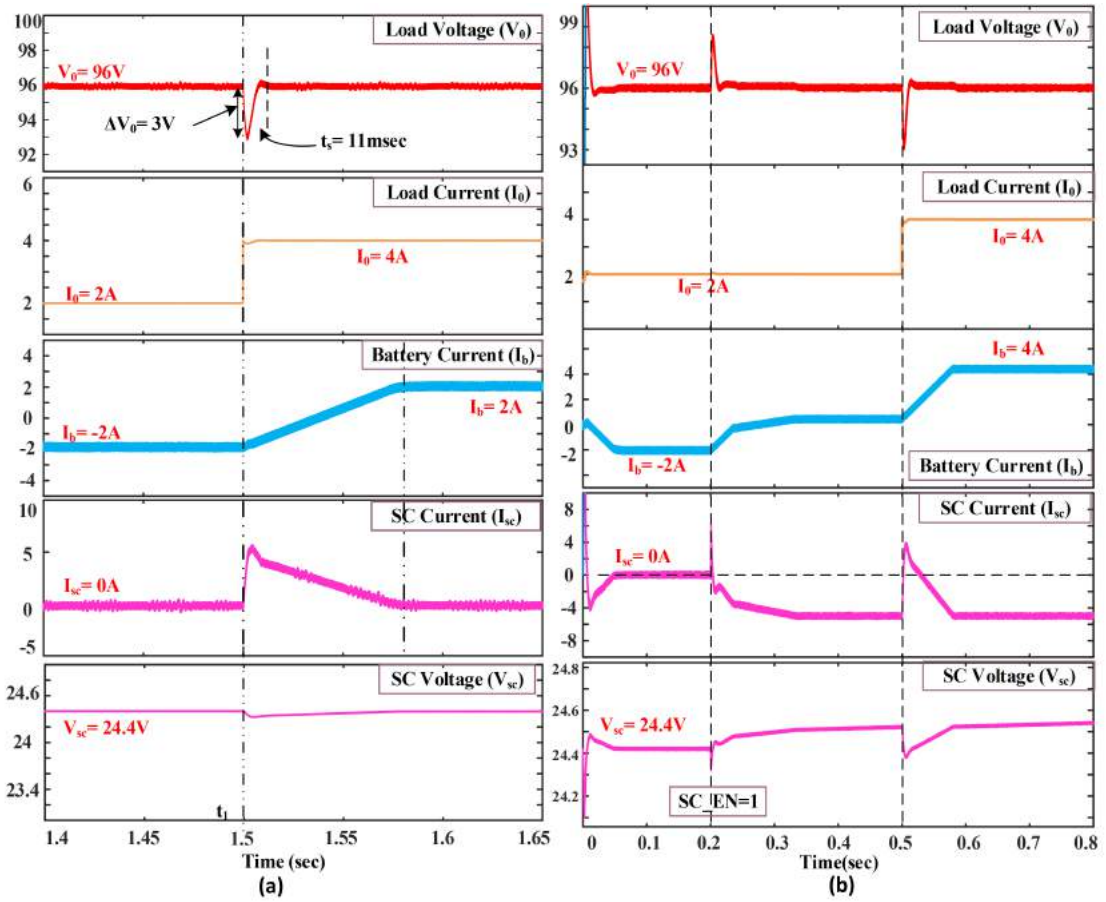

Figure 6.5: Simulation results: a) enlarged view of scenario-III with 50% SC voltage b) super capacitor charging under load disturbance.

6.3.2 System operation under 50 % of supercapacitor voltage

The battery and SC current sharing during scenario- III with 50 % SC voltage is shown in Fig: 6.5 (a). At t= t_1, the load current is increased from 2 A to 4 A. The battery current changes to the new state from charging to discharging with a slow rate of change, and the SC delivers the excess power demand. The enlarged portion compares the time taken by load current, battery current and SC current to reach the final state. With 80 % of SC voltage, the DC bus fluctuates nearly 2 V, and with 50 % voltage, the DC bus voltage variation is 3 V. Compared to the traditional control technique, the reduction in SC voltage has less impact on DC bus voltage. Further to verify the charging of SC from the main system, scenario-III with $SC\_EN = 1$ is considered in Fig: 6.5 (b). Initially, the system is at a steady state with PV= excess power mode, battery= charging mode, V_0= 96 V, I_b= -2 A and I_{sc}= 0 A. At t= 0.2 sec, the SC charging is enabled such that battery current change to positive and 2 % voltage rise occur in the DC bus. Now the battery

is discharging, and the SC is charging. At t= 0.5 sec, load disturbance is applied. The maximum peak overshoot at the time of disturbance is 3.1 %, and the SC acts quickly to mitigate the transient power. It can be seen that the change in battery current is slow during charging and disturbance, which is important for battery life enhancement. Moreover, the battery and SC act quicker, such that the DC bus voltage has minimal oscillations.

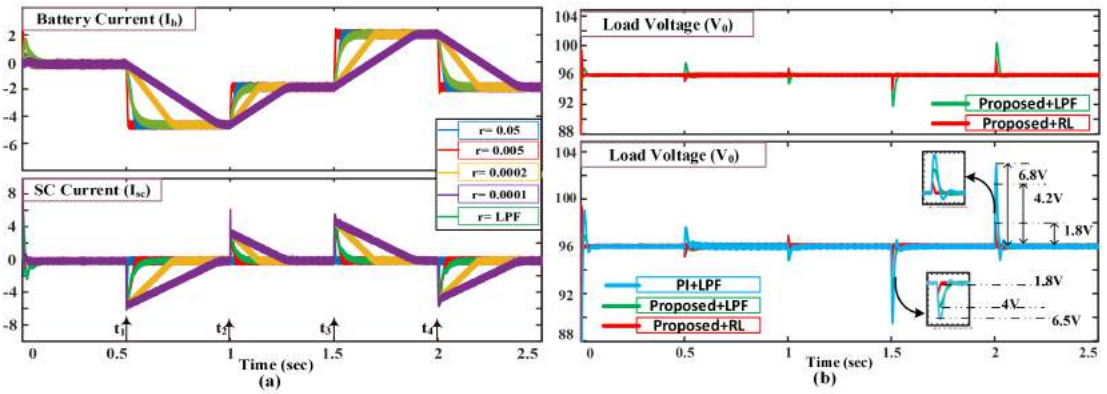

Figure 6.6: Comparison of a) effect of variation in 'r' and LPF with cut off frequency 31 rad/sec on battery and SC current b) corresponding load voltage and comparison of load voltage for Table: 6.2.

6.3.3 System operation with variation in rate limiter constant

Further simulation studies are conducted to examine the system's performance with variation in the 'r' value. Figure 6.6 (a) shows the load voltage, battery current and SC current variation with the decrease in 'r' value and with a LPF of 31 rad/sec for the same hybrid controller. The rate limiter-based method shows that it limits the over-discharge of the battery compared to the LPF. Further, the 'r' allows the designer to select the battery's discharge rate based on application. The hybrid controller with a rate limiter has less overshoot and settling time than the hybrid controller with a LPF, as shown in the DC bus voltage waveform. A comparative study with traditional PI, proposed + LPF and proposed + rate limiter are shown in Fig: 6.6 (b). The traditional system requires 50 msec to 120 msec to reach the final state, while the proposed system with a LPF requires 20 msec to 50 msec to settle the DC bus voltage. The proposed system with a rate limiter only requires 7 msec to 12 msec to settle the oscillations in DC bus voltage. A detailed comparison of different topologies operating with 80 % of SC voltage is given in Table: 6.2.

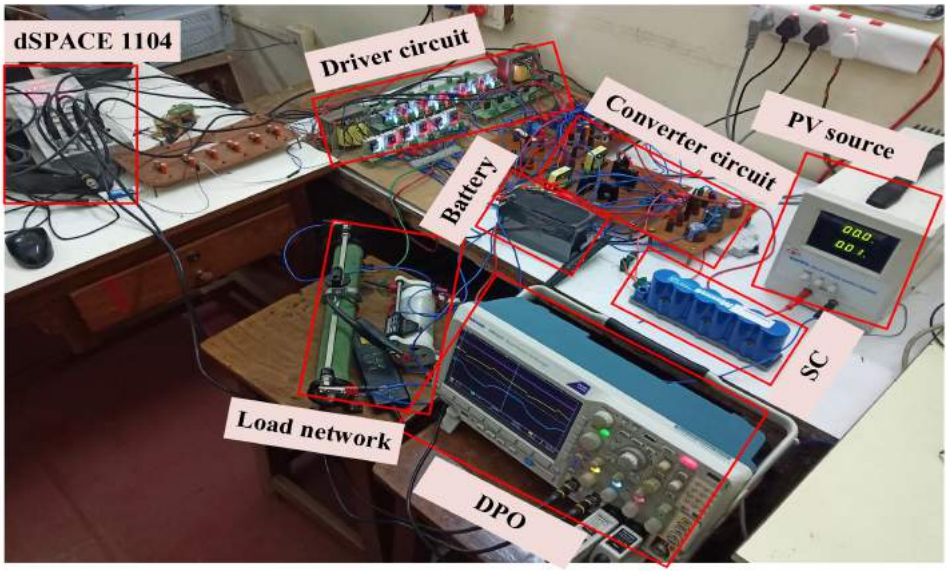

Figure 6.7: The experimental setup developed for PV-DC microgrid.

6.4 Experimental Results

The isolated DC microgrid with PV source, battery, the SC is shown in Fig: 6.7. The experimental setup consists of PV emulated DC source, Exide 12 V, 7Ah lead-acid battery, Maxwell BMOD0058 E016 B02 SC, IRF460 MOSFETS, censor and driver circuit, dSPACE 1104 real-time controller, linear load and other passive components. The system is designed for 100 W power, and the nominal power is 48 W. The output capacitor, PV converter inductor, battery converter inductor and SC inductor values are 470 μF, 2 mH, 2.3 mH and 4.1 mH respectively. The system operates with a DC bus voltage of 24 V. The system is verified under sudden variation in PV source and load. The hardware results are shown to evaluate the performance of the system.

6.4.1 System operation under irradiance variations

To analyse the performance of the proposed controller, disturbances are created at t_1, t_2, t_3, and t_4 similar to scenarios as shown in Fig: 6.8. The four traces represent DC bus voltage, PV current, battery current, and load current. The variation in incident PV panel irradiation is reflected as change in PV current as shown in t= t_1 and t= t_2. Initially, PV generation was sufficient to meet the load demand, and the battery current was almost zero. At t_1, the PV generation increases from 24 W to 48 W. The excess power is absorbed by the battery and DC bus voltage regulated at 24 V. At t_2, the PV generation is reduced to 24 W. As a result, the battery current is reduced to near zero,

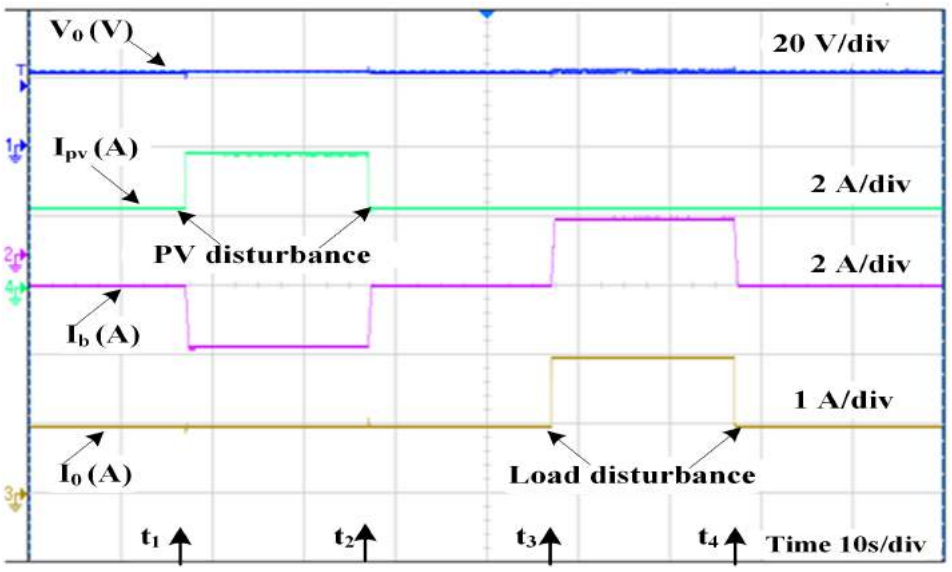

Figure 6.8: Experimental results: load voltage, load current, PV current and battery current for different scenarios.

and DC bus voltage is maintained constant with minimal variation. The slow change in battery current indicates that the SC is absorbing/ supplying the transient power. An enlarged portion of PV variation is presented in Fig: 6.9. Initially, the battery current is almost zero, and PV meets the load demand. At the time of disturbance, the DC bus voltage and load current have a small oscillation and settle back to the original value. The battery current changes slowly according to the power sharing algorithm. The SC supplies the transient power, which helps to get faster system dynamics.

6.4.2 System operation under load variation

The load variation is applied by changing the connected load as shown in Fig: 6.8. At t_3, the load demand increases to 48 W from 24 W and reduced to 24 W at t= t_4. Since the PV generation is constant, and the battery current varies to meet the excess power demand. The DC bus voltage is regulated constant, and the battery current changes slowly compared to the change in load current. At t_3, the load demand increase by 1 A. The battery current increases to meet the additional power requirement. At t_4, the battery current reduces near 0 A since load demand is reduced to 1 A. For further understanding, the enlarged portion of battery and SC current sharing is illustrated in Fig: 6.10. Initially, the load is taking 2 A from PV and battery together. The enlarged portion shows the reduction in load current to 1 A. As a result, the battery current reduces to a new value based on the rate limiter algorithm. The SC absorbs the additional power

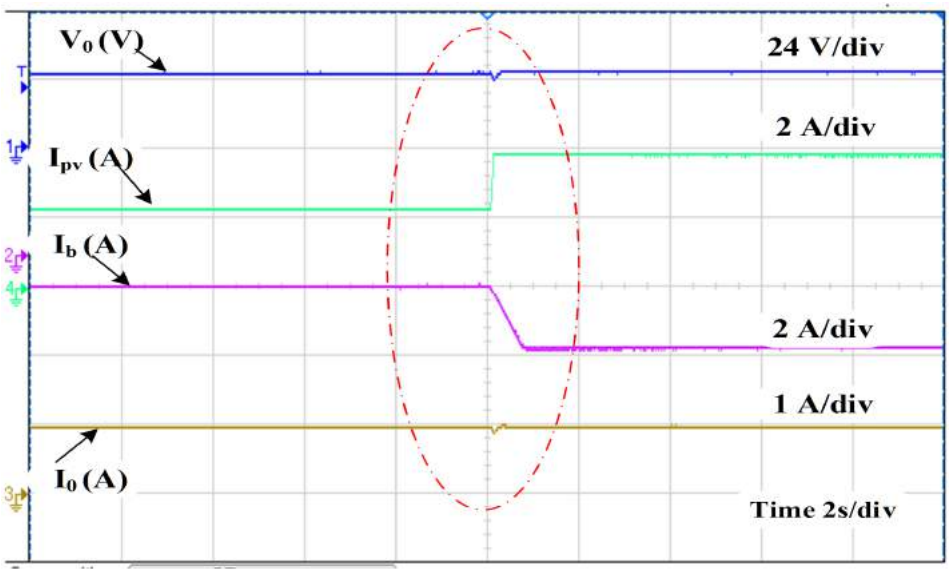

Figure 6.9: Experimental results: current sharing between PV and battery during PV increment

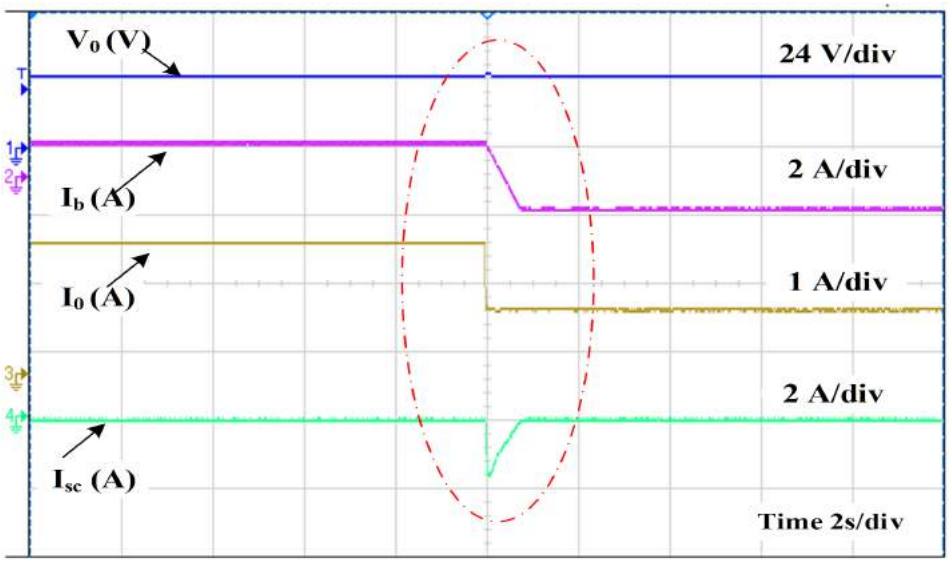

Figure 6.10: Experimental results: current sharing between battery and supercapcitor during load decrement.

created in the DC bus. Hence SC current is negative in this operation.

6.4.3 System operation under supercapacitor charging

To analyze the SC charging, excess PV generation and battery charging conditions are considered. Initially, the battery current is negative, and the SC current is almost zero.

At $t = t_1$, the SC_EN made unity, thus charging of SC is started. It can be seen from Fig: 6.11 that the battery current undergoes a smooth transition from negative current to the positive current during SC charging. The SC voltage slowly increases, and load voltage is maintained constant at 24 V. The combined system enables smooth SC charging without any disturbance in load voltage and battery current.

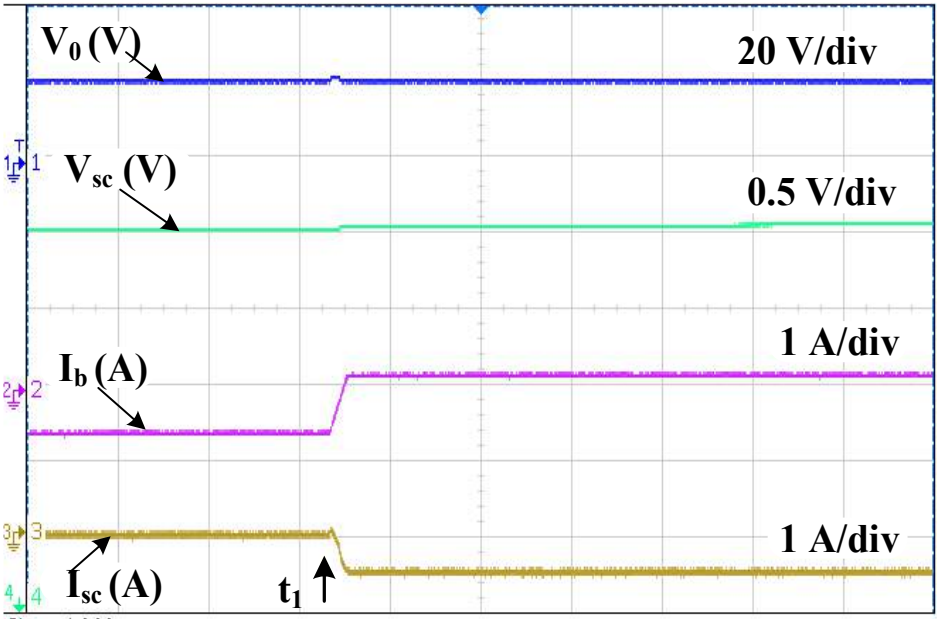

Figure 6.11: Experimental results: charging of SC in excess power mode with SC_EN= 1.

6.4.4 System operation with variation in '*r*'

The key feature of dynamic power sharing is the ability to control the battery discharge rate. A comparison is made for the analysis of battery and SC current sharing with different 'r' values as shown in Fig: 6.12 (a) and (b). The slope of battery current reduces as the 'r' value increase from 0.0002 to 0.0005. The battery current takes more time to reach the final value when r= 0.0002 as shown in Fig: 6.12 (a). It is clear from waveforms that the SC supplies the oscillatory current, and the battery supply the average current component. Further, the DC bus voltage is maintained at 24 V irrespective of the rate limiter constant 'r'.

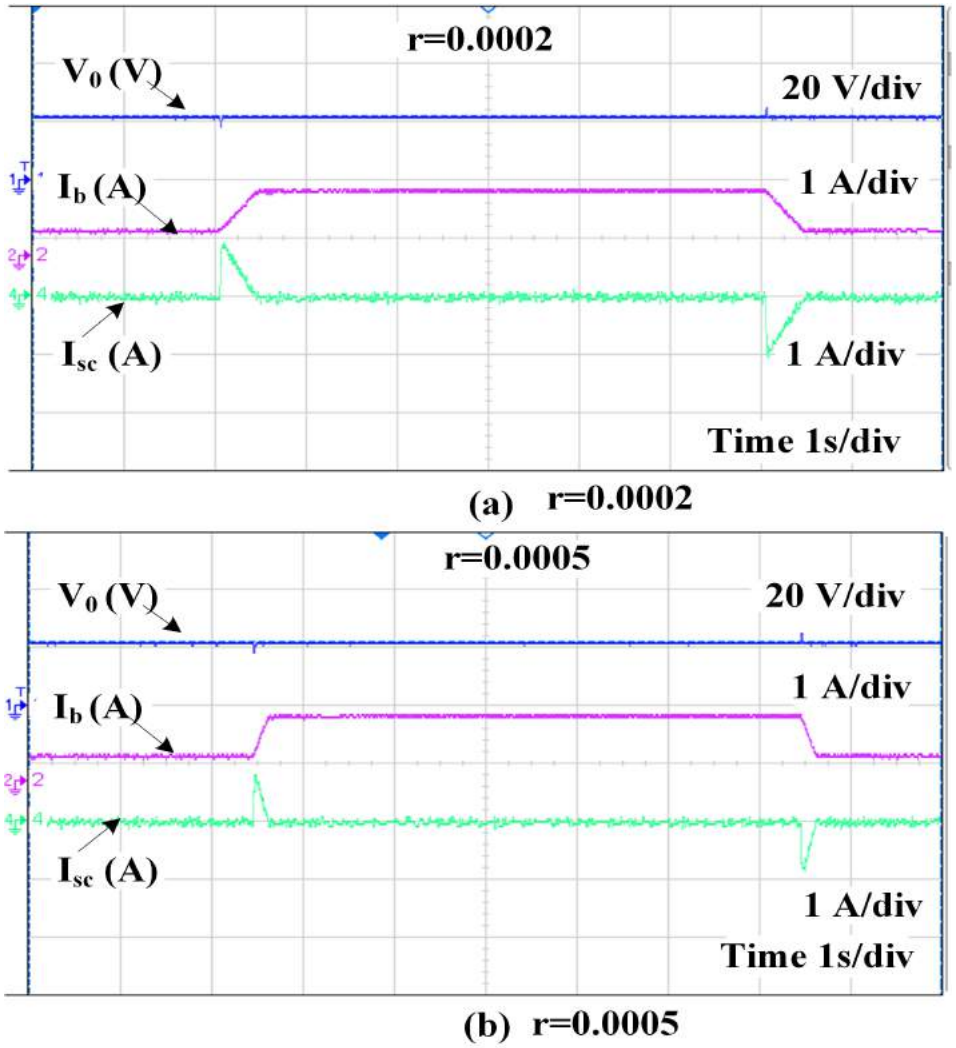

Figure 6.12: Experimental results: a) DC bus voltage, battery current and SC current when r= 0.0002. b) DC bus voltage, battery current and SC current when r= 0.0005.

6.4.5 Comparison with previous works

To further assess the performance of the hybrid control strategy, a comparison with prior studies is conducted and shown in Table: 6.2. The main parameter considered for comparison is percentage overshoot (%MP) and settling time taken by the DC bus voltage under various disturbances. The percentage overshoot in DC bus voltage [98] is given by equation (6.18).

$$\%\ Maximum\ peak\ overshoot(\%MP) = \frac{V_{ref} - V_0}{V_0} X100\% \tag{6.18}$$

Table 6.2: Comparison between proposed controller based on rate limiter (RL), proposed controller with LPF (LPF) and traditional PI methods

Parameter	**PI+ LPF [140]**	**PI+LPF enhanced [141]**	**Proposed with LPF**	**proposed with RL**
%Mp load disturbance	6-8%	4-5%	3.6-4.5%	1.5-2%
%Mp PV disturbance	2-3%	1.5-2.5%	1.5-2.5%	0.5-1%
Settling time (msec)	60-120	25-50	20-50	7-15

Table: 6.2 shows that the proposed hybrid control strategy has a lesser peak overshoot and settling time compared to the methods in [140] and [141]. This implies better DC bus voltage regulation under different source and load variations. Also, the settling time of the proposed method is less than 15 msec for the rate limiter method. This is because of the reduction in system delay due to the combined action of rate limiter and inner duty predictive control. The proposed control strategy with a LPF shows better performance than the traditional method; however, the delay imposed by the filter increases the settling time. From the above analysis, the proposed hybrid control strategy with rate limiter ensures SC to supply the transient power demand quickly until the battery compensates for the average power demand. In summary, the proposed control reduces the battery stress and achieves excellent DC bus voltage regulation with a simple control approach.

6.5 Summary

This chapter has presented a dual loop hybrid control scheme by combining traditional PI and predictive control schemes to control the battery and SC in a PV-DC microgrid. The conventional PI -LPF-based HESS control strategies experience slow dynamic response due to low order LPF. Further, there is no specific method to select the LPF cutoff frequency to control battery charge/discharge rates. Hence, a hybrid control strategy with a discrete rate limiter power-sharing scheme is introduced for HESS. Using a rate limiter for the power splitting scheme enables a systematic approach to include battery discharge rate. It helps to eliminate slow response and the nonlinear nature of the LPF. The simulation study shows that the proposed method minimizes peak overshoot below 2 % and settling time below 15 ms with stabilized DC bus voltage. Furthermore, the variation analysis with rate limiter constant shows that battery charge/discharge rates

can be regulated independently without affecting the system dynamics. The SC charging is enabled using SC_EN below 50 % of SC voltage and verified. The experimental studies reveal that the results follow the simulation study. The hardware results show that DC bus voltage has fewer oscillations and controls power-sharing between the battery and the SC. To sum up, the proposed HESS controller integrated DC microgrid is able to reduce the controller complexity and effectively tackles the required objectives such as limiting the rate of change of battery current, uninterruptible SC charging without affecting the DC bus voltage and battery dynamics, ensuring that the battery is supplied only for the steady-state power demand and SC is supplying the transient period and limiting DC bus voltage fluctuations with minimum variation.

Chapter 7
Conclusion

In this thesis, different control and energy management strategies are developed to improve the performance of PV-fed DC microgrids with HESS. The main objective is to achieve power balance in the DC microgrid and enhance the battery's life span by diverting the transient power to SC. The main contributions of the work include i) accurate modelling of HESS by incorporating a battery, SC, and LPF characteristics, ii) A new power splitting scheme for HESS that eliminates the direct aid of LPF in the battery reference current generation, iii) An EMS for battery and SC to mitigate the negative effect of SC voltage variation, iv) A hybrid control strategy to improve the DC microgrid dynamics as well as reduce the lag effect on controllers, and v) a hybrid control incorporated with discrete rate limiter for controlled power-sharing between battery and SC in HESS. The proposed methods are verified in an active HESS topology integrated PV-DC microgrid. Furthermore, the system is analyzed mathematically, simulated in MATLAB/Simulink®and validated experimentally. The detailed summary of each work is presented below, and the comparison between different proposed methods is presented in Table: 7.1.

7.1 Summary and Important Finding

7.1.1 Modelling and analysis of fully-active hybrid energy storage system

This chapter dealt with the complete modelling of active battery- SC hybrid energy storage system topology for DC microgrid applications. The conventional design procedure neglects the battery current to voltage transfer function and LPF effect on outer voltage control loop design to minimize the complexity. The proposed design combines both battery and SC effects on the voltage control loop and considers the LPF while designing the outer voltage controller parameters. The controller parameters are designed based on the PM and BW of each control loop. The advantage of the proposed method is that it provides enough bandwidth for the outer loop so that faster settling of DC bus voltage is ensured. Further, the calculated PI parameters are verified in simulation as well as experimental studies. Finally, the results show that the active hybrid energy stor-

age system can incorporate ESS with different voltage levels into a common DC bus with controlled power-sharing. The SC voltage waveform shows that it can take sudden system disturbances and reduce the utilization at a steady state. Combining SC with battery improves the system response and enhances battery life.

7.1.2 Supercapacitor voltage based power sharing and EMS for DC microgrid

This chapter proposed a new power-sharing and energy management scheme for PV-DC microgrid integrated with HESS. The main contributions are i) direct calculation of battery reference current without the direct aid of LPF, ii) A new energy management strategy to address SC voltage variation and mitigate its negative effect on DC bus voltage and iii) designing and modelling of proposed HESS control strategy by combining battery, SC and LPF effect on controller design. The proposed control strategy successfully separates the LPF effect from the battery control loop, and the VBLPF based EMS leads to better SC utilization at different SC voltage ranges. The developed EMS addresses the DC microgrid in various operating modes and produces a stable and desirable performance. The HESS is implemented with MPPT controlled PV-DC microgrid and verified for different source and load variations. Several features are illustrated, including quick DC bus voltage regulation, reduced battery current stress, SC charging operation, and mode shift.

7.1.3 Hybrid controller assisted voltage regulation for HESS in DC microgrid

This chapter proposes a hybrid controller for HESS in a PV-DC microgrid. Using the suggested control method, the performance of the HESS is examined under various source and load perturbations. The main contributions include i) developing a hybrid control scheme to minimize the difficulty in parameter tuning, ii) incorporating an SC voltage regulation scheme based on duty regulation and iii) combining the hybrid control with less LPF aided power splitting scheme to reduce the delay in DC bus dynamics. The proposed hybrid control strategy can stabilize the DC bus voltage during different disturbances. The charge and discharge waveforms of the battery are observed at different PV generation and load changes. The proposed controller calculates the duty ratio in a single iteration and reduces the processor complexity. The suggested power splitting strategy decreases the latency in the battery control loop and improves the DC microgrid's performance. The experimental study verified the proposed controller, and the

Table 7.1: Comparative study of proposed strategies and conventional method

S.No	Parameters	Conventional [140]	Proposed-I Chapter-4	Proposed-II Chapter-5	Proposed-III Chapter-6
1	%Mp load disturbance	6-8.5%	3.8-4.6%	3.6-4.2%	1.5-2%
2	%Mp PV disturbance	2-3%	1-1.6%	1-1.2%	0.5-1%
3	Settling time (ms)	60-100	25-40	20-30	7-15
4	Control strategy	PI	PI	Hybrid	Hybrid
5	SC voltage regulation regulation	No	Yes	Yes	Yes
6	No. of tuning parameters (HESS)	6	6	2	2

results show better regulation of DC bus voltage. According to the findings, combining PI with predictive control improves the dynamics of the DC microgrid and assures proper power-sharing of HESS.

7.1.4 Controlled power sharing of HESS in PV fed DC microgrid

This chapter has presented a dual loop hybrid control scheme by combining traditional PI and predictive control schemes to control the battery and supercapacitor in a PV-DC microgrid. To eliminate the slow response and nonlinear nature of the low pass filter, a rate limiter-based power splitting scheme is proposed, which provides a systematic approach for incorporating battery discharge rate into the controller. The proposed controller reduces the controller complexity and effectively tackles the required objectives such as i) limiting the rate of change of battery current, ii) uninterruptible supercapacitor charging without affecting the DC bus voltage and battery dynamics iii) ensuring that the battery is supplied only for the steady-state power demand and supercapacitor is supplying the transient period and iv) limiting DC bus voltage fluctuations with minimum variation. The simulation study verifies the system under different source and load variations. In addition, the variation with rate limiter constant and supercapacitor charging are analyzed. The simulation and experimental studies reveal that the proposed system has fewer oscillations at DC bus voltage and better transient and steady-state performance than traditional approaches. The proposed hybrid control scheme improves the power-sharing between battery and supercapacitor and DC bus voltage regulation with and without a supercapacitor charging scheme.

7.2 Future Scope

Any research never ends without leaving an open window for further research. Future researchers may look at the following aspects:

7.2.1 Development of HESS integrated hybrid microgrids with multiple RES and its energy management strategies

The proposed research mainly focused on integrating HESS into PV fed DC microgrid. The work needs to incorporate AC load, primary grid and other renewable energy sources. One of the main challenges regarding grid integrated DC microgrid is the power-sharing and EMS strategies. The following problems can be addressed while considering the research:

1. Operation of DC microgrid with multiple RES with MPPT control and integration of energy storage.
2. Energy management strategies for HESS in grid connected and isolated mode with different RES by considering cost and peak load shaving.
3. Autonomous charging of SC in grid connected microgrids.

7.2.2 Development of hybrid control strategies for HESS assisted electric vehicles

The developed control strategies can be extended to EVs applications to improve the vehicle dynamics and battery life extension. In such applications, analysis of SC voltage variation is needed. The proposed EMS can be extended to mitigate the negative effect of SC voltage variation in EVs. The following points can be considered while developing hybrid control strategies for EV application.

1. Analysis of battery life extension with the help of SC for different EV driving cycles.
2. Autonomous charging of supercapacitor in regenerative mode.
3. Analysis of effect of SC voltage variation on EV driving range.

Bibliography

[1] "Renewables 2020 global status report." https://www.ren21.net/gsr-2020/. Accessed: 06-05-2022 [Online].

[2] "Current status | ministry of new and renewable energy, government of india." https://mnre.gov.in/solar/current-status/. Accessed: 06-05-2022 [Online].

[3] N. Hatziargyriou, *Microgrids: architectures and control*. John Wiley & Sons, 2014.

[4] R. Lasseter, A. Akhil, C. Marnay, J. Stephens, J. Dagle, R. Guttromson, A. Meliopoulous, R. Yinger, and J. Eto, "The certs microgrid concept," *White paper for Transmission Reliability Program, Office of Power Technologies, US Department of Energy*, vol. 2, no. 3, p. 30, 2002.

[5] M. H. Bollen, "The smart grid: Adapting the power system to new challenges," *Synthesis Lectures on Power Electronics*, vol. 2, no. 1, pp. 1–180, 2011.

[6] T. Hailu, L. Mackay, M. Gajic, and J. Ferreira, "From voltage stiff to voltage weak dc distribution grid: Opportunities and challenges," in *2016 IEEE 2nd Annual Southern Power Electronics Conference (SPEC)*, pp. 1–6, IEEE, 2016.

[7] F. Chen, R. Burgos, and D. Boroyevich, "Efficiency comparison of a single-phase grid-interface bidirectional ac/dc converter for dc distribution systems," in *2015 IEEE Energy Conversion Congress and Exposition (ECCE)*, pp. 6261–6268, IEEE, 2015.

[8] N. R. Tummuru, M. K. Mishra, and S. Srinivas, "Integration of pv/battery hybrid energy conversion system to the grid with power quality improvement features," in *2013 IEEE International Conference on Industrial Technology (ICIT)*, pp. 1751–1756, IEEE, 2013.

[9] X. Liu, P. Wang, and P. C. Loh, "A hybrid ac/dc microgrid and its coordination control," *IEEE Transactions on smart grid*, vol. 2, no. 2, pp. 278–286, 2011.

[10] J. M. Guerrero, P. C. Loh, T.-L. Lee, and M. Chandorkar, "Advanced control architectures for intelligent microgrids—part ii: Power quality, energy storage,

and ac/dc microgrids," *IEEE Transactions on industrial electronics*, vol. 60, no. 4, pp. 1263–1270, 2012.

[11] F. Blaabjerg, R. Teodorescu, M. Liserre, and A. V. Timbus, "Overview of control and grid synchronization for distributed power generation systems," *IEEE Transactions on industrial electronics*, vol. 53, no. 5, pp. 1398–1409, 2006.

[12] D. E. Olivares, A. Mehrizi-Sani, A. H. Etemadi, C. A. Cañizares, R. Iravani, M. Kazerani, A. H. Hajimiragha, O. Gomis-Bellmunt, M. Saeedifard, R. Palma-Behnke, *et al.*, "Trends in microgrid control," *IEEE Transactions on smart grid*, vol. 5, no. 4, pp. 1905–1919, 2014.

[13] G. Koeppel and M. Korpås, "Improving the network infeed accuracy of non-dispatchable generators with energy storage devices," *Electric Power Systems Research*, vol. 78, no. 12, pp. 2024–2036, 2008.

[14] A. T. D. Perera, V. M. Nik, D. Mauree, and J.-L. Scartezzini, "Electrical hubs: An effective way to integrate non-dispatchable renewable energy sources with minimum impact to the grid," *Applied Energy*, vol. 190, pp. 232–248, 2017.

[15] T. Chaudhury and D. Kastha, "A high gain multiport dc–dc converter for integrating energy storage devices to dc microgrid," *IEEE Transactions on Power Electronics*, vol. 35, no. 10, pp. 10501–10514, 2020.

[16] A. Foles, L. Fialho, and M. Collares-Pereira, "Techno-economic evaluation of the portuguese pv and energy storage residential applications," *Sustainable Energy Technologies and Assessments*, vol. 39, p. 100686, 2020.

[17] N. Kularatna and K. Gunawardane, *Energy Storage Devices for Renewable Energy-based Systems: Rechargeable Batteries and Supercapacitors*. Academic Press, 2021.

[18] U. Akram, M. Nadarajah, R. Shah, and F. Milano, "A review on rapid responsive energy storage technologies for frequency regulation in modern power systems," *Renewable and Sustainable Energy Reviews*, vol. 120, p. 109626, 2020.

[19] H. Xiaoliang, T. Hiramatsu, and H. Yoichi, "Energy management strategy based on frequency-varying filter for the battery supercapacitor hybrid system of electric vehicles," in *2013 World Electric Vehicle Symposium and Exhibition (EVS27)*, pp. 1–6, 2013.

[20] L. Chen, X. Zhang, P. Han, H. Chen, Y. Xu, L. Ren, and Y. Tang, "Optimization of smes-battery hybrid energy storage system for wind power smoothing," in *2020 IEEE International Conference on Applied Superconductivity and Electromagnetic Devices (ASEMD)*, pp. 1–2, 2020.

[21] T. Bocklisch, "Hybrid energy storage approach for renewable energy applications," *Journal of Energy Storage*, vol. 8, pp. 311–319, 2016.

[22] Q. Sun, D. Xing, H. Alafnan, X. Pei, M. Zhang, and W. Yuan, "Design and test of a new two-stage control scheme for smes-battery hybrid energy storage systems for microgrid applications," *Applied Energy*, vol. 253, p. 113529, 2019.

[23] P. Naderi and F. Fallahi, "A novel structure proposal for distributed generation using smes and pv system with relative controllers design," *Energy Systems*, vol. 6, no. 2, pp. 153–172, 2015.

[24] I. Azizi and H. Radjeai, "A new strategy for battery and supercapacitor energy management for an urban electric vehicle," *Electrical Engineering*, vol. 100, no. 2, pp. 667–676, 2018.

[25] A. A. K. Arani, G. B. Gharehpetian, and M. Abedi, "A novel control method based on droop for cooperation of flywheel and battery energy storage systems in islanded microgrids," *IEEE Systems Journal*, vol. 14, no. 1, pp. 1080–1087, 2019.

[26] S. Singh *et al.*, "Selection of non-isolated dc-dc converters for solar photovoltaic system," *Renewable and Sustainable Energy Reviews*, vol. 76, pp. 1230–1247, 2017.

[27] N. Femia, G. Petrone, G. Spagnuolo, and M. Vitelli, "Optimization of perturb and observe maximum power point tracking method," *IEEE Transactions on Power Electronics*, vol. 20, no. 4, pp. 963–973, 2005.

[28] M. Killi and S. Samanta, "Modified perturb and observe mppt algorithm for drift avoidance in photovoltaic systems," *IEEE transactions on Industrial Electronics*, vol. 62, no. 9, pp. 5549–5559, 2015.

[29] D. Kumar, F. Zare, and A. Ghosh, "Dc microgrid technology: system architectures, ac grid interfaces, grounding schemes, power quality, communication networks, applications, and standardizations aspects," *Ieee Access*, vol. 5, pp. 12230–12256, 2017.

[30] T. Thomas and M. K. Mishra, "Control strategy for a pv-wind based standalone dc microgrid with hybrid energy storage system," in *2019 IEEE 1st International Conference on Energy, Systems and Information Processing (ICESIP)*, pp. 1–6, IEEE, 2019.

[31] A. M. Gee, F. V. Robinson, and R. W. Dunn, "Analysis of battery lifetime extension in a small-scale wind-energy system using supercapacitors," *IEEE transactions on energy conversion*, vol. 28, no. 1, pp. 24–33, 2013.

[32] P. Srinivas and U. B. Manthati, "Modelling of a double-input bidirectional dc–dc converter for hess and unified controller design for dc microgrid applications," *International Journal of Power and Energy Systems*, vol. 40, no. 3, 2020.

[33] H. Liao, J. Peng, Y. Wu, H. Li, Y. Zhou, X. Zhang, and Z. Huang, "Adaptive split-frequency quantitative power allocation for hybrid energy storage systems," *IEEE Transactions on Transportation Electrification*, vol. 7, no. 4, pp. 2306–2317, 2021.

[34] M. A. Zabara, C. B. Uzundal, and B. Ülgüt, "Performance modeling of unmanaged hybrid battery/supercapacitor energy storage systems," *Journal of Energy Storage*, vol. 43, p. 103185, 2021.

[35] H. Zhou, T. Bhattacharya, D. Tran, T. S. T. Siew, and A. M. Khambadkone, "Composite energy storage system involving battery and ultracapacitor with dynamic energy management in microgrid applications," *IEEE transactions on power electronics*, vol. 26, no. 3, pp. 923–930, 2010.

[36] M. Momayyezan, D. B. W. Abeywardana, B. Hredzak, and V. G. Agelidis, "Integrated reconfigurable configuration for battery/ultracapacitor hybrid energy storage systems," *IEEE Transactions on Energy Conversion*, vol. 31, no. 4, pp. 1583–1590, 2016.

[37] S. Kotra, M. K. Mishra, and N. P. Chaithanya, "Design and small signal analysis of dc microgrid with hybrid energy storage system," in *2017 IEEE PES Asia-Pacific Power and Energy Engineering Conference (APPEEC)*, pp. 1–6, IEEE, 2017.

[38] T. Mahlia, T. Saktisahdan, A. Jannifar, M. Hasan, and H. Matseelar, "A review of available methods and development on energy storage; technology update," *Renewable and sustainable energy reviews*, vol. 33, pp. 532–545, 2014.

[39] G. Venkataramani, P. Parankusam, V. Ramalingam, and J. Wang, "A review on compressed air energy storage–a pathway for smart grid and polygeneration," *Renewable and sustainable energy reviews*, vol. 62, pp. 895–907, 2016.

[40] T. Ise, M. Kita, and A. Taguchi, "A hybrid energy storage with a smes and secondary battery," *IEEE Transactions on Applied Superconductivity*, vol. 15, no. 2, pp. 1915–1918, 2005.

[41] A. Khaligh and Z. Li, "Battery, ultracapacitor, fuel cell, and hybrid energy storage systems for electric, hybrid electric, fuel cell, and plug-in hybrid electric vehicles: State of the art," *IEEE transactions on Vehicular Technology*, vol. 59, no. 6, pp. 2806–2814, 2010.

[42] F. Akar, Y. Tavlasoglu, E. Ugur, B. Vural, and I. Aksoy, "A bidirectional nonisolated multi-input dc–dc converter for hybrid energy storage systems in electric vehicles," *IEEE Transactions on Vehicular Technology*, vol. 65, no. 10, pp. 7944–7955, 2015.

[43] S. Kotra and M. K. Mishra, "A supervisory power management system for a hybrid microgrid with hess," *IEEE Transactions on Industrial Electronics*, vol. 64, no. 5, pp. 3640–3649, 2017.

[44] N. R. Tummuru, M. K. Mishra, and S. Srinivas, "Dynamic energy management of renewable grid integrated hybrid energy storage system," *IEEE Transactions on Industrial Electronics*, vol. 62, no. 12, pp. 7728–7737, 2015.

[45] J. Li, A. M. Gee, M. Zhang, and W. Yuan, "Analysis of battery lifetime extension in a smes-battery hybrid energy storage system using a novel battery lifetime model," *Energy*, vol. 86, pp. 175–185, 2015.

[46] J. Li, R. Xiong, H. Mu, B. Cornélusse, P. Vanderbemden, D. Ernst, and W. Yuan, "Design and real-time test of a hybrid energy storage system in the microgrid with the benefit of improving the battery lifetime," *Applied energy*, vol. 218, pp. 470–478, 2018.

[47] T. Weitzel, M. Schneider, C. H. Glock, F. Löber, and S. Rinderknecht, "Operating a storage-augmented hybrid microgrid considering battery aging costs," *Journal of Cleaner Production*, vol. 188, pp. 638–654, 2018.

[48] F. Ongaro, S. Saggini, and P. Mattavelli, "Li-ion battery-supercapacitor hybrid storage system for a long lifetime, photovoltaic-based wireless sensor network," *IEEE Transactions on Power Electronics*, vol. 27, no. 9, pp. 3944–3952, 2012.

[49] S. Mane, M. Mejari, F. Kazi, and N. Singh, "Improving lifetime of fuel cell in hybrid energy management system by lure–lyapunov-based control formulation," *IEEE Transactions on Industrial Electronics*, vol. 64, no. 8, pp. 6671–6679, 2017.

[50] H. Aouzellag, K. Ghedamsi, and D. Aouzellag, "Energy management and fault tolerant control strategies for fuel cell/ultra-capacitor hybrid electric vehicles to enhance autonomy, efficiency and life time of the fuel cell system," *International journal of hydrogen energy*, vol. 40, no. 22, pp. 7204–7213, 2015.

[51] Y. Shan, J. Hu, K. W. Chan, Q. Fu, and J. M. Guerrero, "Model predictive control of bidirectional dc–dc converters and ac/dc interlinking converters—a new control method for pv-wind-battery microgrids," *IEEE Transactions on Sustainable Energy*, vol. 10, no. 4, pp. 1823–1833, 2018.

[52] P. Zhao, J. Wang, and Y. Dai, "Capacity allocation of a hybrid energy storage system for power system peak shaving at high wind power penetration level," *Renewable Energy*, vol. 75, pp. 541–549, 2015.

[53] S. Wang, Y. Tang, J. Shi, K. Gong, Y. Liu, L. Ren, and J. Li, "Design and advanced control strategies of a hybrid energy storage system for the grid integration of wind power generations," *IET Renewable Power Generation*, vol. 9, no. 2, pp. 89–98, 2015.

[54] H. Lee, B. Y. Shin, S. Han, S. Jung, B. Park, and G. Jang, "Compensation for the power fluctuation of the large scale wind farm using hybrid energy storage applications," *IEEE Transactions on Applied Superconductivity*, vol. 22, no. 3, pp. 5701904–5701904, 2011.

[55] N. R. Tummuru, U. Manandhar, A. Ukil, H. B. Gooi, S. K. Kollimalla, and S. Naidu, "Control strategy for ac-dc microgrid with hybrid energy storage under different operating modes," *International Journal of Electrical Power & Energy Systems*, vol. 104, pp. 807–816, 2019.

[56] D. Shin, Y. Kim, J. Seo, N. Chang, Y. Wang, and M. Pedram, "Battery-supercapacitor hybrid system for high-rate pulsed load applications," in *2011 Design, Automation & Test in Europe*, pp. 1–4, IEEE, 2011.

[57] C. R. Lashway, A. T. Elsayed, and O. A. Mohammed, "Hybrid energy storage management in ship power systems with multiple pulsed loads," *Electric Power Systems Research*, vol. 141, pp. 50–62, 2016.

[58] M. Farhadi and O. A. Mohammed, "Performance enhancement of actively controlled hybrid dc microgrid incorporating pulsed load," *IEEE Transactions on Industry Applications*, vol. 51, no. 5, pp. 3570–3578, 2015.

[59] M. Farhadi and O. A. Mohammed, "Real-time operation and harmonic analysis of isolated and non-isolated hybrid dc microgrid," *IEEE Transactions on Industry Applications*, vol. 50, no. 4, pp. 2900–2909, 2014.

[60] A. Lahyani, A. Sari, I. Lahbib, and P. Venet, "Optimal hybridization and amortized cost study of battery/supercapacitors system under pulsed loads," *Journal of Energy Storage*, vol. 6, pp. 222–231, 2016.

[61] M. Farhadi and O. Mohammed, "Adaptive energy management in redundant hybrid dc microgrid for pulse load mitigation," *IEEE Transactions on Smart Grid*, vol. 6, no. 1, pp. 54–62, 2014.

[62] A. Lahyani, P. Venet, A. Guermazi, and A. Troudi, "Battery/supercapacitors combination in uninterruptible power supply (ups)," *IEEE transactions on power electronics*, vol. 28, no. 4, pp. 1509–1522, 2012.

[63] Z. Shuai, Y. Sun, Z. J. Shen, W. Tian, C. Tu, Y. Li, and X. Yin, "Microgrid stability: Classification and a review," *Renewable and Sustainable Energy Reviews*, vol. 58, pp. 167–179, 2016.

[64] A. Cansiz, C. Faydaci, M. T. Qureshi, O. Usta, and D. T. McGuiness, "Integration of a smes–battery-based hybrid energy storage system into microgrids," *Journal of Superconductivity and Novel Magnetism*, vol. 31, no. 5, pp. 1449–1457, 2018.

[65] L. Yang, N. Tai, and C. Fan, "Regulation and stabilization by ice storage air-conditioning and battery energy storage system in microgrids," *IEEJ Transactions on Electrical and Electronic Engineering*, vol. 12, no. 2, pp. 176–184, 2017.

[66] L. Chen, H. Chen, Y. Li, G. Li, J. Yang, X. Liu, Y. Xu, L. Ren, and Y. Tang, "Smes-battery energy storage system for the stabilization of a photovoltaic-based microgrid," *IEEE Transactions on Applied Superconductivity*, vol. 28, no. 4, pp. 1–7, 2018.

[67] H. Alafnan, M. Zhang, W. Yuan, J. Zhu, J. Li, M. Elshiekh, and X. Li, "Stability improvement of dc power systems in an all-electric ship using hybrid smes/battery," *IEEE Transactions on Applied Superconductivity*, vol. 28, no. 3, pp. 1–6, 2018.

[68] F. Ju, Q. Zhang, W. Deng, and J. Li, "Review of structures and control of battery-supercapacitor hybrid energy storage system for electric vehicles," in *2014 IEEE international conference on automation science and engineering (CASE)*, pp. 143–148, IEEE, 2014.

[69] J. J. Jose and U. B. Manthati, "Two-input bidirectional converter controlled hybrid energy storage system (hess) for micro grids," in *2016 IEEE 1st international conference on power electronics, intelligent control and energy systems (ICPEICES)*, pp. 1–4, IEEE, 2016.

[70] J. P. Zheng, T. R. Jow, and M. Ding, "Hybrid power sources for pulsed current applications," *IEEE transactions on aerospace and electronic systems*, vol. 37, no. 1, pp. 288–292, 2001.

[71] R. A. Dougal, S. Liu, and R. E. White, "Power and life extension of battery-ultracapacitor hybrids," *IEEE Transactions on components and packaging technologies*, vol. 25, no. 1, pp. 120–131, 2002.

[72] Q. Zhang and G. Li, "Experimental study on a semi-active battery-supercapacitor hybrid energy storage system for electric vehicle application," *IEEE Transactions on Power Electronics*, vol. 35, no. 1, pp. 1014–1021, 2019.

[73] Z. Song, J. Li, X. Han, L. Xu, L. Lu, M. Ouyang, and H. Hofmann, "Multi-objective optimization of a semi-active battery/supercapacitor energy storage system for electric vehicles," *Applied Energy*, vol. 135, pp. 212–224, 2014.

[74] Z. Song, H. Hofmann, J. Li, X. Han, X. Zhang, and M. Ouyang, "A comparison study of different semi-active hybrid energy storage system topologies for electric vehicles," *Journal of Power Sources*, vol. 274, pp. 400–411, 2015.

[75] J. Cao and A. Emadi, "A new battery/ultracapacitor hybrid energy storage system for electric, hybrid, and plug-in hybrid electric vehicles," *IEEE Transactions on power electronics*, vol. 27, no. 1, pp. 122–132, 2011.

[76] L. Zhang, Y. Tang, S. Yang, and F. Gao, "A modular multilevel converter-based grid-tied battery-supercapacitor hybrid energy storage system with decoupled power control," in *2016 IEEE 8th International Power Electronics and Motion Control Conference (IPEMC-ECCE Asia)*, pp. 2964–2971, IEEE, 2016.

[77] R. Mo and H. Li, "Hybrid energy storage system with active filter function for shipboard mvdc system applications based on isolated modular multilevel dc/dc converter," *IEEE Journal of Emerging and Selected Topics in Power Electronics*, vol. 5, no. 1, pp. 79–87, 2016.

[78] W. Jiang, S. Xue, L. Zhang, W. Xu, K. Yu, W. Chen, and L. Zhang, "Flexible power distribution control in an asymmetrical-cascaded-multilevel-converter-based hybrid energy storage system," *IEEE Transactions on Industrial Electronics*, vol. 65, no. 8, pp. 6150–6159, 2017.

[79] L. Piris-Botalla, G. G. Oggier, and G. O. García, "Extending the power transfer capability of a three-port dc–dc converter for hybrid energy storage systems," *IET Power Electronics*, vol. 10, no. 13, pp. 1687–1697, 2017.

[80] Z. Ding, C. Yang, Z. Zhang, C. Wang, and S. Xie, "A novel soft-switching multiport bidirectional dc–dc converter for hybrid energy storage system," *IEEE transactions on power electronics*, vol. 29, no. 4, pp. 1595–1609, 2013.

[81] S. Punna, U. B. Manthati, and A. Chirayarukil Raveendran, "Modeling, analysis, and design of novel control scheme for two-input bidirectional dc-dc converter for hess in dc microgrid applications," *International Transactions on Electrical Energy Systems*, vol. 31, no. 10, p. e12774, 2021.

[82] P. Bajpai and V. Dash, "Hybrid renewable energy systems for power generation in stand-alone applications: A review," *Renewable and Sustainable Energy Reviews*, vol. 16, no. 5, pp. 2926–2939, 2012.

[83] Y. Zhang, Z. Jiang, and X. Yu, "Control strategies for battery/supercapacitor hybrid energy storage systems," in *2008 IEEE Energy 2030 Conference*, pp. 1–6, IEEE, 2008.

[84] U. Manandhar, A. Ukil, H. B. Gooi, N. R. Tummuru, S. K. Kollimalla, B. Wang, and K. Chaudhari, "Energy management and control for grid connected hybrid energy storage system under different operating modes," *IEEE Transactions on Smart Grid*, vol. 10, no. 2, pp. 1626–1636, 2017.

[85] U. Manandhar, B. Wang, A. Ukil, and H. B. Gooi, "Dynamic evolution control based power sharing method for hybrid energy storage system," *IET Power Electronics*, vol. 12, no. 2, pp. 276–283, 2018.

[86] P. Lin, P. Wang, Q. Xu, J. Xiao, I. U. Nutkani, and C. F. Hoong, "An integral-droop based dynamic power sharing control for hybrid energy storage system in dc microgrid," in *2017 IEEE 3rd International Future Energy Electronics Conference and ECCE Asia (IFEEC 2017-ECCE Asia)*, pp. 338–343, IEEE, 2017.

[87] Q. Xu, X. Hu, P. Wang, J. Xiao, P. Tu, C. Wen, and M. Y. Lee, "A decentralized dynamic power sharing strategy for hybrid energy storage system in autonomous dc microgrid," *IEEE transactions on industrial electronics*, vol. 64, no. 7, pp. 5930–5941, 2016.

[88] S. Teleke, M. E. Baran, S. Bhattacharya, and A. Q. Huang, "Rule-based control of battery energy storage for dispatching intermittent renewable sources," *IEEE Transactions on Sustainable Energy*, vol. 1, no. 3, pp. 117–124, 2010.

[89] K. Jin, X. Ruan, M. Yang, and M. Xu, "A hybrid fuel cell power system," *IEEE Transactions on Industrial Electronics*, vol. 56, no. 4, pp. 1212–1222, 2008.

[90] R. Cozzolino, L. Tribioli, and G. Bella, "Power management of a hybrid renewable system for artificial islands: A case study," *Energy*, vol. 106, pp. 774–789, 2016.

[91] U. Manandhar, N. R. Tummuru, S. K. Kollimalla, A. Ukil, G. H. Beng, and K. Chaudhari, "Validation of faster joint control strategy for battery-and supercapacitor-based energy storage system," *IEEE Transactions on Industrial Electronics*, vol. 65, no. 4, pp. 3286–3295, 2017.

[92] S. K. Kollimalla, A. Ukil, H. Gooi, U. Manandhar, and N. R. Tummuru, "Optimization of charge/discharge rates of a battery using a two-stage rate-limit control," *IEEE Transactions on Sustainable Energy*, vol. 8, no. 2, pp. 516–529, 2016.

[93] Z. Cabrane, D. Batool, J. Kim, and K. Yoo, "Design and simulation studies of battery-supercapacitor hybrid energy storage system for improved performances of traction system of solar vehicle," *Journal of Energy Storage*, vol. 32, p. 101943, 2020.

[94] U. Manandhar, B. Wang, A. Ukil, G. H. Beng, N. R. Tummuru, and S. K. Kollimalla, "A new control approach for pv system with hybrid energy storage system," in *IECON 2017-43rd Annual Conference of the IEEE Industrial Electronics Society*, pp. 2739–2743, IEEE, 2017.

[95] H. Guentri, T. Allaoui, M. Mekki, and M. Denai, "Power management and control of a photovoltaic system with hybrid battery-supercapacitor energy storage based on heuristics methods," *Journal of Energy Storage*, vol. 39, p. 102578, 2021.

[96] S. K. Kollimalla, M. K. Mishra, A. Ukil, and H. Gooi, "Dc grid voltage regulation using new hess control strategy," *IEEE Transactions on Sustainable Energy*, vol. 8, no. 2, pp. 772–781, 2016.

[97] M. C. Joshi and S. Samanta, "Improved energy management algorithm with time-share-based ultracapacitor charging/discharging for hybrid energy storage system," *IEEE Transactions on Industrial Electronics*, vol. 66, no. 8, pp. 6032–6043, 2018.

[98] B. Wang, U. Manandhar, X. Zhang, H. B. Gooi, and A. Ukil, "Deadbeat control for hybrid energy storage systems in dc microgrids," *IEEE Transactions on Sustainable Energy*, vol. 10, no. 4, pp. 1867–1877, 2018.

[99] Y. Zhang, G. Du, and Y. Lei, "Deadbeat control with power sharing for supercapacitor/battery-based hybrid energy storage systems in dc microgrids," in *IECON 2020 The 46th Annual Conference of the IEEE Industrial Electronics Society*, pp. 1785–1790, IEEE, 2020.

[100] P. Singh and J. Lather, "Dynamic current sharing, voltage and soc regulation for hess based dc microgrid using cpismc technique," *Journal of Energy Storage*, vol. 30, p. 101509, 2020.

[101] A. J. Abianeh and F. Ferdowsi, "Sliding mode control enabled hybrid energy storage system for islanded dc microgrids with pulsing loads," *Sustainable Cities and Society*, vol. 73, p. 103117, 2021.

[102] S. Kotra and M. K. Mishra, "Design and stability analysis of dc microgrid with hybrid energy storage system," *IEEE Transactions on Sustainable Energy*, vol. 10, no. 3, pp. 1603–1612, 2019.

[103] S. Anand and B. Fernandes, "Modified droop controller for paralleling of dc–dc converters in standalone dc system," *IET Power Electronics*, vol. 5, no. 6, pp. 782–789, 2012.

[104] R. K. Sharma and S. Mishra, "Dynamic power management and control of a pv pem fuel-cell-based standalone ac/dc microgrid using hybrid energy storage," *IEEE Transactions on Industry Applications*, vol. 54, no. 1, pp. 526–538, 2017.

[105] Q. Xu, J. Xiao, X. Hu, P. Wang, and M. Y. Lee, "A decentralized power management strategy for hybrid energy storage system with autonomous bus voltage restoration and state-of-charge recovery," *IEEE Transactions on Industrial Electronics*, vol. 64, no. 9, pp. 7098–7108, 2017.

[106] K. Shreelekha and S. Arulmozhi, "Multiport isolated bidirectional dc-dc converter interfacing battery and supercapacitor for hybrid energy storage application," in *2016 International Conference on Electrical, Electronics, and Optimization Techniques (ICEEOT)*, pp. 2763–2768, IEEE, 2016.

[107] Q. Song and J. Chen, "A decentralized energy management strategy for a battery/supercapacitor hybrid energy storage system in autonomous dc microgrid," in *2018 IEEE 27th International Symposium on Industrial Electronics (ISIE)*, pp. 19–24, IEEE, 2018.

[108] D. N. Huu, "An adaptive control of hybrid battery-supercapacitor storage for integration of wind and solar," in *2016 IEEE International Conference on Sustainable Energy Technologies (ICSET)*, pp. 157–162, IEEE, 2016.

[109] Q. Xu, J. Xiao, P. Wang, X. Pan, and C. Wen, "A decentralized control strategy for autonomous transient power sharing and state-of-charge recovery in hybrid energy storage systems," *IEEE Transactions on Sustainable Energy*, vol. 8, no. 4, pp. 1443–1452, 2017.

[110] Y. Zhang and Y. W. Li, "Energy management strategy for supercapacitor in droop-controlled dc microgrid using virtual impedance," *IEEE Transactions on Power Electronics*, vol. 32, no. 4, pp. 2704–2716, 2016.

[111] M. Shi, X. Chen, J. Zhou, Y. Chen, J. Wen, and H. He, "Advanced secondary voltage recovery control for multiple hesss in a droop-controlled dc microgrid," *IEEE Transactions on Smart Grid*, vol. 10, no. 4, pp. 3828–3839, 2018.

[112] Q. Zhang, L. Wang, G. Li, and Y. Liu, "A real-time energy management control strategy for battery and supercapacitor hybrid energy storage systems of pure electric vehicles," *Journal of Energy Storage*, vol. 31, p. 101721, 2020.

[113] Z. Cabrane, M. Ouassaid, and M. Maaroufi, "Battery and supercapacitor for photovoltaic energy storage: a fuzzy logic management," *IET Renewable Power Generation*, vol. 11, no. 8, pp. 1157–1165, 2017.

[114] J. Faria, J. Pombo, M. d. R. Calado, and S. Mariano, "Power management control strategy based on artificial neural networks for standalone pv applications with a hybrid energy storage system," *Energies*, vol. 12, no. 5, p. 902, 2019.

[115] S. Zhang, R. Xiong, and F. Sun, "Model predictive control for power management in a plug-in hybrid electric vehicle with a hybrid energy storage system," *Applied energy*, vol. 185, pp. 1654–1662, 2017.

[116] G. Wu, K. Y. Lee, L. Sun, and Y. Xue, "Coordinated fuzzy logic control strategy for hybrid pv array with fuel-cell and ultra-capacitor in a microgrid," *IFAC-PapersOnLine*, vol. 50, no. 1, pp. 5554–5559, 2017.

[117] H. Yin, W. Zhou, M. Li, C. Ma, and C. Zhao, "An adaptive fuzzy logic-based energy management strategy on battery/ultracapacitor hybrid electric vehicles," *IEEE Transactions on transportation electrification*, vol. 2, no. 3, pp. 300–311, 2016.

[118] N. Chettibi, A. Mellit, G. Sulligoi, and A. M. Pavan, "Adaptive neural network-based control of a hybrid ac/dc microgrid," *IEEE Transactions on Smart Grid*, vol. 9, no. 3, pp. 1667–1679, 2016.

[119] F. Garcia-Torres and C. Bordons, "Optimal economical schedule of hydrogen-based microgrids with hybrid storage using model predictive control," *IEEE Transactions on Industrial Electronics*, vol. 62, no. 8, pp. 5195–5207, 2015.

[120] F. Garcia-Torres, L. Valverde, and C. Bordons, "Optimal load sharing of hydrogen-based microgrids with hybrid storage using model-predictive control," *IEEE Transactions on Industrial Electronics*, vol. 63, no. 8, pp. 4919–4928, 2016.

[121] B. Hredzak, V. G. Agelidis, and M. Jang, "A model predictive control system for a hybrid battery-ultracapacitor power source," *IEEE Transactions on Power Electronics*, vol. 29, no. 3, pp. 1469–1479, 2013.

[122] B. R. Ravada and N. R. Tummuru, "Control of a supercapacitor-battery-pv based stand-alone dc-microgrid," *IEEE Transactions on Energy Conversion*, vol. 35, no. 3, pp. 1268–1277, 2020.

[123] S. Hajiaghasi, A. Salemnia, and M. Hamzeh, "Hybrid energy storage system for microgrids applications: A review," *Journal of Energy Storage*, vol. 21, pp. 543–570, 2019.

[124] W. Jing, C. H. Lai, S. H. W. Wong, and M. L. D. Wong, "Battery-supercapacitor hybrid energy storage system in standalone dc microgrids: areview," *IET Renewable Power Generation*, vol. 11, no. 4, pp. 461–469, 2017.

[125] J. Shen and A. Khaligh, "A supervisory energy management control strategy in a battery/ultracapacitor hybrid energy storage system," *IEEE Transactions on transportation electrification*, vol. 1, no. 3, pp. 223–231, 2015.

[126] A. Mohamed, V. Salehi, and O. Mohammed, "Real-time energy management algorithm for mitigation of pulse loads in hybrid microgrids," *IEEE Transactions on Smart Grid*, vol. 3, no. 4, pp. 1911–1922, 2012.

[127] A. Arabali, M. Ghofrani, M. Etezadi-Amoli, M. S. Fadali, and Y. Baghzouz, "Genetic-algorithm-based optimization approach for energy management," *IEEE Transactions on Power Delivery*, vol. 28, no. 1, pp. 162–170, 2012.

[128] Q. Zhang, W. Deng, and G. Li, "Stochastic control of predictive power management for battery/supercapacitor hybrid energy storage systems of electric vehicles," *IEEE Transactions on Industrial Informatics*, vol. 14, no. 7, pp. 3023–3030, 2017.

[129] T. Mesbahi, N. Rizoug, P. Bartholomeüs, R. Sadoun, F. Khenfri, and P. Le Moigne, "Optimal energy management for a li-ion battery/supercapacitor hybrid energy storage system based on a particle swarm optimization incorporating nelder–mead simplex approach," *IEEE Transactions on Intelligent Vehicles*, vol. 2, no. 2, pp. 99–110, 2017.

[130] "Mathworks. implement generic battery model - simulink - mathworks united kingdom." `http://www.mathworks.co.uk/help/physmod/powersys/ref/battery.html`. Accessed February, 09,2020 [Online].

[131] O. Tremblay and L.-A. Dessaint, "Experimental validation of a battery dynamic model for ev applications," *World electric vehicle journal*, vol. 3, no. 2, pp. 289–298, 2009.

[132] "Mathworks. implement generic supercapacitor model - simulink - mathworks india." `https://in.mathworks.com/help/physmod/sps/powersys/ref/supercapacitor.html`. Accessed February, 09,2020[Online].

[133] K. B. Oldham, "A gouy–chapman–stern model of the double layer at a (metal)/(ionic liquid) interface," *Journal of Electroanalytical Chemistry*, vol. 613, no. 2, pp. 131–138, 2008.

[134] "Discrete varying low pass filter." `https://www.mathworks.com/help/control/ref/varyinglowpassfilter.html`. Accessed: 09-12-2020 [Online].

[135] S. Punna, U. B. Manthati, and A. Chirayarukil Raveendran, "Modeling, analysis, and design of novel control scheme for two-input bidirectional dc-dc converter for hess in dc microgrid applications," *International Transactions on Electrical Energy Systems*, vol. 31, no. 10, p. e12774, 2021.

[136] Y. Zhou, Z. Huang, H. Liao, H. Li, Y. Jiao, and J. Peng, "A predictive set-point modulation energy management strategy for hybrid energy storage systems," *IEEE Transactions on Industry Applications*, vol. 55, no. 6, pp. 6266–6277, 2019.

[137] C. Arunkumar, U. B. Manthati, and S. Punna, "Supercapacitor voltage based power sharing and energy management strategy for hybrid energy storage system," *Journal of Energy Storage*, vol. 50, p. 104232, 2022.

[138] M. Ghiasi, "Detailed study, multi-objective optimization, and design of an ac-dc smart microgrid with hybrid renewable energy resources," *Energy*, vol. 169, pp. 496–507, 2019.

[139] C. Shah, J. D. Vasquez-Plaza, D. D. Campo-Ossa, J. F. Patarroyo-Montenegro, N. Guruwacharya, N. Bhujel, R. D. Trevizan, F. A. Rengifo, M. Shirazi, R. Tonkoski, *et al.*, "Review of dynamic and transient modeling of power electronic converters for converter dominated power systems," *IEEE Access*, vol. 9, pp. 82094–82117, 2021.

[140] W. Jing, C. H. Lai, W. S. Wong, and M. D. Wong, "A comprehensive study of battery-supercapacitor hybrid energy storage system for standalone pv power system in rural electrification," *Applied Energy*, vol. 224, pp. 340–356, 2018.

[141] S. K. Kollimalla, M. K. Mishra, and N. L. Narasamma, "Design and analysis of novel control strategy for battery and supercapacitor storage system," *IEEE Transactions on Sustainable Energy*, vol. 5, no. 4, pp. 1137–1144, 2014.

Author's Publications

International Journals (Published/Accepted)

1. **Arunkumar C. R.**, , Udaya Bhasker Manthati, and Srinivas Punna. "Supercapacitor voltage based power sharing and energy management strategy for hybrid energy storage system."Journal of Energy Storage 50 (2022): 104232. https://doi.org/10.1016/j.est.2022.104232.

2. **Arunkumar C.R.**, Manthati, U.B. & Punna, S. Supercapacitor-based transient power supply for DC microgrid applications.Electrical Engineering, Springer (2021). https://doi.org/10.1007/s00202-021-01312-7.

3. **Arunkumar C.R.**, Manthati, U.B. & Srinivas, P. Accurate modelling and analysis of battery–supercapacitor hybrid energy storage system in DC microgrid systems.Energy System , Springer (2021). https://doi.org/10.1007/s12667-021-00467-3

International Conferences (Published/Accepted)

4. **Arunkumar C.R.** and U. B. Manthati, "Design and Small Signal Modelling of Battery-Supercapacitor HESS for DC Microgrid," TENCON 2019 - 2019 IEEE Region 10 Conference (TENCON), Kochi, India, 2019, pp. 2216-2221, doi: 10.1109/TENCON.2019.8929544

International Journals (Under Review)

5. **Arunkumar C.R.** &U. B. Manthati, "A Hybrid Controller Assisted Voltage Regulation and Power Splitting Strategy for Battery/ Supercapacitor System in Isolated DC Microgrid", *Submitted in IEEE Transactions on Energy Conversion*, 2022.

6. **Arunkumar C.R.** &U. B. Manthati, "Dynamic Power Sharing Assisted Hybrid Controller for PV Fed Isolated DC Microgrid", *Submitted in IEEE System Journal*, 2022.